Stony Brook University

Photooxidation Processes on Single Crystal TiO_2(110) Surfaces

A Dissertation Presented

by

David Philip Sporleder

to

The Graduate School

in Partial Fulfillment of the

Requirements

for the Degree of

Doctor of Philosophy

in

Chemistry

Stony Brook University

December 2008

Stony Brook University

The Graduate School

David Philip Sporleder

We, the dissertation committee for the above candidate for the Doctor of Philosophy degree, hereby recommend acceptance of this dissertation.

Michael G. White, Ph. D., Advisor
Professor, Department of Chemistry

Philip M. Johnson, Ph. D., Chairperson
Professor, Department of Chemistry

Joseph W. Lauher, Ph. D., Third Member
Professor, Department of Chemistry

Jan Hrbek, Ph. D., Outside Member
Senior Chemist, Brookhaven National Laboratory

This dissertation is accepted by the Graduate School

Lawrence Martin
Dean of the Graduate School

Abstract of the Dissertation

Photooxidation Processes on Single Crystal TiO_2(110) Surfaces

by

David Philip Sporleder

Doctor of Philosophy

in

Chemistry

Stony Brook University

2008

There is considerable interest in light induced chemistry on TiO_2 surfaces due to its numerous applications, one of the most common being the destruction of hazardous bacterial matter and organic pollutants in wastewaters or air. In some cases, the complete oxidation of organic compounds to CO_2 and H_2O is observed. The work presented here focuses on thermally induced or photoinduced processes occurring on TiO_2 surfaces with the goal of better understanding the decomposition mechanism of such pollutants and identifying the intermediates involved. Final state velocity distributions of molecules ejected from the TiO_2 surface upon photoexcitation were determined under ultrahigh vacuum (UHV) conditions to gain insight into the energy transfer processes that occur. The velocity distributions were measured by using a pump-probe, time-of-flight (TOF) method along with one photon, vacuum ultraviolet (VUV) ionization of gas phase products for product detection. Temperature program desorption (TPD) studies were employed to identify surface bound products.

Adsorbed molecular oxygen has been shown to be essential in the removal of organic compounds on TiO_2, hence initial investigations concentrated on the interaction of O_2 with single crystal rutile TiO_2(110) surfaces. Velocity distributions of molecular oxygen desorbed from the surface via a photo-induced process were determined and are shown to be consistent with a hole capture, substrate mediated excitation mechanism. In addition, the distributions indicate that different initial states of adsorbed oxygen, perhaps different O_2 species (i.e. O_2^- or O_2^{2-}), binding sites, or geometries exist on the surface of TiO_2(110).

An investigation of the photodecomposition mechanism of organic molecules was performed by exploring the dynamics of desorbates produced from photoreactions of model carbonyl compounds (acetone and 2-butanone) on TiO_2(110) surfaces. Consistent with previous studies, it was found that in order for the system to be active for photodecomposition adsorbed molecular oxygen is required. Evidence that an active oxygen species involved is an O atom is presented. The primary photooxidation pathway yields two products, a gas phase alkyl radical and surface bound carboxylate which are generated by photo-induced fragmentation of the ketones. Velocity distributions of the alkyl radicals were determined to be bimodal indicating two channels for photodecomposition operate under the conditions explored. In the case of 2-butanone the two channels may be described by the slow channel involving excess energy partitioning into excitation of the pyramidal bending mode of the methylene group of the ejected ethyl radical. Additionally, no evidence for secondary chemistry involving alkyl radicals was observed under the UHV conditions employed.

For Brian

Table of Contents

List of Abbreviations

AES: Auger electron spectroscopy

CMA: Cylindrical mirror analyzer

DOF: Degrees of freedom

EPR: Electron paramagnetic resonance

E_t: Translational energy

HREELS: High resolution electron energy loss spectroscopy

L: Langmuir

LEED: Low energy electron diffraction

LN: Liquid nitrogen

MCP: Multichannel plates

ML: Monolayer

PES: Photoelectron spectroscopy

PMT: Photomultiplier tube

PV: Pulsed valve

PSD: Photon stimulated desorption

QMS: Quadrupole mass spectrometer

STM: Scanning tunneling microscopy

TMP: Turbo molecular pump

TOF-MS: Time-of-flight mass spectrometer

TPD: Temperature program desorption

UHV: Ultra high vacuum

VUV: Vacuum ultraviolet

List of Tables

List of Figures

Acknowledgments

It gives me great pleasure to acknowledge the help and support I received throughout my graduate career at Stony Brook University. First, I would like to thank my research advisor Professor Michael White for his generosity with his time as well as the guidance and advice he has provided me for my dissertation research. Also, I wish to thank my advisement committee members Professors Philip Johnson, Joseph Lauher and Dr. Jan Hrbek for their guidance and the time they committed to my career development.

I am grateful to my fellow group members, both past and present for their help, support and advice. Of these I should like to mention Dr. Robert Beuhler for offering his knowledge of instrumentation to help with my experiments as well as his assistance in developing the sample holder used for collecting the data in this dissertation. My sincere thanks to Daniel Wilson for the many long hours shared running experiments as well as for the fine work he has done modifying our software used for data collection which has greatly enhanced our photochemistry machine.

Also thanks are due to the Department of Energy, Basic Energy Sciences Directorate for the financial support of the work in this dissertation.

Finally, I am indebted to my wife, Xiaojie Zhou, and family Phil Sporleder, Linda and James Freitag, Chris and Caroline Sporleder, and Brain Sporleder for the unwavering support and encouragement as well as the advice they have given me throughout the years.

1. Introduction

The focus of this dissertation is to gain a better understanding of the photooxidation processes that occur on a semiconductor photocatalyst such as titania (TiO_2). TiO_2 is often used as a model system in fundamental investigations of the surface chemistry of metal oxides. Also, numerous applications for titania have been developed over the years based on its optical and electrical properties, and have inspired an extensive number of studies on the chemistry at titania interfaces.[1-7] One of the most common applications is the photooxidation of organic compounds for environmental remediation. The research presented in this dissertation employed model systems to investigate thermally induced and photo-induced processes occurring at titania interfaces with the goal elucidating the initial mechanistic steps during the oxidation of organic material as well as identifying the intermediates involved. Investigations of photooxidation processes on TiO_2 are presented in two parts in this dissertation. Given that it has previously been shown that adsorbed O_2 is needed for photodecomposition of organic molecules on TiO_2 yet the mechanism and state of oxygen is not known,[1-7] a study of the simple system of O_2 and TiO_2 single crystals was conducted and is reported in Chapter 3. The experimental approach was to focus on the photo-induced reaction dynamics by determining final state velocity distributions of desorbed O_2 molecules which can reflect on their initial bound states. Subsequently, photo-induced reactions of simple ketones, acetone and 2-butanone, on a titania sample co-adsorbed with O_2 were examined and presented in Chapter 4. Again, final state velocity distributions of species ejected into the vacuum were measured and TPD experiments were employed to identify any surface bound products.

Interest in light induced chemistry on titania surfaces began to gain momentum after the photoelectrolysis of water into H_2 and O_2 using a TiO_2 electrode was first reported by Fujishima and Honda in Nature in 1972.[2,8] Some of the more commonly researched applications of TiO_2 today make use of its photo-induced hydrophilicity for self-cleaning and antifogging surfaces, or its photooxidation properties for the degradation of pollutants in wastewater or air. One of the first reports on the use of titania for the photooxidation of pollutants, was presented in 1977 by Frank and Bard and it showed the ability of TiO_2 to oxidize aqueous CN^- in the presence of sunlight.[9] Since then, the photodecomposition of bacteria and organics has been demonstrated many times over and in some cases, organic compounds were completely oxidized to CO_2, H_2O, and NO_3^-.[5] Most investigations on titania today, focus on enhancing technological applications as well as clarifying the photooxidation mechanism for such processes.

Widespread use of TiO_2 as a photocatalyst stems from the fact that it is relatively inexpensive, harmless to humans and the environment, and resistant to degradation during illumination.[1-7] TiO_2 particles have been shown to retain much of their photocatalytic ability even after repeated catalytic cycles and can also be recovered by filtration or centrifugation if used unanchored in solution.[5] Moreover, titania in aerated water has proven to be the most active photocatalyst for the breakdown of harmful pollutants.[5] Two structures of TiO_2 are typically used for photochemical applications, rutile and anatase, with the latter form having demonstrated higher activity for photooxidation processes.

Generally speaking in semiconductor photocatalysis, incident light is converted into chemical energy. The fundamental process for photoexcitation of a semiconductor

mediated chemical reaction is well known, with the initial step being electronic excitation by absorption of photons.[1,5,6,10]

In the band theory of solids, semiconductors are characterized as having band structure where a high density region of states are associated with covalent bonding between lattice atoms and designated as the valence band.[11] This band is considered to be essentially a continuum of mostly filled states that would be completely filled at T = 0 K. Lying higher in energy than the valence band is a second high density region of mostly empty states referred to as the conduction band. The energy region between the two bands or band gap is defined as the region void of states, extending from the top of the valence band edge to the bottom of the conductance band edge. The magnitude of the gap determines the population of the conduction band at a given temperature and thus the electrical conductivity of the solid. It should be noted that a "real" crystal may have states lying within the band gap region associated with lattice irregularities. Absorption of supra-band gap radiation creates electron vacancies (holes) by promoting electrons from the valence band to the conduction band. Photo-generated electrons (or holes) can rapidly undergo relaxation to the conduction band (or valence band) edge but further relaxation of electrons and holes occurs on a longer time scale.

An adsorbed species on the surface can undergo interfacial charge transfer by accepting a conduction band electron as long as an adsorbate orbital in lower in energy than the conduction band edge and the charge transfer rate is competitive with the rate of recombination. Additionally, if a filled or partially filled adsorbate orbital is higher in energy than the valence band edge, the adsorbate may donate an electron to the valence band hole. The rate and probability of such reduction and oxidation processes depends

on the relative positions of the adsorbate energy levels and the conduction and valence band edges.

In order for TiO_2 to be a viable catalyst for photooxidation, the electron-hole pair recombination rate needs to be suppressed by charge carrier trapping at surface or bulk lattice irregularities (defects). Electronic states of these defects differ in energy from those in the regular band structure and can act to trap electrons or holes and thus reduce the rate of recombination. EPR spectroscopy has been used to demonstrated charge carrier trapping in TiO_2 where electrons and holes are trapped to form Ti^{III} sites and O^- sites respectively, as described by the following equations.[12]

$$TiO_2 + h\nu \rightarrow e_{CB} + h_{VB} \qquad \text{charge generation} \qquad (1.1)$$

$$Ti^{IV} + e_{CB} \rightarrow Ti^{III} \qquad \text{electron trapping} \qquad (1.2)$$

$$O^{2-} + h_{VB} \rightarrow O^- \qquad \text{hole trapping} \qquad (1.3)$$

Throughout this dissertation, the IV and III superscripts represent the + 4 and + 3 oxidation states of the elements, respectively.

Another factor that can influence photocatalytic processes is alteration of the electrostatic potential of valence and conduction band edges when a semiconductor is brought into contact with another phase (i.e. solid, liquid or gas).[1,5,6] Charge transfer between the two phases can result in the formation of an electric field in the near surface region of the semiconductor (space charge region). For an n-type semiconductor (such as TiO_2) where lattice defects contribute excess mobile electrons, charge transfer to an adsorbate can result in a negative charge at the interface and thus, a near surface region depleted of electrons. The space charge region is termed a depletion layer in this case, and electron-hole pairs formed in this region by absorption of a photon separate with the

electron moving towards the bulk and the hole moving toward the surface. This is commonly referred to as band bending since the potential energy for an electron at the interface differs from that in the bulk, and in the case of a depletion layer the band edges bend up toward the interface. Band bending can have an effect on the oxidation and reduction abilities of a semiconductor by shifting the band energy levels relative to the electron accepting or donating orbital of the adsorbate of interest. Moreover, transfer of electrons to adsorbates can increase the lifetimes of photo-generated holes in the semiconductor by reducing the recombination rate.

In photooxidation processes on titania, adsorbed oxygen species (O_2^-, O adatoms, $OH^{\cdot}$) have been shown to be essential, particularly for the decomposition of organic compounds. The oxygen species involved and its specific role has not yet been explicitly determined. It has been proposed that O_2 scavenges photo-generated electrons, therefore increasing the lifetime of holes, and thus the probability of an organic species undergoing oxidation by donating an electron (hole capture). Others studies have suggested that reactive oxygen species can directly interact with organic molecules or intermediate species. Given the importance of oxygen in photodegradation processes on TiO_2 the interaction of O_2 with titania surfaces have been thoroughly investigated. An O_2 PSD study which focuses on the desorption dynamics was conducted and is presented in Chapter 3 of this dissertation.

Many studies on TiO_2 photooxidation are designed to replicate conditions similar to how the photocatalyst is actually used in many applications. Studies such as these, typically use powdered and polycrystalline titania substrates that are not well defined, for photooxidation under relatively high pressure leading to conditions favorable to

secondary chemistry (i.e. reactions involving the intermediates formed in initial mechanistic steps of the photooxidation process). However initial reaction steps and intermediates can be difficult to discern in this manner. For example, a variety of different intermediate species have been identified in photooxidation reactions studied under such conditions. The experimental approach used for the investigations presented in this dissertation was to employ model systems in an attempt to determine the early mechanistic steps in photooxidation processes on TiO_2 with interest in illuminating the role O_2 plays as well as identify any initial intermediate species that form. To this end, photo-induced processes were studied under UHV conditions for better control of reactant gases, as well as reduction of background contaminates and secondary chemistry. Furthermore, well characterized single crystal TiO_2(110) surfaces were employed as the semiconductor substrate for their thermal stability and the relative ease by which the (110) surfaces can be reduced and oxidized.

A schematic of the (1 × 1)-TiO_2(110) (rutile) surface is displayed in Figure 1.1, where the red spheres represent in-plane oxygen atoms, the gray spheres represent fivefold coordinated titanium atoms in the + 4 oxidation state, designated as Ti^{IV}(5f) in this dissertation, and the dark red spheres correspond to bridging oxygen atoms (O_{br}).[1] The O_{br} atoms are bridge bonded to two Ti^{IV} in-plane atoms and protrude above the surface plane. It is well known that the presence of defects states in TiO_2 greatly alter the chemistry it undergoes with adsorbate molecules. For example, the presence of defect states are a prerequisite for O_2 adsorption on titania surfaces in the absence of photo-generated conduction band electrons. An oxygen vacancy is one of the most common types of defects in metal oxides. TiO_2 is readily reduced upon thermal annealing,

yielding defects associated with O vacancies and at least two have been identified as Ti^{III} interstitials, label as $Ti^{III}(i)$ here, and O_{br} vacancies on the surface.[13] The O_{br} vacancy sites are comprised of two exposed Ti^{III} atoms associated with excess electron density and an example of such a defect is schematically shown in Figure 1.1. Since most photooxidation processes on TiO_2 require adsorbed O_2, all of the experiments reported in this dissertation were performed on reduced samples unless otherwise stated.

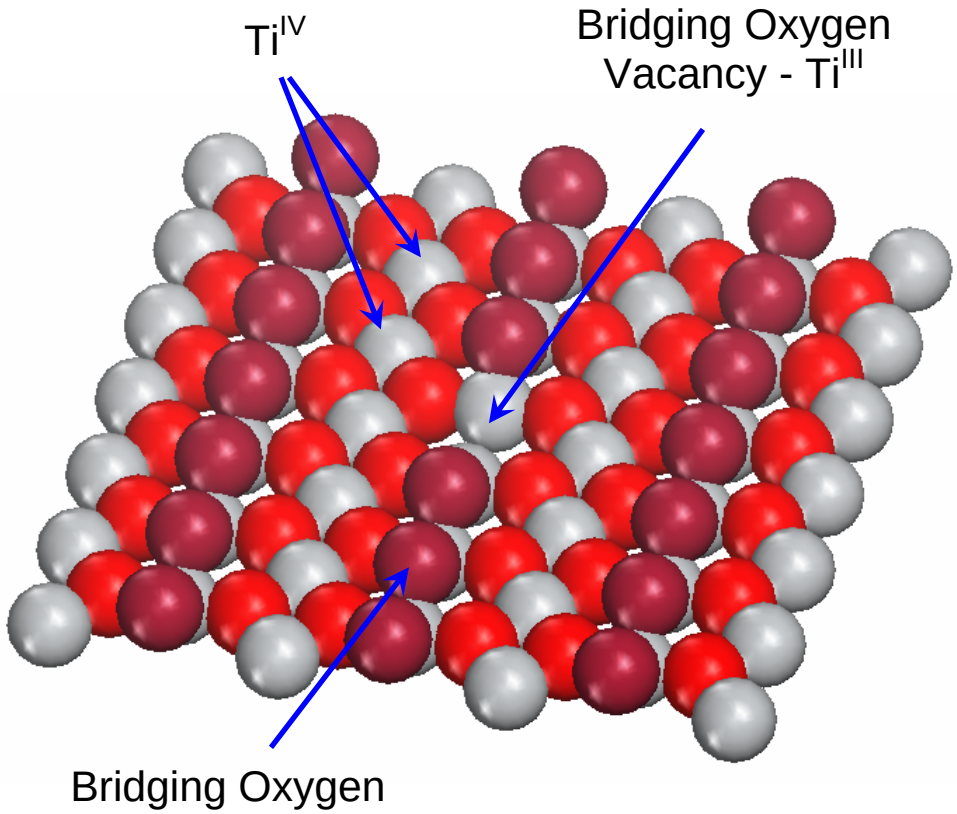

Figure 1.1: Schematic of the TiO_2(110) surface. Red spheres represent in-plane oxygen atoms, grey spheres represent Ti atoms, and the dark red spheres correspond to bridging oxygen atoms.

2. Experimental Section

The surface photochemistry apparatus used for data collection has been described elsewhere,[14,15] however, since that time there has been extensive modifications to the machine and it is described in detail in the following section (2.1). Sample preparation and characterization methods are discussed in section (2.2), followed by a description of the procedures used for determining final state velocity distributions and generation of VUV radiation which are presented in section (2.3).

2.1 Surface photochemistry apparatus

The surface photochemistry apparatus used for these experiments consists of two vacuum chambers, a main surface science chamber with a base pressure of about 5×10^{-10} Torr, and a smaller chamber which serves as a windowless VUV source. The two chambers are connected by a doubly differentially pumped capillary light guide to allow passage of the VUV probe radiation while maintaining the UHV environment of the main chamber. The main chamber, which is pumped by two turbo molecular pumps, is comprised of two levels. The titania sample is positioned between the two chamber levels and aligned with respect to the various instruments by an XYZ translator. Figure 2.1 shows the upper level which is used for sample preparation and characterization. It contains an ion gun (NGI3000-SE, LK Technologies) used for cleaning the titania surface by ion bombardment and a directional doser for exposing the sample to the various small molecules to be investigated. Additionally, the upper level includes a LEED apparatus (RVL 8-120, Princeton Research Instruments, Inc.) for surface characterization and an apertured QMS (HAL 511/3F PIC, Hiden Analytical)) enclosed in a cryogenically cooled

shroud for thermal desorption measurements. A CMA (10-155A, Physical Electronics) was used for AES to test for impurities at the TiO_2(110) surface and is not shown in the figure. The chamber does not have the required number of large diameter ports for both the LEED apparatus and CMA to be mounted simultaneously, thus these instruments occupied the same port and were interchanged as necessary. The CMA was primarily used during the early stages of the project for development of sample preparation methods.

Figure 2.2 displays the lower level of the main chamber where the photochemistry experiments were performed. The lower level contains a directional doser as well as a time-of-flight mass spectrometer for species identification and velocity measurements. The VUV source chamber is also shown in Figure 2.2 along with the capillary light guide that links the two chambers. The source chamber is made up of a six way cross and contains a TMP and a piezo-driven, pulsed molecular beam valve for generation of a free jet expansion of nitrogen (or a noble gas) directed perpendicular to the beam path of the UV light used for VUV generation. The details for generation of the VUV light are given below. Once generated, the VUV light entered the capillary in the source chamber, propagated by total internal reflection into the lower level of the main chamber, and exited the capillary into the extraction region of the TOF-MS perpendicular to the axis of the spectrometer.

2.2 Sample preparation

An orientated rutile TiO_2(110) crystal (CrysTec Kristalltechnologie) with an area of 100 mm^2 and 2 mm thick was used in these experiments. A commercial button heater

(HeatWave) utilized a Re/Pt filament for resistively heating the sample. The TiO_2 crystal was mounted to the button heater as shown in Figure 2.3. A Mo support collar encircling the heater was fastened to the heater with Mo screws and connected to the sample manipulator by a threaded Mo support rod. Two clips constructed out of Ta foil press on ledges that were machined onto opposite sides of the TiO_2 crystal to assure the sample was in good contact with the heater. For improved heat transfer, Au foil (25 μm thick) was sandwiched between the button heater and sample. The temperature was monitored with a type K thermocouple (chromel-alumel alloy) that was inserted into a small hole in the edge of the crystal and held in place with high temperature chemical set cement (OMEGABOND 600, Omega). The manipulator, a stainless steel tube, served to connect the sample holder to the XYZ translator as well as act as a LN reservoir for sample cooling. A crystal temperature range of 100 to 900 K could be achieved with this sample mount.

The TiO_2 crystal was initially bulk reduced and the surface was cleaned by sputtering at a crystal temperature of 850 K, first with 3 keV Ar^+ ions, followed by 500 eV ions in order to repair damage caused by the higher energy sputtering.[16] Annealing at 850 K was continued for 30 minutes after sputtering. This procedure was repeated until impurity levels, which were determined by AES, were below the spectrometer detection limits. Typical contaminants were K^+ and Ca^+ ions. After an extensive number of cleaning cycles, the sample obtained a dark blue color. A LEED pattern consistent with a (1×1)-$TiO_2(110)$ rutile surface was obtained after the reducing/cleaning procedure, confirming that the sample maintained long range order. The QMS was employed for TPD experiments of D_2O to quantify the surface bridging

oxygen vacancies.[17,18] The oxygen vacancy population was determined to be about 0.06 ML.

At the beginning of each experiment, prior to a thermal or photochemistry measurement, the crystal was sputtered and annealed to provide a clean, reduced TiO_2(110) sample surface. The sample preparation methods differed slightly between the two studies presented in this dissertation, and the details of the surface cleaning procedures are given in the experimental sections of the appropriate chapters.

A QMS was used to perform TPD experiments for characterization of the O_2, D_2O, acetone, or butanone coverage as well as for TPD measurements following UV irradiation of the surface in order to probe surface bound products. A Eurotherm 2408 process control unit maintained a constant heating rate of 2 Ks^{-1} during all TPD measurements. The sample was held at a potential of negative 70 to 90 volts to prevent any electrons that escaped from the ionization region of the mass spectrometer from inducing chemistry at the TiO_2-vacuum interface.

A stainless steal inlet system pumped with a 50 L s^{-1} turbo molecular pump was employed to introduce O_2, D_2O, acetone, and butanone. Reagent grade acetone (Fisher Scientific), butanone (Aldrich), and D_2O samples were purified by several freeze-pump-thaw cycles. The cycles were continued until the pressure above the liquid samples did not significantly decrease between consecutive freeze-pump-thaw cycles. Vapor above acetone, butanone, or D_2O samples were introduced to the TiO_2 surface via a directional doser at a crystal temperature of 100 K. Research purity oxygen obtained from Matheson Tri-Gas was introduced by either backfilling the chamber or through a directional doser at a crystal temperature of 100 K.

2.3 Velocity measurements

Species ejected from the TiO_2 surface upon UV excitation of the adsorbate-oxide interface were detected by employing a one photon ionization method using coherent VUV radiation and TOF-MS. Detection of molecular oxygen was enhanced by making use of the H $^3\Pi_u \leftarrow$ X $^3\Sigma_g^-$ (6,0) (94.7-94.9 nm) resonant transition in which the excited Rydberg state undergoes auto-ionization. Measurements of the photodecomposition of acetone on TiO_2 also utilized a photon energy of 13.1 eV (94.74 nm), however in this case product detection was by non-resonant ionization. For measurements of butanone photodecomposition products, two different photon energies for non-resonant ionization of desorbates were used in order to aid in product identification, 13.1 eV and 10.8 eV (114.42 nm).

Generation of 13.1 eV photons was done by nonresonant third harmonic generation (THG; $\omega_{vuv} = 3\omega_{uv}$) in a free jet expansion of N_2 gas that was produced by a piezo-driven, pulsed molecular beam valve. A Nd:YAG pumped dye laser system (Spectra-Physics GCR-230 (20 Hz), Laser Analytics LDL 20505 dye laser) with Rhodamine 590 laser dye produced light with a wavelength of 568.44 nm. Second harmonic generation (SHG; $\omega_{uv} = 2\omega_v$) of the dye laser output in an angle-tuned KDP crystal (INRAD Autotracker II) produced UV (ω_{uv}) laser light with a wavelength of 284.22 nm that was focused inside the smaller vacuum chamber and into the free jet expansion of N_2 by a achromatic lens with a focal length of 10 cm. Both the VUV and UV radiation were captured by a Pyrex capillary light guide (35 cm long, 1 mm i.d.) and directed into the extraction field of the TOF mas spectrometer perpendicular to the TOF axis. Photons of 10.8 eV were produced by the same method except LDS 698 laser dye

was employed to make 343.25 nm wavelength radiation, and third harmonic generation of the UV light was carried out in a free jet expansion of Xe gas in the VUV source chamber.

Chemistry at the adsorbate-oxide interface was induced by irradiating the sample surface with UV laser light of the wavelength of interest at an incident angle of 45º relative to the surface normal. UV light with wavelengths of 298 nm, 335 nm, or 359 nm was generated when Rhodamine 610, LDS 698 with DCM, and LDS 722 laser dyes were used, respectively, in conjunction with a second Nd:YAG pumped dye laser system (Spectra-Physics GCR-190 (20 Hz), Sirah PRSC-D-18 dye laser). The visible dye laser output was used to produce the desired UV frequencies by SHG in angle-tuned KDP crystals (INRAD Autotracker II), and the visible light was removed from the beam path by an INRAD 752-104 UV harmonic separator. A Galilean type telescope used in conjunction with a 7 mm aperture fixed the UV beam size at 0.7 cm diameter, yielding an ellipse of 0.5 cm^2 at the sample face. The beam path contained two Glan-Thompson polarizers (Lambrecht), one established p-polarized light relative to the crystal face, while the other was used to regulate the power. Calibrated fused-silica neutral density filters further attenuated the laser power to the desired level.

The TOF mass spectrometer includes a three-electrode electrostatic lens array (capable of velocity vector focusing[19]) with a total applied acceleration potential of 98.3 V and a flight path of 40 cm from the ionization laser to the detector. Ions were detected via an assembly consisting of two microchannel plates, 4.0 cm in diameter, and a phosphor screen. The emission of the phosphor was converted into an electrical current by a PMT and displayed on a digital oscilloscope that was triggered by the VUV probe

laser, and connected to a personal computer. A LabVIEW program recorded the signal as well as controlled a digital delay generator (DG 535, Stanford Research System, Inc.) that either fixed or scanned the delay between the probe laser and the excitation laser.

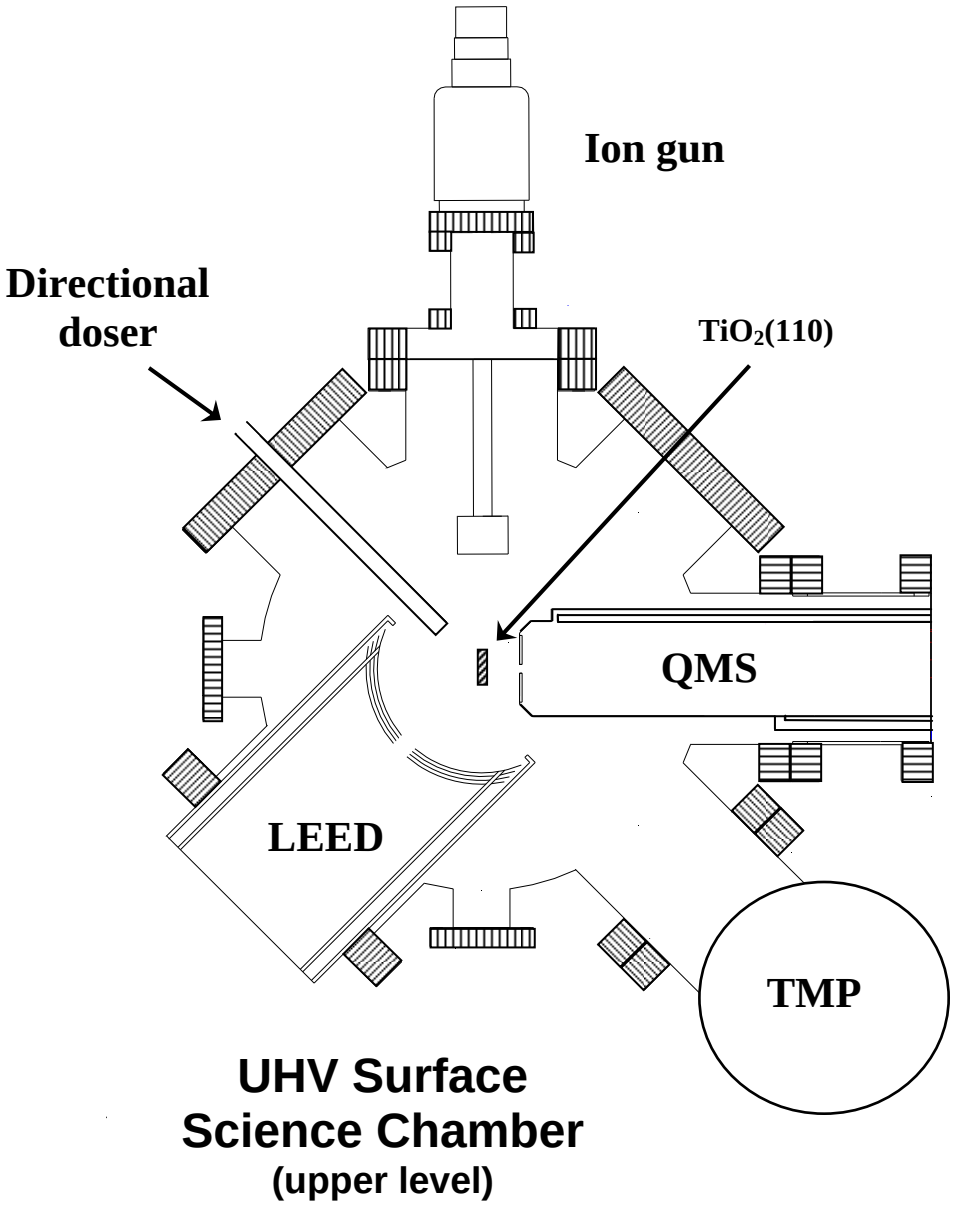

Figure 2.1: Schematic of the main surface science chamber (upper level) used for sample preparation and characterization.

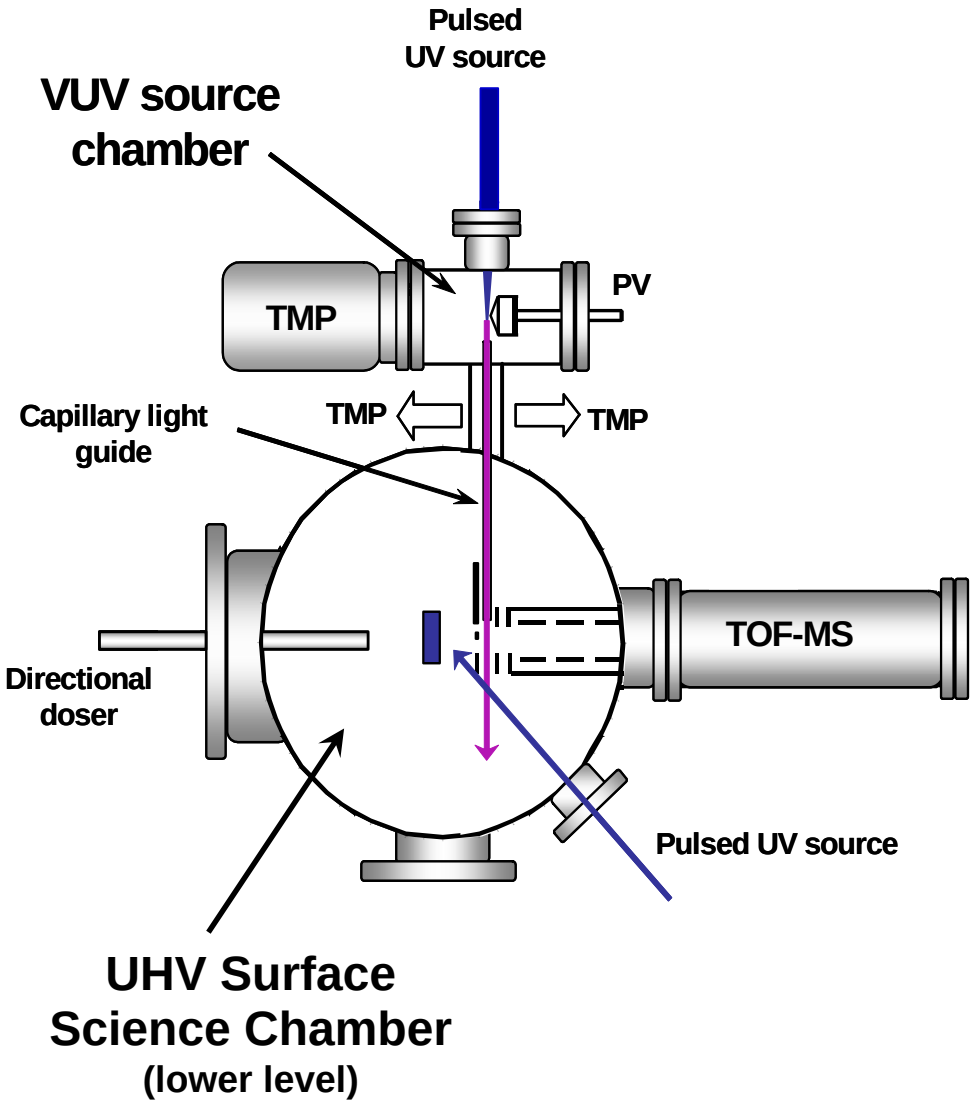

Figure 2.2: Schematic of the lower level of the main surface science chamber and the VUV source chamber. The two chambers are connected via a doubly differentially pumped capillary light guide to allow passage of the VUV radiation from the point of generation to the extraction region of the TOF-MS. The TiO_2(110) sample is shown in the center of the main chamber. The excitation UV light is incident on the sample (110) face 45° to the surface normal.

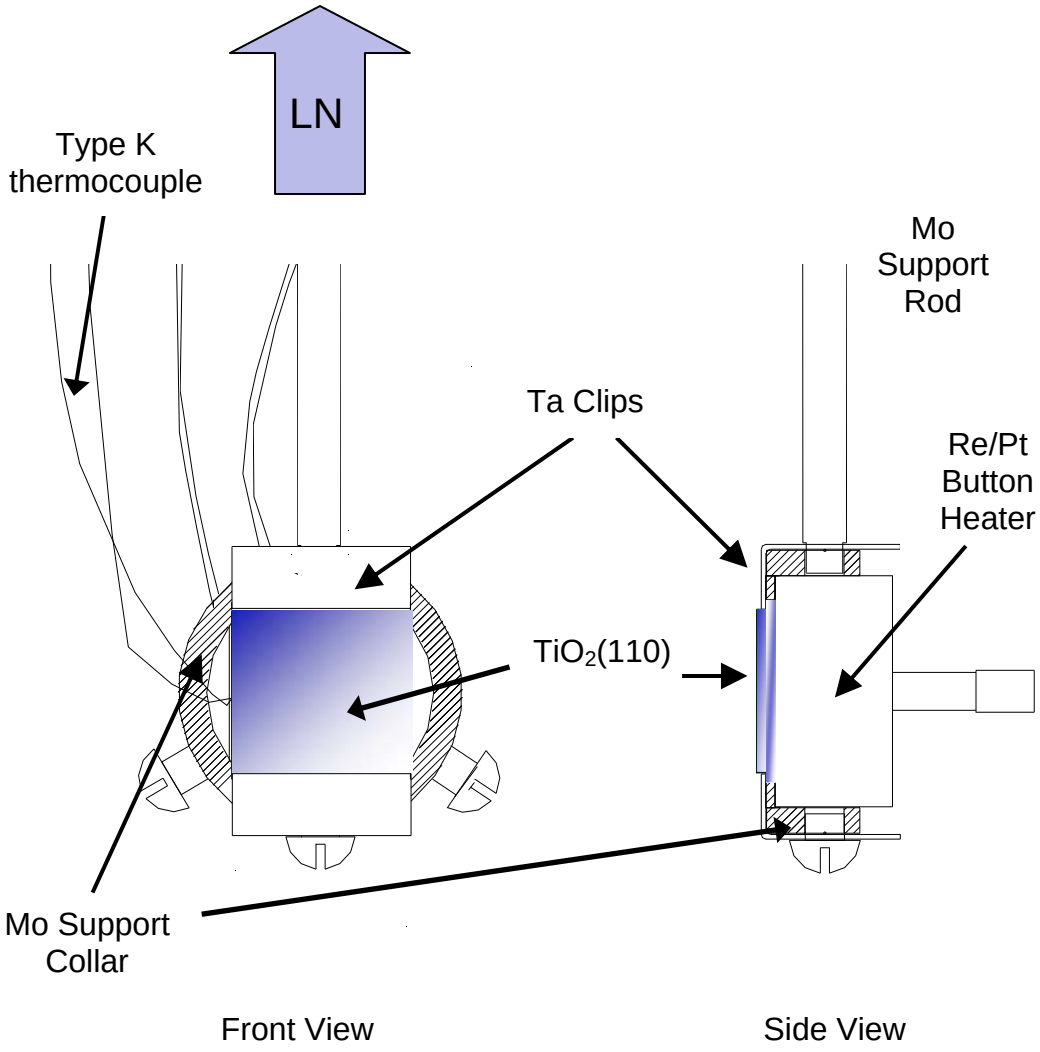

Figure 2.3: Schematic of the sample holder used in the experiments reported here. A commercial button heater (Heatwave) utilized a Re/Pt heating element for resistively heating the TiO_2(110) sample. A temperature range of 100 to 850 K could be obtained and was monitored with a type K thermocouple.

3. Photo-Induced Desorption of Molecular Oxygen from TiO_2(110) Surfaces

This section is to be published.

3.1 Introduction

The vast number of studies on chemistry at titania interfaces have been performed and are motivated by the variety of applications for the semiconductor as discussed in the general introduction.[1-7] The work performed for this dissertation is primarily concerned with the use of titania as a photocatalyst to decompose organic molecules. Although adsorbed molecular oxygen has been shown to be essential in these photodecomposition processes, its precise role as either a direct participant in reactions, or as a scavenger of photo-generated electrons has not been unambiguously determined.[1-7] Chemistry at the TiO_2 interface has proved to be quite rich, and despite the large number of investigations of even the relatively simple process of O_2 PSD from single crystal TiO_2(110) surfaces, so far no direct link between the desorption kinetics and initial binding site(s) of chemisorbed oxygen has been made. Gaining insight into how oxygen contributes in photooxidation reactions occurring on titania surfaces will aid in improving technological applications of TiO_2 as a photocatalysts.

It is well known that the introduction of defect states within the band gap of TiO_2 due to loss of O atoms greatly enhances the chemical reactivity of the oxide.[1,6,7] The increased reactivity of the reduced sample has been attributed to the donating ability of electrons that are associated with these defects states ($Ti^{III}(i)$ or O_{br} vacancies). For instance, molecular oxygen only weakly interacts with a fully oxidized TiO_2 surface, undergoing physisorption at low temperature (< 70 K).[20] However chemisorption of O_2

occurs on an oxygen deficient (reduced) titania surface via charge transfer from either defect states or photo-generated electrons.[21] A TiO_2 crystal is readily reduced under ultra high vacuum conditions by electron impact, annealing, or ion bombardment.[1,7,22] While electron impact forms defects which can be "healed" by exposure to O_2 at 100 K and have been attributed to O_{br} vacancies, vacuum annealing and ion bombardment introduce O_{br} vacancies as well as another defect that is not completely "healed" by O_2 exposure at 100 K.[22] The identity of this second defect may come from a recent study by Wendt et al. which provides evidence for $Ti^{III}(i)$ atoms in a reduced sample that provide a means for O_2 chemisorption.[13] Photo-electron spectroscopy and density functional theory calculations have allowed for Wendt et al. to assign the defect state lying within the band gap, 0.85 eV below the Fermi level, to $Ti^{III}(i)$ atoms which can diffuse to the near surface region at high temperature. The studies performed in this dissertation, use the more common experimental approach of vacuum annealing to create a reduced TiO_2 sample for investigations of its interfacial chemistry.

Oxygen may interact with a titania surface by physisorption, chemisorption, or dissociation. On oxidized TiO_2, molecular oxygen will only interact at low temperature and undergo physisorption. When the metal oxide has electrons available for charge transfer from either defect states or absorption of photons, O_2 can chemisorb or dissociate at the interface. It has been demonstrated that oxygen chemisorbs on TiO_2 as either a superoxide (O_2^-) anion,[12,23-25] or atomic O^{2-} species,[21] while other oxygen species such as the peroxide (O_2^{2-}) anion have been postulated.[26] A recent study by Kimmel and Petrik also suggest a O_4^{2-} species may exist on TiO_2 when exposed to O_2 at very low temperature.[27] Additionally, dissociative adsorption of O_2 occurs at O_{br} vacancy sites for

temperatures ≥ 100 K with one O atom filling the vacancy and the other binding to a Ti^{IV}(5f) site. O_2 adsorbed at Ti^{III}(*i*) can also dissociate upon thermal activation at temperatures around 300 K leaving two O adatoms at Ti^{IV}(5f) sites which may form an Ti_xO_y adlayer.[13]

Based on a King and Wells type of study to measure O_2 sticking on TiO_2 at 100 K, Henderson et al. suggested that three oxygen molecules bind to the surface per O_{br} vacancy.[21] These authors presented a model in which one O_2 binds at an O_{br} site and the other two O_2 bind at Ti^{IV}(5f) sites adjacent to the vacancy. This model was qualitatively supported by theoretical studies that predicted electron density associated with O_{br} vacancies is highly delocalized, however neither study considered Ti^{III}(*i*) defects as possible adsorption sites.[28] Thermal desorption studies have shown a peak at 410 K that is thought to be due to O_2^- species bound at Ti^{IV}(5f) sites that do not dissociate upon thermal activation. These O_2^- species are also active for photodesorption as shown in this work. It is possible that molecular oxygen adsorbed at Ti^{IV}(5f) sites have a wide range of binding energies or configurations that depend on their proximity to Ti^{III}(*i*) or O_{br} vacancy defects. In fact, several theoretical investigations have predicted that molecular oxygen adsorbs in a number of geometries, spin states, and with a range of binding energies.[25,29-31] If these different initial states desorb via different transition states, measurements of the O_2 translational energy distribution should be able to distinguish the different desorption channels.

Several studies that focused on the desorption kinetics of O_2 PSD from TiO_2(110) surfaces pre-adsorbed with O_2 employed cw excitation (UV lamps) and detection (electron impact mass spectroscopy) techniques.[26,32-35] It was determined that molecular

oxygen photodesorption did not follow exponential kinetics and photoyields and rates were strongly temperature dependent. Originally the kinetic behavior for photodesorption at low temperature (~120 K) was attributed to two initial O_2 states (α_1-O_2, α_2-O_2).[33] However, further analysis led to a reinterpretation of the data in which a model for PSD of a single species (α-O_2) was provided.[35] This model explained the non-exponential desorption kinetics by a coverage dependence of the electron transfer along one direction of the crystal (001) which leads to a change in electron-hole recombination rates as a function of O_2 coverage. Another state (β-O_2) was suggested to arise by irreversibly converting the low temperature state(s) (α-O_2) upon thermal activation of the substrate to about 200 K or above. The β-O_2 state is distinguishable from α-O_2 by its much higher photodesorption cross section for and ability to photo-oxidize CO. Taken together, the above arguments seem to indicate multiple initial adsorption states for O_2 though the correlation with binding sites is unknown.

It is generally accepted that the O_2 photo-induced desorption mechanism is substrate mediated and governed by the optical properties of the semiconductor substrate. However at least one theoretical study has predicted a direct optical excitation of the adsorbate-substrate complex as a desorption pathway.[36] Investigating the desorption dynamics of O_2 from the TiO_2 surface will assess the validity a direct adsorbate-substrate complex excitation mechanism since the final state distributions of O_2 desorbing via this channel would be sensitive to the energy and polarization of the excitation source.

In this chapter, results from an investigation of the PSD of molecular oxygen from well characterized single crystal TiO_2(110) surfaces pre-adsorbed with O_2 are presented. Reduced TiO_2 surfaces created by vacuum annealing were used and contained an O_{br}

vacancy concentration of about 0.06 ML as determined by H_2O TPD measurements. Pulsed lasers were used for UV excitation and time-delayed VUV one-photon ionization of desorbing O_2 molecules. Once ionized, O_2^+ was detected via time-of-flight mass spectroscopy which provided mass identification and allowed for time-delayed pump-probe velocity measurements. Final state velocity distributions of O_2 were determined as a function of substrate temperature and UV excitation energy.

3.2 Experimental Section

The experimental set-up and general procedures were described in section 2.1 of this dissertation and only the procedures unique to the experiments performed in this chapter are given below. The titania sample was prepared at the beginning of each experiment in the following manner. Prior to a thermal or photochemistry measurement, a bulk reduced crystal was sputtered with 500 eV ions while being maintained at a temperature of 300 K for 10 minutes followed by annealing to 850 K for 30 minutes. This provided a clean, reduced TiO_2(110) surface. Annealing to 850 K for 10 minutes between consecutive TPD or photochemistry measurements was done to replenish the defect population in the near surface region since thermal or photo-induced dissociation of adsorbed O_2 will oxidize the sample.

Photo-induced desorption of molecular oxygen was investigated by measuring O_2 velocity distributions as a function of excitation energy and substrate temperature, using a pump-probe TOF-MS technique. A TiO_2(110) surface pre-adsorbed with O_2 was irradiated with either 298 nm, 335 nm, or 359 nm light to induce molecular desorption. For these experiments a photon flux on the order of 10^{13} per cm^2 s was used. No O_2

desorption occurred from a bare TiO_2 surface (not pre-exposed with O_2) unless the photon density was increased by at least two orders of magnitude relative that used in a typical desorption measurement. Additionally, only a small signal was detected when this higher fluence was used. Thus we conclude that no significant contribution of the signal attributed to desorption of pre-adsorbed O_2 was due to ablation of the titania surface. Photodesorbed molecular oxygen was detected by employing a one photon ionization method using coherent VUV radiation (13.1 eV) and TOF-MS. The details of the detection scheme are discussed in section 2.3 of this dissertation.

The raw data for the velocity measurements were collected as a function of delay time (delay curve) between the desorption (pump) and ionization (probe) lasers. Scanning the laser delay is equivalent to scanning the flight time of the neutral oxygen molecules over the fixed distance from the sample surface to the probe laser, 28 mm, and thus equal to scanning the O_2 velocity. In order to improve signal to noise for delay curves, at least three or more measurements were made and averaged together. A second type of measurement (depletion curve) was performed at a fixed delay to measure the rate at which O_2 was depleted from the substrate. An example depletion curve is shown in Figure 3.1 for PSD of O_2 from a TiO_2 substrate at 100 K, an excitation energy of 3.7 eV, and a laser delay of 27 μsec (E_t = 180 meV). Signal intensity for delay measurements was corrected for oxygen depletion from the surface using desorption rates obtained by fitting depletions curves to bi-exponential decay functions (dashed line). The solid line in Figure 3.1 is a single exponential decay and the significance of this decay function discussed in section 3.4.6. Also, due to experimental constraints, the delay measurements that spanned over a broad range of flight times had to be collected in two or three smaller

ranges and then overlapped to normalize their intensities relative to each other. All delay curves were converted to flux distributions by weighting by t^{-1} since laser ionization is a density sensitive detection method. The flight time and distance was used in conjunction with the proper Jacobian to transform the distributions from time-of-flight to velocity and translational energy.

3.3 Results

Figure 3.2 displays a TPD spectrum of D_2O from the TiO_2 crystal face. Three main features are observed, two narrow peaks at 175 K, 270 K, and a broader feature at 500 K. The higher temperature peak is also displayed magnified 10 times for ease of viewing. In agreement with others[37,38], these three features are assigned to water hydrogen bonded to O_{br} atoms, molecularly adsorbed at in-plane Ti^{IV}(5f) atoms, and dissociatively adsorbed at O_{br} vacancies, respectively. By following Perkins et al.[17] the relative areas of the peaks corresponding to water at Ti^{IV}(5f) sites and O_{br} vacancy sites can be used to estimate the oxygen vacancy population. For the data in Figure 3.2, the oxygen vacancy population was 0.06 ML.

A TiO_2 surface exposed to O_2 via a directed doser was characterized by TPD experiments. A typical TPD spectrum obtained in this study of O_2 adsorbed on the reduced TiO_2 surface is given in trace (a) of the upper panel of Figure 3.3. Here, two features are present: a broad peak ranging from 120 to 460 K, and a narrow peak at 400 K. Both of these features have been previously observed by others.[21,39,40] TPD experiments of O_2 adsorbed on oxidized TiO_2 (not shown here for brevity) show that the high temperature state is absent in agreement with studies done by Henderson et al.[21]

The high temperature feature was assigned by Henderson et al. to molecular oxygen associated with a Ti(5f) site that is partially reduced by electron density from an adjacent O_{br} vacancy defect. However, a recent study by Wendt et al. reported that $Ti^{III}(i)$ sites in the near surface region can also provide electron density for molecular adsorption of O_2.[13] These authors further postulate that a charge competition model can explain the temperature dependence of molecular oxygen adsorption and dissociation on TiO_2 observed by Henderson et al. Specifically, the 0.8 eV loss feature observed by Henderson et al. in electron energy loss (EEL) spectra of a reduced TiO_2 sample is consistent with the presence of $Ti^{III}(i)$ defects.

Curve (b) in the upper panel of Figure 3.3 shows a TPD spectrum of a TiO_2 surface which has been exposed first to O_2, and then to photons of 300 ± 20 nm energy using a mercury arc lamp with a monochromator (Oriel Corporation). It is clear upon inspection of Figure 3.3 that while the low temperature feature is essentially unchanged after UV irradiation, the 400 K peak is completely absent after exposure to UV light. Thus, the state(s) that undergo thermal desorption at 400 K contribute to the photon stimulated desorption of molecular oxygen observed in the experiments reported in this dissertation. Similarly, Perkins et al. determine the state of O_2 that thermally desorbs at 400 K is active for PSD at low temperature and that the broad low temperature TPD feature is largely due to O_2 desorbing from their sample holder.[17] Thompson and Yates observed O_2 photodesorption from $TiO_2(110)$ surfaces prepared by two different methods of TiO_2 reduction: one method was to prepared the sample by sputtering and annealing, while the other method involved only annealing the TiO_2 crystal.[40] Samples produced by the former method yielded both low and high temperature peaks in TPD experiments, and

successive O_2 PSD experiments performed without annealing in between measurements exhibited a decrease in desorption yield. Similar results were obtained in this work as well as those presented by Perkins and Herderson.[17] However, the procedure that involved only annealing produced samples which exhibited only the low temperature thermal desorption peak, and successive PSD experiments showed no drop in O_2 yield.[26,32,41] Thompson and Yates suggest the difference in O_2 thermal and photodesorption behavior can be attributed to different degrees of bulk reduction of the sample leading to varying degrees of thermally activated dissociation and molecular desorption.[40] Consistent with this idea, an argument is made in the next section based on our O_2 photodesorption results and existing literature that the 400 K peak of our thermal desorption spectra can likely be attributed to a highly reduced sample containing $Ti^{III}(i)$ defects.

All of the velocity measurements of O_2 photodesorbing from TiO_2 in this study were performed on a crystal that was exposed to 80 L O_2 (1 L = 1×10^{-6} Torr s^{-1}) by backfilling the chamber with O_2 gas. A TPD spectrum obtained after an 80 L exposure is displayed in the lower panel of Figure 3.3, prior to irradiation of the surface with 335 nm light from a pulsed laser system (a), and afterwards (b). Before UV irradiation sharp peaks at 100 K, 155 K, and 400 K appear along with a broad feature that ranges between 120 and 500 K. The very narrow feature at 100 K emerges before an increase in the crystal temperature can be detected (< 1 K) indicating the source of this peak is likely O_2 desorbing from a portion of the sample holder such as the Re/Pt heating element rather then the TiO_2 surface. It is likely that the origin of the 155 K peak is also from the sample holder. This feature is only seen when oxygen exposure occurs by backfilling the

chamber or for large exposures via the directed doser. Comparing oxygen TPD spectra for samples exposed to an approximately equal number of O_2 molecules (equal 400 K peak areas) by the two different dosing methods it was noted that only those experiments in which the surface was prepared by backfilling O_2 contained the 155 K feature, indicating this peak does not correspond to oxygen from the TiO_2 surface. A thermal desorption feature at 145 K has been observed by others, also only when exposing the TiO_2 sample to oxygen by backfilling the chamber. The broad low temperature peak is significantly more intense in the TPD spectra of the lower panel, suggesting that most of the oxygen responsible for this feature is from the sample holder; however it is also present in the TPD results we obtain after directly exposing the sample to O_2, even at the lower coverages. Although the origin of the broad peak is not clear, upon inspection of Figure 3.3 it is obvious that only the state leading to O_2 thermal desorption at 400 K is active for photon stimulated desorption.

Flux corrected distributions of O_2 as a function of laser delay are given in Figure 3.4a for a substrate temperature of 100 K and three different excitation energies of 3.45 eV, 3.70 eV, and 4.16 eV, with the latter two displaced vertically for clarity. The x.axis of the distributions is plotted on a common log scale for ease of viewing the peaks at early times. All three curves are trimodel exhibiting two narrow peaks at 16 μsec and 29 μsec corresponding to "fast" (prompt) desorption channels, and a broad peak at about 120 μsec that tails to long delay times and corresponds to a "slow" desorption channel. In order to obtain mean translational energies for the individual desorption channels, the trimodal distributions in the velocity domain were fit with multiple functions. The fitting procedure and example fits are given in Appendix A of this dissertation.

Velocity distributions of the delay data in panel (a) are presented in panel (b) of Figure 3.4. The velocity distributions of desorbing O_2 molecules peak at three velocities, 175 ms^{-1}, 950 ms^{-1}, 1750 ms^{-1}. Oxygen molecules desorb via the slow channel with an average kinetic energy of 0.016 eV, while O_2 species desorb through the two prompt channels with average kinetic energies of 0.14 eVand 0.54 eV. It is evident upon inspection of Figure 3.4 that over the excitation energy range investigated in this study, there is little difference in the measured velocity distributions of PSD of molecular oxygen.

The velocity distributions for O_2 desorbing from TiO_2 are shown in Figure 3.5 for different sample temperatures. For all of these experiments, oxygen was first dosed at 100 K, and a 4.16 eV excitation energy was used. Oxygen desorption from a sample with a temperature of 100 K (a) has velocity peaks appearing at 175 ms^{-1}, 950 ms^{-1}, and 1750 ms^{-1}, and is the same data that is displayed as the uppermost curve of Figure 3.4. The data from an experiment in which a sample pre-exposed to O_2 at 100 K was flashed to 260 K and subsequently allowed to cool to 100 K prior to exposure to UV light is displayed as trace (b) with three peaks at 200 ms^{-1}, 950 ms^{-1}, and 1750 ms^{-1}. Trace (c) shows the data from an experiment conducted at a sample temperature of 260 K. Three peaks are present in trace (c) at 350 ms^{-1}, 950 ms^{-1}, and 1750 ms^{-1}, corresponding to average energies of 0.042 ± 0.004 eV, 0.18 ± 0.02 eV, and 0.51 ± 0.05 eV respectively. Note the temperature dependence of the slow channel portion of the velocity distributions shifts from an average energy of 0.016 eV at a surface temperature of 100 K to 0.042 eV at a temperature of 260 K. Traces (a) and (b) in which the photoexcitation occurred with a surface temperature of 100 K, show that the slow channel occurs at nearly the same

position, indicating the process responsible for the shift in trace (c) is almost completely reversible. Changes in the prompt desorption channels are less obvious. There is a slight shift in the middle peak to higher $\langle E_t \rangle$, while the state responsible for the most energetic desorption channel remains fixed. Also, the intensity of the middle channel slightly decreases with increasing surface temperature.

3.4 Discussion

3.4.1 Excitation energy dependence

A recent theoretical study by de Lara-Castells et al.[25,36] investigated the possibility of a direct optical excitation mechanism of the adsorbate-substrate bond for O_2 desorption. Specifically, a vertical transition between a strongly bound O_2^- species (ground state) to a loosely bound physisorbed O_2 molecule (excited state) was examined. The authors justified this mechanism based on the magnitude of the calculated dipole moment between the two electronic states, and predicted the maximum desorption probability to occur at a photon energy of about 3.7 eV with an average kinetic energy of 0.12 eV for the ejected neutrals.

For a direct optical excitation mechanism one would expect the translational energy of desorbing molecules to be sensitive to the excitation energy. Photons of increasingly larger energies would excite the adsorbate-substrate complex from the ground state to increasingly larger energies on the repulsive wall of the excited state potential energy surface. As long as the photon energies were large enough to produce an excited complex with a potential energy above the desorption limit, different excitation energies should then lead to different average translational energies for the desorbing

species. Of course, the degree to which the translational energy distribution of a system is sensitive to excitation energy will depend on several factors, including the shape of the excited state PES and the relative equilibrium bond distance to the surface for O_2 in both the ground state and excited state. Given that the Franck-Condon distribution calculated by de Lara-Castells is reasonably narrow, comparing the velocity distributions for PSD of O_2 from TiO_2 at different excitation energies in the region of the predicted transition should be a good test for this model.

The velocity distributions measured in the present study for PSD of O_2 from a TiO_2 substrate at 100 K are trimodal as seen in Figure 3.4. Here, it is shown that the velocity distributions are unchanged for the three photoexcitation energies used. The desorption profile reflects the Franck-Condon distribution and has a maximum at a photon energy of 3.7 eV (middle curve) whereas the predicted probability is very small for 3.45 eV (lower curve) and 4.16 eV (upper curve). The fact that the three velocity distributions display no dependence on excitation energy, argues against desorption by a direct optical excitation mechanism for the energy region investigated.

Given the above arguments, as well as the fact that the onset for PSD of O_2 coincides with the band gap energy for bulk rutile TiO_2 (3.05eV),[26] the results presented here are more consistent with a substrate mediated excitation mechanism then a direct excitation mechanism. It has been suggested that O_2^- photodesorption proceeds via a hole capture mechanism where holes (h) formed in the near surface region by irradiation with photon energies greater than the band gap migrate towards the surface.[26,36] In the vicinity of each other, a photo-generated hole and superoxide anion can undergo charge transfer followed by desorption of the neutral O_2 molecule. Similar hole capture

mechanisms have also been previously proposed for PSD of adsorbed anions on semiconductor surfaces. Two such examples are NO photodesorption from Si(111) 7×7,[42] and CO_2 photodesorption from ZnO.[43] Thompson et al. developed a kinetic model for O_2 PSD from TiO_2(110) surfaces based on a hole capture mechanism to explain their observed desorption yield dependence on the square root of the incident photon flux.[34] Consistent with this proposed hole capture model, the initial yield of all three desorption channels observed in the measurements presented here, also depend on the square root of the photon flux.

3.4.2 Origin of the slow desorption channel (thermal)

Figure 3.5 displays the velocity distributions for PSD of O_2 from a reduced TiO_2(110) surface at substrate temperatures of 100 Kand 260 K (traces a and c). Upon comparison of these two curves, it is apparent that the two prompt desorption channels do not significantly shift with increasing substrate temperature. The relative intensities of the prompt channels slightly change with the middle velocity peak decreasing relative to the other prompt desorption feature, perhaps due to a modification of the relative number of different adsorbed states of O_2 as the sample temperature increases. An argument is made below that two different adsorption states of O_2 account for desorption via the two prompt channels. In contrast to the prompt desorption channels, the slow channel undergoes a dramatic shift towards higher velocity with increasing substrate temperature. Another photodesorption experiment (not shown here for brevity) was performed with a sample temperature of 200 K and is consistent with a trend of increasing mean velocity for the slow desorption channel with increasing substrate temperature. The mean

translational energies of O_2 desorption via the slow channel for substrate temperatures of 100 K, 200 K, and 260 K are 16 meV, 31 meV, and 42 meV respectively. The slow desorption channel portion of the velocity distribution shown in trace (b) compares well with that observed for O_2 desorption from a substrate at 100 K, trace (a). Thus, the shift to increasing velocity with increasing substrate temperature for O_2 desorption via the slow channel is reversible. The behavior of the slow desorption channel (low mean translational energies and the dependence on sample temperature) is consistent with a thermal desorption mechanism. The mean translational energy for a flux of gas molecules (in equilibrium) moving though an arbitrary area is described by an average energy given by 2kT, where k is the Boltzmann constant.[44] This expression describes the kinetic energy of molecules striking a surface, and the same expression can be applied for molecules leaving a surface since it describes a gas in thermal equilibrium. The flux $\mathbf{<}E_t\mathbf{>}$ for a gas at 100 K, 200 K, and 260 K are 17 meV, 35 meV, and 45 meV respectively. Thus, the measured kinetic energy distributions for O_2 desorbing by way of the slow channel are reasonably described by a thermal distribution. This is shown graphically in Figure 3.6, which displays plots of the velocity distributions for two different substrate temperatures along with Boltzmann distributions for molecules desorbing from a surface at the corresponding temperatures.

It should be noted that the geometric arrangement of the TiO_2 sample and the TOF-MS precludes detection of desorbing species with angles greater then 40º from the surface normal. Molecules that desorb more slowly are defocused, meaning they have a broader desorption angle profile. The cause of this arises from thermal motions parallel to the surface which have a greater influence on the desorption angle of slower molecules

leaving the surface. Thus, the slower molecules will be detected with a lower probability. Consequently, the velocity distributions measured here slightly overestimate the true velocity distributions. It is likely this only significantly affects the slowest channel since the mean translational energies of molecules desorbing via the prompt channels are much larger relative to the thermal energy of the surface. The true mean translational energy distributions for the slow channel are then likely to be slightly lower than the measured distributions reported here. PSD of O_2 via the slow channel is consistent with a mechanism in which the O_2 is trapped momentarily on the surface in a physisorption well prior to desorption. This allows energy transfer via collisions between O_2 and the surface to obtain $\langle E_t \rangle$ for desorbing oxygen that is close to the energy of a gas in equilibrium with the substrate. As indicated by the sub-thermal velocity distributions for the slow channel, the lifetime of the oxygen species on the surface after interfacial charge transfer is obviously not long enough for O_2 to come into equilibrium with the sample surface.

3.4.3 Origin of prompt desorption channels (dynamical loss)

All of the measured velocity distributions in this study indicate the existence of three different channels for photo-induced desorption of O_2 from TiO_2(110) surfaces. In order to explain the origin of the multiple desorption channels, only the two prompt channels will be examined since the velocity measurements can only yield direct information on the state of the system immediately before the final O_2 state (transition state). Therefore, oxygen that is trapped on the surface may have originally been excited equivalently to one or both of the prompt channels, prior to being trapped.

We first consider the case where molecular oxygen that is ejected from the surface exists in a single initial state. In this case the observation of multiple peaks in the velocity distributions must be attributed to a fraction of the desorbing O_2 molecules undergoing a dynamical energy loss prior to leaving the surface. Here, a dynamical loss refers to an energy loss in addition to expenditure of energy to overcome the binding energy and any adsorption barrier. A desorbing species may typically lose energy due to an excitation of a intramolecular vibration, surface phonon, adsorbate-substrate bond vibration, or a conversion of O_2 spin states. The desorption channel corresponding to the highest translational energy for molecules leaving the surface would be due to O_2 molecules which undergo no dynamical energy loss.

A close examination of the two prompt desorption channels argues against a dynamical energy loss as the source of multiple channels. First, let us consider the intramolecular O_2 vibration. The fundamental vibration of the free O_2 molecule has a frequency corresponding to about 193 meV,[45] significantly lower than the mean energy difference between the two prompt desorption channels reported here (400 meV). Although, the O_2 vibrational frequency is likely to be altered upon adsorption on the reduced TiO_2 surface, at least two different theoretical studies predict a lengthening of the O–O bond from its gas phase equilibrium position,[29,30] indicating a weaker bond and thus a lower vibrational frequency. Based on these findings, it seems unlikely that the excitation of an intramolecular O_2 vibration is responsible for the observation of multiple peaks in the velocity distributions. Secondly, excitation of a surface phonon mode may lead to a loss in energy for desorbing O_2 molecules. Rocker et al. examined vibrations of a thermally reduced TiO_2(110) sample and observed three fundamental surface optical-

phonons modes ν_1, ν_2, and ν_3, corresponding to energies of 54 meV, 95 meV, and 46 meV, respectively.[46] Again, the energies reported here are too low to account for the observed difference in translational energy for the two prompt desorption channels shown in Figures 3.4 and 3.5. Thirdly, energy transfer to an excitation of an adsorbate-substrate vibration is examined. The O_2 bond to the TiO_2 substrate is likely significantly weaker then the O=O bond in the free molecule which as stated above is too weak to account for a loss equal to the energy difference observed in these experiments (400 meV). In fact, binding energies for a variety of spin states, geometric arrangements, and adsorption sites for O_2 molecules bonded to a TiO_2 surface containing O_{br} vacancies have been calculated, and the highest value reported was 3.61 eV.[25,29-31] The zero point dissociation energy of the free O_2 molecule is 5.08 eV.[45] Given the relative strengths of these two bonds and the larger reduced mass for the O_2-substrate system versus the free molecule, the frequency for adsorbate-substrate vibration will likely be less then the O_2 intramolecular vibration. Since the O_2 intramolecular vibrational frequency was not large enough to account for the observed difference between the prompt channels, an adsorbate-substrate vibration can be ruled out as a loss mechanism. Finally, conversion of the spin state of the desorbing oxygen is considered as a mechanism for the observed energy difference between the two prompt channels. If the O_2 triplet and singlet PES partially overlap, then it is possible that some of the desorbing O_2 experience intersystem crossing, and then the two prompt desorption channels correspond to products with different spin states. If this were true, their translational energies would differ by 0.977 eV (ν_{00} between the $^3\Sigma_g^-$ and $^1\Delta_g$ states of the free molecule). This result is obviously too large to account for the energy

difference of the prompt channels. Thus it seems unlikely that a dynamical energy loss could explain the observation of multiple peaks in the velocity distributions.

3.4.4 Initial oxygen states on TiO_2(110)

Given the above arguments, the multiple features in the measured distributions can likely be attributed to different initial states for oxygen adsorbed on the TiO_2(110) surface. An ideal TiO_2(110) stoichiometric surface contains a single form of exposed Ti^{IV} atoms that are fivefold-coordinated, Ti^{IV}(5f).[1] Upon the introduction of bridging oxygen vacancies, a second type of Ti atom is exposed which has been proposed to be in the + 3 oxidation state. It is well known that O_2 dissociates at these bridging vacancy sites, in effect "healing" the vacancy and leaving an O adatom on a nearby Ti(5f) cation.[1] However, it is not known to what extent the dissociation is activated. While both theoretical and experimental studies suggest O_2 at vacancies exists intact in the molecular form at 120 K,[21,25,26,29-33,36,41] a more recent scanning tunneling microscopy (STM) study show that oxygen dissociates at vacancy sites at this temperature.[13] The authors suggest that sub-surface Ti^{III}(*i*) defects are responsible for molecular oxygen adsorption, and the thermal desorption peak at 400 K. In agreement with their findings, a two-photon photoemission study by Onda and Petek suggests two different defect states can exist at the reduced TiO_2 interface, one at the surface, likely O_{br} vacancies, and the other in the sub-surface region, likely Ti^{III}(*i*).[22] In this study by Onda and Petek, surface defects were shown to be healed upon O_2 exposure at 100 K while oxidation of the sub-surface defects required heating in the presence of adsorbed O_2. The extent to which each of these defect states formed was dependent on the sample preparation method. The two prompt

channels in the velocity distributions reported in this dissertation for substrate temperatures of 100 K or 260 K are essentially the same. At 260 K there is general agreement in the literature that O_2^- dissociates at the vacancies, thus we conclude that for the experiments reported here, the vacancies are "healed" even at 100 K. Based on the above arguments, the possibility of photo-induced desorption of O_2 from the O_{br} vacancy sites is ruled out.

Of course, a real (110) TiO_2 surface will also contain extended defects such as steps along the <001> or <1$\bar{1}$1> directions as previously observed in STM images by Diebold et al.[47] Some of the Ti and O surface atoms at the steps are in lower coordination states then terrace atoms, perhaps increasing their chemical reactivity. It was determined that the surface consisted of terraces about 100 Å wide, which would lead to a low percentage of atoms occurring at steps. It is possible that oxygen desorption from O_2 initially bond at different extended defects such as steps is the source for multiple adsorption sites. However, given that adsorption of O_2 amounts to about three times the O_{br} vacancy concentration (about 20% a monolayer in the present experiments), it is unlikely such extended defect sites are numerous enough to be the source of the photodesorbed O_2.

In addition to different binding sites, other initial states for O_2 on titanium dioxide may be due to different chemical species such as O_2^- or O_2^{2-}, adsorption geometries, or spin states. A variety of different stable binding geometries and spin states have been proposed by theoretical studies.[25,29-31] As discussed above, singlet O_2 and triplet O_2 will differ by a potential energy of 0.982 eV at infinite distance from the surface. Thus if they desorb through the same transition state their translational energy would differ by this

amount assuming the desorbing oxygen are not vibrationally excited. Therefore, we have ruled out a dynamical loss by this mechanism. However, if O_2 is initially present on the substrate in two different spin states, each of these species may desorb via different transition states. Since the experiments reported here probe the energy difference between transition states and final states, singlet and triplet O_2 desorbing through different intermediate states may differ in translational energy by more or less than the difference in potential energy of the free O_2 species (0.983 eV). Consequently, one can not rule out this desorption pathway as an explanation for the observed multiple peaks in the velocity distributions.

As a result of the above arguments, we believe the transfer of electrons associated with $Ti^{III}(i)$ defect states leads to at least two different initial adsorbed O_2 states active for PSD. Both initial adsorption states of O_2 thermally desorb at 400 K, or perhaps one desorbs while the other dissociates on the surface upon thermal activation. Although, we have discussed several different types of initial states arising from varying adsorption sites, geometries, amounts of charge transfer, and spin states of adsorbates, the measurements reported here can not distinguish between them.

3.4.5 Model for desorption

A reaction mechanism for the overall photodesorption process is proposed here and is represented by the following expressions. Also, Figure 3.7 qualitatively shows the potential energy of the O_2/TiO_2 system throughout the reaction progress.

$$TiO_2 + h\nu \rightarrow e_{CB} + h_{VB} \quad (3.1)$$

$$O_2^-(a) + h_{VB} \rightarrow O_2^*(a) \quad (3.2)$$

$$O_2^*(a) \rightarrow O_2^*(g) \quad (3.3a)$$

$$O_2^*(a) \rightarrow O_2(g) + \text{heat} \quad (3.3b)$$

Initially O_2 is chemisorbed on the surface in at least two different states, and negatively charged after undergoing charge transfer with defect states within the forbidden band. Both theory and experiments have proposed the electrons that undergo charge transfer in the adsorption process are initially associated with Ti*3d* defect states corresponding to a O_{br} vacancy, $Ti^{III}(i)$, or Ti^{III} sub-surface lattice site.[13,48,49] Recent studies suggest $Ti^{III}(i)$ or sub-surface lattice atoms provide the electron density that is transferred to O_2 at 100 K[13,22] The first step in the desorption process is the formation of electron-hole pairs in the near surface region upon irradiation of the sample with UV light above the band gap energy. Chemisorbed O_2^- in the vicinity of a newly photo-generated hole creates a highly energetic transition state (TS1) resulting from Coulombic attraction between the separated charges. As shown in Figure 3.7, O_2 desorption from a chemisorption state (CS) via this transition state creates a barrier to desorption which is overcome with photons of sufficient energy to generate e/h pairs. In the second step O_2^-(a) is neutralized by a photo-generated hole. It is postulated that the electron transfer occurs on a much shorter time scale than the nuclear motion, and can be considered to occur via a vertical transition. Thus after charge transfer, oxygen remains in a highly energetic state (O^*_2(a), TS2) on the repulsive wall of the neutral molecule-substrate PES. Excited oxygen molecules proceed to desorb by one of two channels. Step 3.3a represents prompt desorption of energetic oxygen upon charge transfer, with the O_2* ejected from the surface translationally hot. The maximum kinetic energy (MKE) is shown schematically in Figure 3.7 as being the difference between the potential energy of

TS2 and the final state (FS) of gas phase O_2. The lack of evidence for O_2 undergoing a vibrational energy loss argues in favor of O_2 coming off vibrationally cold and for the FS to be at the potential energy of the asymptotic limit of the neutral molecule-substrate PES. According to our model the two prompt desorption channels observed in our velocity measurements correspond to two initial oxygen adsorption states being ejected from the surface translationally hot (equation 3.3a). Finally, equation 3.3b represents the second pathway for desorption, in which the highly energetic intermediate undergoes relaxation via collisions with the surface and is momentarily trapped in a physisorption well. A physisorption state (PS) for O_2 on stoichiometric TiO_2(110) surfaces has been observed in previously TPD studies.[20] Given that the O_2 thermal desorption peak in the aforementioned study was observed between about 60 Kand 70 K, physisorbed O_2 will have a short lifetime on a surface at a substrate temperature of 100 K. At the temperatures used in this study, physisorbed oxygen likely enters the gas phase before coming into equilibrium with the substrate, thus explaining the observed non-Boltzmann like velocity distributions and sub-thermal mean translational energies for the slow channel.

3.4.6 Connection with previous studies

Several early reports by the Yates research group concerning the PSD of O_2^- from TiO_2(110) single crystal surfaces modeled the O_2 desorption kinetics using bi-exponential functions.[33] They suggested that the reaction was first order in O_2^-(a) coverage and two initial O_2 adsorption states had two different desorption cross sections, hence giving rise to the observed bi-exponential kinetic behavior. More recently, the

same research group further investigated PSD of O_2^- from TiO_2 and determined that the desorption kinetics were better explained by mechanism in which a single O_2^-(a) state desorbed, and the e/h recombination rate is coverage dependant.[35] Despite the difference in thermal desorption behavior (whether or not the 400 K peak is observed), PSD of O_2 followed similar kinetic behavior in the present study as that observed by the Yates group. Both studies found that the O_2^- desorption kinetics are not described well by a single exponential decay. Although the velocity distributions reported here are consistent with multiple adsorption states of O_2, the non-exponential kinetic behavior is not directly linked to the occurrence of multiple O_2 states. For instance, if multiple adsorption states justified the apparent non-first order rate, then O_2 desorbing via each of the individual prompt channels that are attributed to initial adsorption states would each follow an exponential decay. However in the measurements reported here, the evolution of O_2 during irradiation of the sample was monitored for each individual laser delay that corresponded to a single peak velocity. All of the decay curves followed similar behavior, and did not follow exponential kinetics. Thus, the O_2 desorption cross sections for both initial states likely depend on oxygen coverage in a manner other then first order.

To offer a possible explanation for this sort of coverage dependence, we turn to the behavior of photo-generated charge carriers in TiO_2. A recent EPR spectroscopy study by Berger et al. has demonstrated that adsorption of molecular oxygen as O_2^- on stoichiometric anatase particles increases the lifetime of holes by trapping a portion of the photo-generated electrons and that this charge separation is stable up to about 300 K.[12] It may be that as O_2^- desorbs from the surface, the enhanced lifetime of the holes due to charge trapping is reduced. Such a mechanism would increase the e/h recombination rate

in a manner that is dependant upon the oxygen coverage, leading to a desorption rate that is not well characterized by an exponential decay.

Additionally, the e/h recombination rates may also explain the temperature dependence of the observed kinetic behavior. Studies by the Yates group on the PSD of molecular oxygen from TiO_2(110) single crystal surfaces measured the rate of O_2 photodesorption for substrate temperatures between 100 to 300 K.[26,32,41] The cross section for O_2 PSD increased irreversibly with substrate temperature. Also, O_2 co-adsorbed with CO on TiO_2 underwent desorption upon irradiation with UV light concurrent with a minor channel of CO oxidation and desorption of CO_2 with an equal desorption cross section. The CO_2 yield decreased with increasing temperature and approached zero at 300 K.[41] The temperature dependence of the rates for PSD of O_2 and photon-induced oxidation and desorption of CO_2 were reproduced in experiments conducted in our laboratory. In contrast to the desorption rates, the velocity distributions do not exhibit an irreversible change with respect to temperature. This is consistent with the O_2^- desorption rate increasing without a significant change in the initial O_2^-(a) states upon annealing to 260 K. The temperature dependence of the rate and velocity measurements may be explained by an increase in the lifetime of the photo-generated hole in the near surface region due to annealing the O_2^-/TiO_2. An activated O_2 dissociation channel that operates near 300 K requires more electronic charge transfer from the substrate then O_2 adsorption, thus the electronic charge available for e/h recombination is diminished.[13] Based on this activated dissociation channel, one may expect the lifetime of photo-generated holes at the interface to increase upon annealing to temperatures high enough to open this channel, which in turn would increase the rate of

hole capture by adsorbed O_2^- species without necessarily altering the initial O_2^- adsorption states. Thus it may be oxygen that dissociates and therefore not detected in these experiments that is responsible for the above mentioned thermal dependence. The reduction in the reactivity of CO may be attributed to a kinetic effect. The lifetime of O_2^- on the surface may be too short after activated O_2 dissociation occurs to allow for a detectable amount of CO to be oxidized.

An alternative rationalization of the data is that the O_2 adsorption states are altered upon thermal activation to create a state of molecular oxygen that has a high rate of desorption and is inert towards CO oxidation.[26,32] However it is likely that different initial adsorption states will desorb from the surface by means of different transition states therefore annealing the O_2/TiO_2 system should induce an irreversible change in the mean translational energies of either or both of the prompt desorption channels. This was not observed in the present study.

3.5 Summary

The PSD of molecular oxygen from single crystal $TiO_2(110)$ surfaces pre-adsorbed with O_2 was investigated and final state velocity distributions of the desorbing O_2 were obtained as a function of excitation energy and substrate temperature. Velocity distributions were determined by a pump-probe technique that used pulsed lasers for UV excitation and time-delayed one photon VUV ionization in conjunction with TOF mass spectroscopy for detection. The results are consistent with a substrate mediated excitation mechanism, with no evidence for a theoretically predicted direct adsorbate-oxide excitation mechanism[36] over the excitation energy range studied (3.45 to

4.16 eV). Molecular oxygen desorption occurs via multiple channels believed to be attributed to at least two initial O_2 adsorption states on the titania surface. It was found that roughly half of the oxygen molecules become momentarily trapped in a physisorption state prior to desorption and come off the surface with a mean translational energy almost equal to the thermal energy available from the substrate (about 2kT).

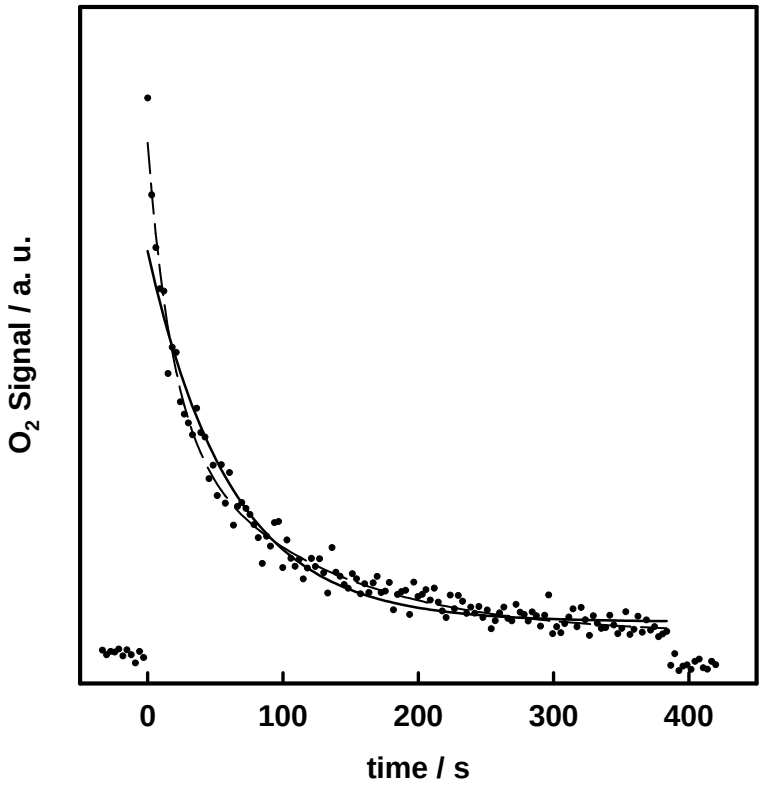

Figure 3.1: Photodesorption signal for mass 32 as a function of time exposed to 335 nm UV radiation at a laser delay of 27 μsec and a substrate temperature of 100 K. Time zero corresponds to the introduction of the UV light. Filled circles are data points, solid line and dashed line are an exponential fit and a bi-exponential fit to the data respectively.

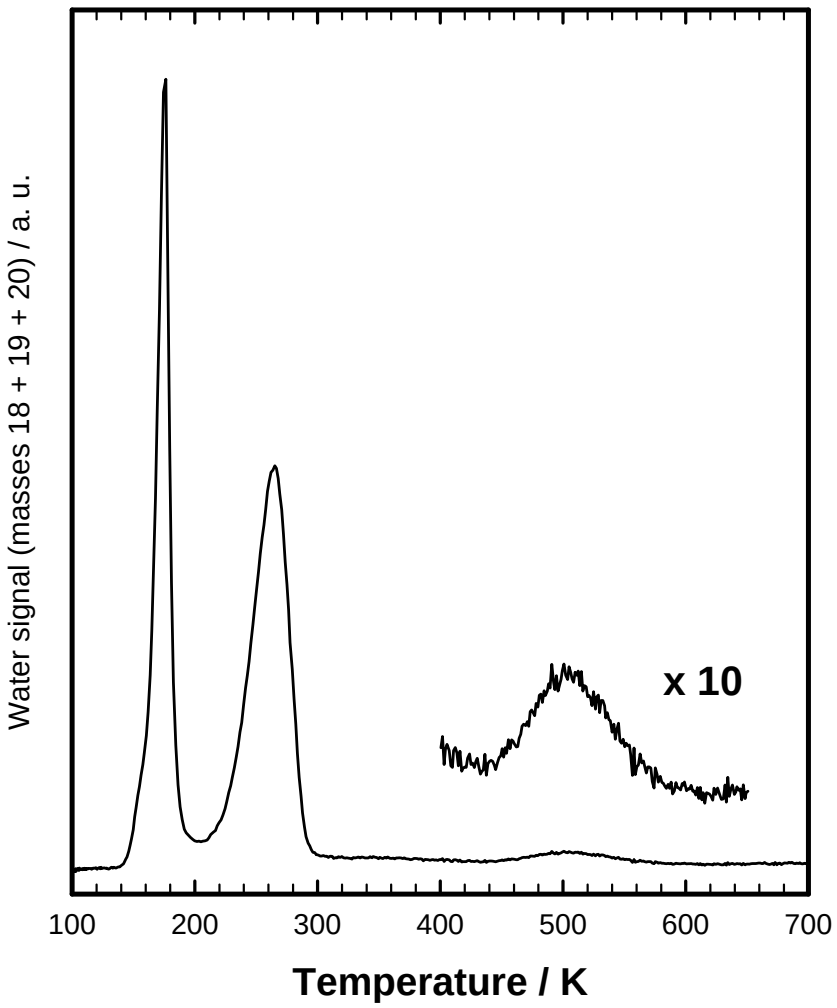

Figure 3.2: Water TPD spectrum for about 1 ML coverage of water adsorbed via a directional doser on a reduced TiO_2(110) surface at about 100 K. Masses 18, 19 and 20 were all summed to give the solid trace presented here.

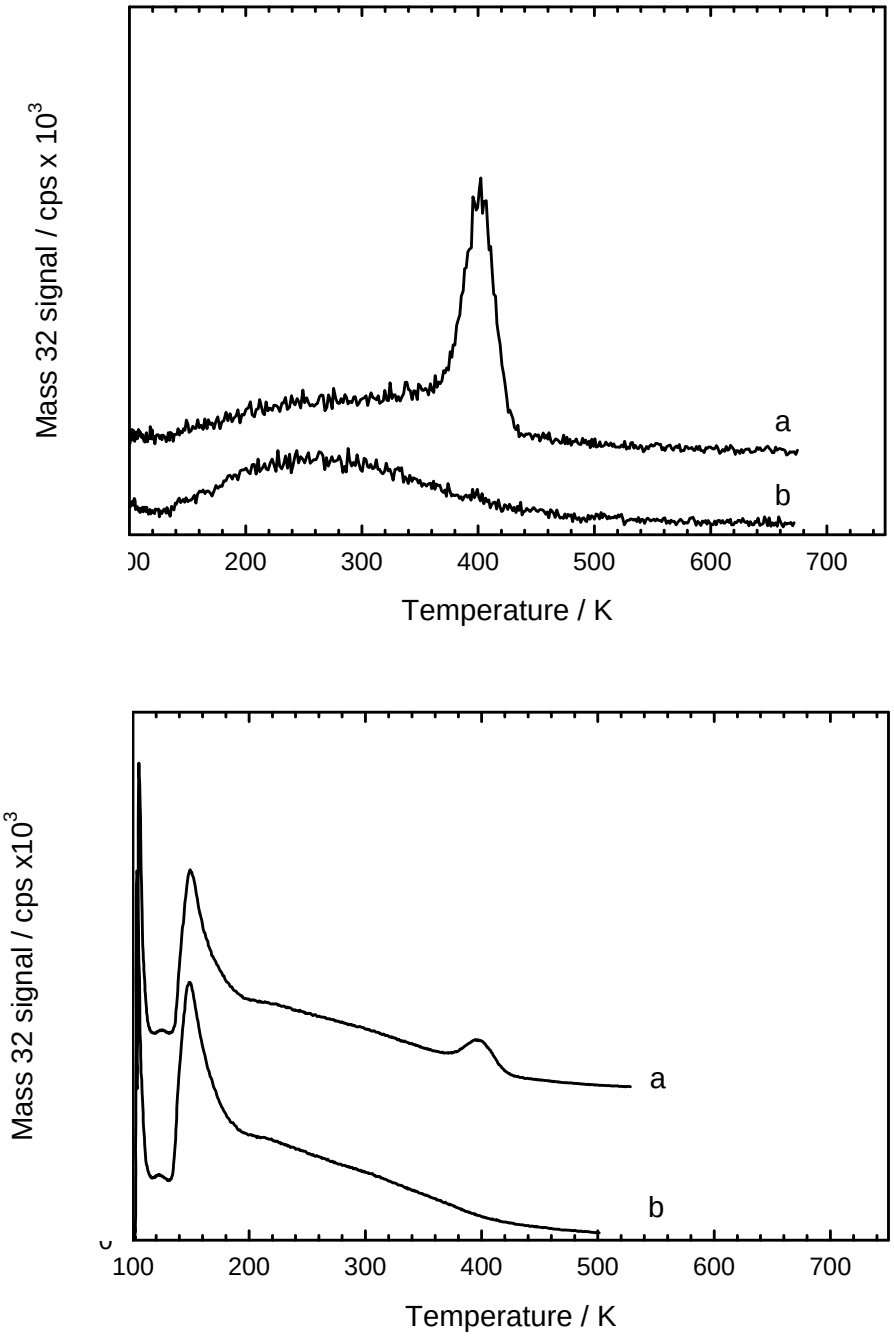

Figure 3.3: Oxygen TPD spectra (m/e = 32) from a reduced TiO_2(110) surface pre-exposed with O_2 at 100 K via a directional doser (*upper panel*), or backfilling the chamber (*lower panel*). Curve (a) was obtained in the dark and (b) collected after UV irradiation of the adsorbate-oxide interface with photons of supra-band gap energy at a substrate temperature of 100 K.

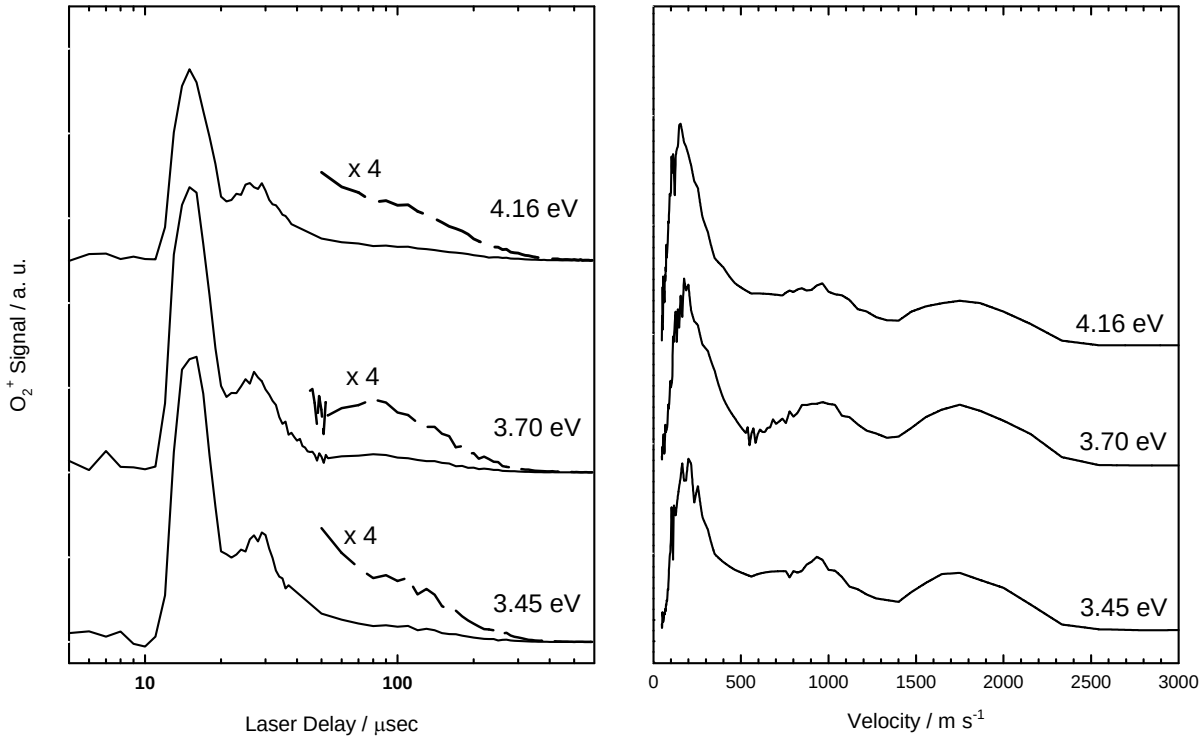

Figure 3.4: *Left panel*: Photodesorption of O_2 from a reduced TiO_2(110) surface pre-exposed to 80 L at 100 K as a function of laser delay and excitation energy. The data shown here has been flux corrected as well as corrected for depletion of oxygen coverage. *Right panel:* Velocity distributions of O_2 PSD as a function of excitation energy. Velocity distributions were obtained by transforming the data shown in the left panel.

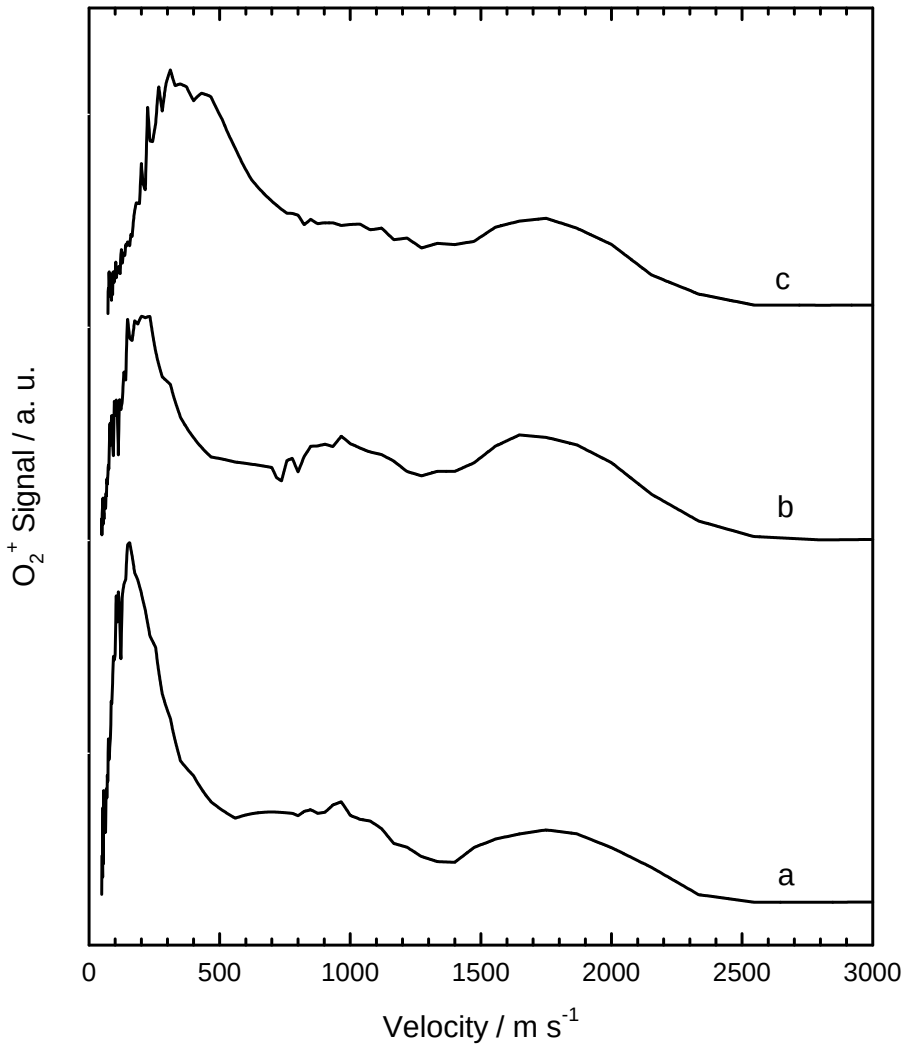

Figure 3.5: Velocity distributions of O_2 PSD from a reduced $TiO_2(110)$ surface pre-exposed to 80 L at 100 K. The excitation energy used was 4.16 eV (298 nm). Trace (a) photodesorption at a substrate temperature of 100 K, (b) O_2 adlayer flashed to 260 K and photodesorption induced at substrate temperature of 100 K, (c) photodesorption at a substrate temperature of 260 K.

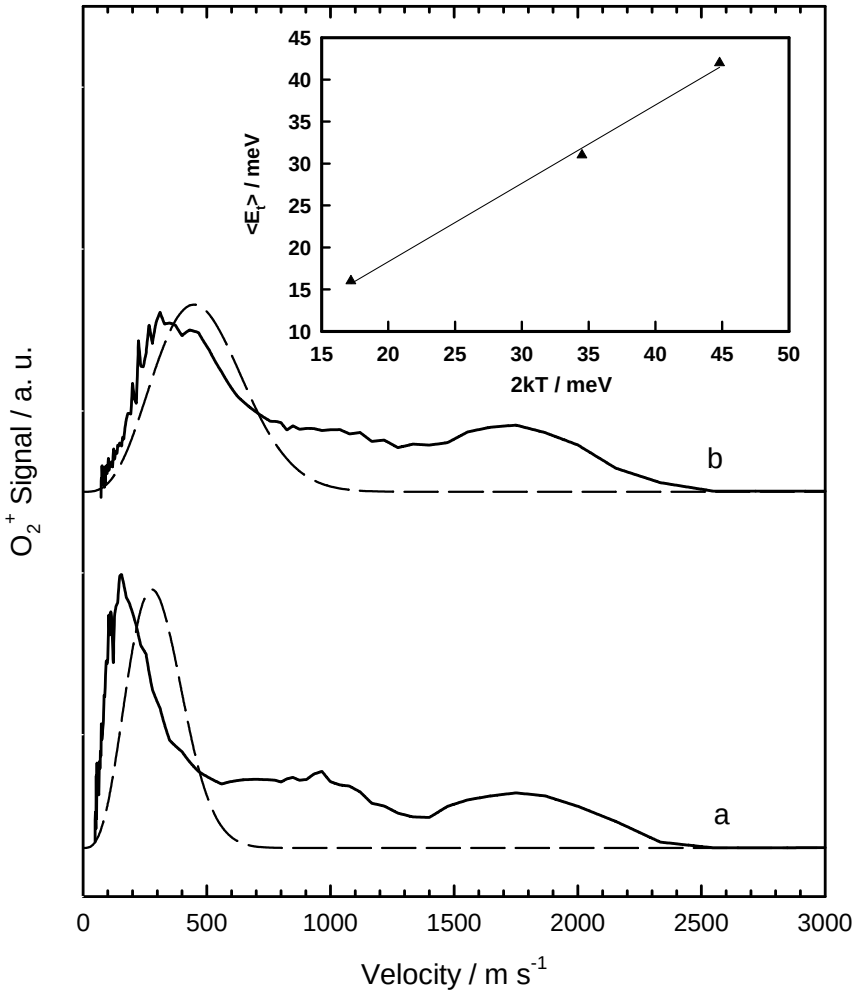

Figure 3.6: Velocity distributions of O_2 PSD from a reduced TiO_2(110) surface pre-exposed to 80 L of O_2 at 100 K. The excitation energy used was 4.16 eV (298 nm). Photodesorption was measured at substrate temperatures of (a) 100 K and (b) 260 K. Solid lines correspond to the flux and depletion corrected experimental data. Dashed lines are Boltzmann distributions for temperatures of (a) 100 K and (b) 260 K. Inset shows a plot of the mean translational energies of the slow channel as a function of substrate temperature. The velocity distribution for the middle point not shown here.

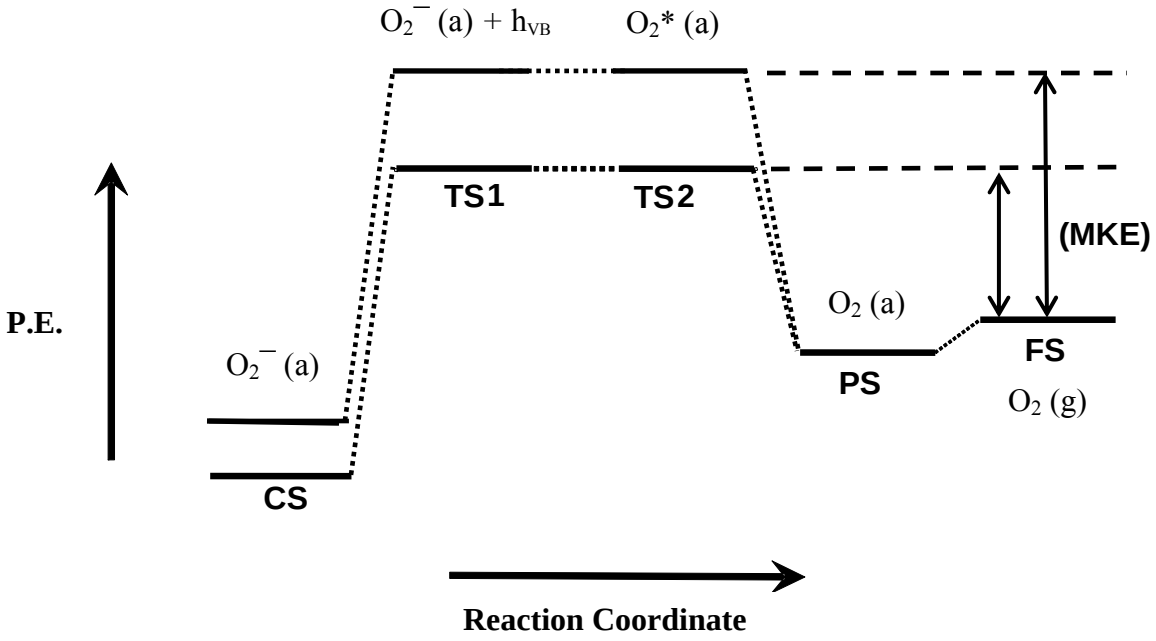

Figure 3.7: A qualitative representation of the potential energy as a function of reaction progress. CS: chemisorption state, TS1 and TS2: first and second transition states, PS: physisorption state, FS: final state, MKE: maximum kinetic energy.

4. Photodecomposition of Acetone and 2-Butanone on TiO_2(110) Surfaces

This section is to be published.

4.1 Introduction

There is a great deal of interest in utilizing titania as a photocatalyst to oxidize organic pollutants in wastewater or air to less harmful species, or to create self-cleaning surfaces. Typically, photooxidation reactions of organics on titania have many branching pathways, and have a interdependence on water and oxygen coverage.[50] We consider acetone photodecomposition on TiO_2 since it is of practical importance given that it is a common solvent and an indoor air pollutant. It also serves as a model for interactions of organic molecules containing carbonyl functional groups on TiO_2. The vast majority of previous studies on acetone photooxidation have been on high surface area substrates such as powders or pellets, with a focus on either evaluating different catalyst or catalyst preparation methods, or on the kinetics of the overall oxidation to CO_2.[16] Taken collectively, the several investigations that have identified multiple substrate bound reaction intermediates in the photodegradation of acetone on TiO_2 demonstrating the complexity of the overall reaction. For instance, the peroxy species $CH_3(CO)CH_2OO\cdot$,[51] as well as acetate, formate, acetaldehyde, and formaldehyde,[52] and a few dimerized acetone species[53] have all been postulated based on data from either EPR,[51] FTIR,[52] or NMR[53] spectroscopy probes. Far fewer studies of photooxidation of 2-butanone over titania have been done, but butanone is also a typical molecule of indoor air pollution.[54]

Mechanistic studies performed on single crystal surfaces and under UHV conditions greatly simplify the reaction system by providing a well defined substrate, and

better control over the ketone, oxygen, and water concentrations. The conditions employed in investigations of this type are quite different from when high surface area and highly defective substrates, or higher pressure conditions are used as in most applications. However, the relevance of investigations using UHV and single crystals in these photooxidation processes has been demonstrated by the similarities of some of the radical intermediates identified with those found when powders are employed.[16] Henderson has studied photooxidation of acetone[16,55] and 2-butanone[50] on single crystal TiO_2(110) surfaces by PSD and post-irradiation TPD with focus on identifying the primary reaction steps. In that work, a cw excitation source with a broad wavelength range (UV lamp) was used, and products were detected with electron impact mass spectroscopy. Decomposition of ketones on TiO_2 required adsorbed O_2 and thus defective (reduced) surfaces created by vacuum annealing were employed. It was determined that the two ketones are not active for photodegradation on the bare TiO_2, and co-adsorbed O_2 was required to activate a photoreaction. Also, the ketones followed similar reaction mechanisms which involve two main steps. It was proposed that first step involved the formation of a thermally activated ketone-oxygen complex between temperatures of 150 K and 250 K that is photoactive and has a diolate structure. Subsequent absorption of photons by the substrate produces charge carriers which initiate α-cleavage (breaking of a carbonyl carbon-carbon bond) yielding a surface bound carboxylate and ejection of a gas phase alkyl radical. For the case of acetone photodecomposition the mechanism is represented by the following equations,

$$\eta^1\text{-acetone} + O^* \rightarrow \text{acetone-oxygen complex (diolate)} \quad (4.1)$$

$$\text{acetone-oxygen complex} + h\nu \rightarrow CH_3\bullet\,(g) + CH_3COO\,(a) \quad (4.2)$$

where O* is an active oxygen species. Butanone differs from acetone in that a methyl group is substituted with an ethyl group and the asymmetry of the molecule allows for the possibility of different α-cleavages to occur. Interestingly, butanone photodecomposition liberated almost exclusively ethyl radical, with very little signal for methyl despite the similar bond energies for the two possible α-cleavages. Also, in the case of acetone, methyl radical is ejected into the vacuum with no further reaction, where as it was suggested with butanone, ethyl radicals are formed and undergo secondary chemistry at the interface to produce other C_2 species (ethane and ethylene).

In this chapter, investigations focusing on the reaction dynamics of the photo-initiated decomposition of acetone and 2-butanone on single crystal TiO_2(110) surfaces is presented. For these studies, TOF mass spectra and post-irradiation TPD were employed for identification of products formed in the primary photooxidation channels. The same pump-probe, TOF techniques were used as in the O_2 photodesorption study presented in Chapter 3 to determine final state velocity distributions of the desorbing alkyl radical species. Also, adlayers of O_2 on TiO_2 were prepared in different manners to shed light on the identity and role of the oxygen species involved in the organic photooxidation reactions. Again, pulsed lasers were employed for a well defined UV excitation source with a narrow bandwidth. Throughout the discussion section of this chapter future experiments using the current methods are suggested where they may aid in clarifying parts of the reaction mechanism.

4.2 Experimental Section

The experimental set-up and general procedures used in this study were described in section 2.1 of this dissertation and only the procedures unique to the experiments performed in this chapter are given below. At the beginning of each experiment, prior to a thermal or photochemistry measurement, the bulk reduced crystal was cleaning by the following procedure. The TiO_2 sample was maintained at a temperature of 300 K and sputtered with 500 eV Ne^+ ions for 10 minutes, annealed to 850 K in vacuum for 30 minutes, and subsequently annealed at 850 K in the presence of O_2 gas (2×10^{-6} Torr). Defects states ($Ti^{III}(i)$, O_{br} vacancies) were introduced into the near surface region by annealing to 850 K for 10 minutes. A 10 minute anneal in vacuum at 850 K was also performed between consecutive TPD or photochemistry measurements in order to replenish the defect population since adsorbed O_2 plus heat or UV radiation will oxidize the sample surface.

In the investigation of the photodecomposition of ketones on TiO_2, the reduced sample was first exposed to molecular oxygen by backfilling the chamber followed by exposure to the ketone to be studied via a directional doser at a substrate temperature of 100 K. Chemistry at the adsorbate-oxide interface was induced by irradiating the sample surface with pulsed UV laser radiation of 3.7 eV (335 nm) energy with a typical photon flux of 10^{13} cm^{-2} s^{-1} in butanone experiments and 10^{14} cm^{-2} s^{-1} in acetone experiments. Species ejected from the adsorbate-oxide interface upon UV excitation of the sample surface were detected by non-resonant one photon ionization using coherent VUV radiation and TOF-MS. Measurements of the photodecomposition of acetone on TiO_2 utilized a photon energy of 13.1 eV (94.74 nm) for ionization of desorbed products. For

measurements of butanone photodecomposition products, two different photon energies for ionization of desorbates were used in order to aid in product identification, 13.1 eV (94.74 nm) and 10.8 eV (114.42 nm). The methods for generation of VUV radiation are discussed in section 2.3 of this dissertation.

As in the study of PSD of O_2 discussed in the previous chapter, the raw data for the velocity measurements were collected as a function of delay time between the excitation laser and ionization laser, thus measuring the flight time of species ejected from the surface over a fixed distance of 28 mm. In order to improve signal to noise for delay curves, at least three or more measurements were made for each curve and averaged together. A second type of measurement (depletion curve) was performed at a fixed delay to measure the decrease of desorbate yield as a function of time due to consumption of reactants on the surface. Signal intensities for delay measurements were corrected for the decrease of reactant coverage by using depletion rates obtained from fits of depletions data to bi-exponential decay functions. Similar to O_2 PSD, most of the depletion measurements for ketone photooxidation were not well described by a single exponential decay function. Due to experimental constraints, the delay measurements for acetone photodecomposition were collected in two laser delay ranges and then overlapped to normalize their intensities. All delay curves were converted to flux distributions by weighting by t^{-1} to correct for laser ionization being a density sensitive detection method. The flight time and distance was used with the relevant Jacobian to transform the data to the velocity distribution and then further converted to the translational energy distribution.

4.3 Results

4.3.1 Acetone on reduced TiO_2

Acetone thermal desorption from reduced TiO_2(110) surfaces has been extensively investigated by Henderson.[56] Thus, in the current study, acetone TPD measurements are primarily used to characterize the acetone coverage and to identify surface bound photo-generated products by comparison of TPD spectra of the acetone-oxygen adlayer obtained in the dark to post-irradiated TPD spectra. According to Henderson, acetone desorbs around 345 K at low coverage. The leading edge of the acetone temperature profile shifts to lower temperature with increasing coverage due to acetone-acetone repulsions becoming more prevalent and weakening the acetone-Ti^{IV}(5f) bond (acetone is believed to be coordinated to Ti^{IV} sites through O lone pair electrons in a η^1 configuration).[56] The narrow feature at 125 K does not saturate with increasing exposure to acetone and was assigned to multilayer acetone. Thermal desorption spectra of acetone on a reduced TiO_2(110) surface are displayed in Figure 4.1. The directed doser used in our study was not calibrated, but an estimate of the acetone coverage was made by comparison of our data to TPD curves of known acetone coverage previously reported by Henderson.[56] The TPD spectra reported here for five different coverages of acetone are similar in peak profile and temperature to those reported by Henderson with the exception of the position of the high temperature edge, and small features above 450 K. High temperature features for acetone thermal desorption from TiO_2(110) surfaces have been observed by Henderson in latter studies and also attributed to surface roughening.[50,55] Of particular importance to the present investigation is that the

photochemistry of acetone on both TiO_2(110) surfaces that yield TPD features above 400 K,[50] and on "smooth" surfaces[16] was found to be similar.

Figure 4.2 (a) displays a TOF mass spectrum for gas phase acetone (1.4×10^{-8} Torr) obtained with a probe photon energy of 13.1 eV. Features due to background gases such as H atoms, H_2, H_2O, and O_2, are labeled in the figure. Note that the oxygen signal is enhanced due to the efficiency of the detection scheme employed as discussed in the previous chapter. The remaining peaks, masses 58 and 43, are assigned to the acetone parent ion and the acetyl ion, respectively. No other gas phase acetone fragments were detected.

Adsorbed oxygen has been shown to be essential in the photodecompostion of acetone and butanone on TiO_2(110) surfaces.[16,50,55] Therefore, the TiO_2 surface was first exposure to 80 L of O_2, followed by deposition of a monolayer of acetone or butanone (as determined by the onset of the appearance of the multilayer peak in separate TPD spectra) at a substrate temperature of 100 K. Additionally, all measurements of the photodecomposition of ketones used a pump energy of 3.7 eV (335 nm) to induce chemistry at the adsorbate-oxide interface. This energy is well above the TiO_2 band gap energy (3.05 eV)[57] and below the energy for the onset of photodissociation of the free acetone molecule.[58] A TOF mass spectrum collected at a sample temperature of 100 K and a pump-probe laser delay of 28 μsec is shown in Figure 4.2 (b) for a UV irradiated TiO_2 surface co-adsorbed with O_2 and acetone. The background gases are also labeled in the figure. Two narrow peaks observed in the TOF spectrum correspond to masses 15 and 32, and are not present when the excitation laser is blocked. Consequently, the peaks due to masses 15 and 32 are attributed to photo-induced chemistry at the adsorbate-oxide

interface and are consistent with ejection of a methyl radical and O_2 PSD, respectively. This assignment is in agreement with the findings of previous studies of acetone photodecomposition on single crystal TiO_2(110) surfaces.[16,50,55]

Note in Figure 4.2 (b) that O_2 desorbing from the surface arrives at a slightly earlier time then O_2 signal attributed to background. This is because species desorbing from the surface have a velocity component along the TOF axis in addition to that induced by the acceleration field of the TOF-MS. Assignment of masses from photo-induced processes must be done carefully since arrival times are altered from those of gas-phase species of the same mass and depend on pump-probe laser delay. Consequently, this provides a good way to test if ion signal corresponds to a species originating from the adsorbate-oxide interface since arrival times of gas phase species are independent of laser delay. Also, since the pump-probe laser delay is a measure of velocity, the shift in arrival time will be independent of the species mass. The influence of the desorption velocity on the arrival time was estimated by comparing arrival times for background O_2 gas with O_2 photodesorbed from the surface at the delay of interest. This allowed for mass assignments based on TOF mass spectra obtained at a fixed laser delay to be made.

In addition to the ejected methyl radicals, previous studies have observed a surface bound product in photodecomposition studies of acetone, and it was identified to be acetate (CH_3COO) by post-irradiation TPD experiments.[16,50,55] Acetate thermally decomposes on TiO_2 and desorbs as ketene (CH_2CO) around 600 K.[16] Figure 4.3 (a) shows TPD measurements that were obtained for 80 L O_2 and (~ 1 ML) acetone co-adsorbed on a TiO_2 surface. Mass 42 has the same temperature profile as acetone

below 500 K and is due to e^- impact cracking. To test for the presence of photo-generated acetate remaining on the TiO_2 surface, a TPD spectrum of mass 42, displayed in Figure 4.3 (b) was obtained after UV illumination of a surface with co-adsorbed O_2 (80 L) and acetone (1 ML). Again, mass 42 below 500 K follows the temperature profile of the parent signal of acetone and is due to unreacted acetone. Previous studies suggest that saturation coverage of O_2 on TiO_2(110) is on the order of one to three times the vacancy concentration (0.06 ML in the present study).[21,26] Thus, acetone is likely in excess of O_2 consistent with the large amount of signal from mass 42 below 500 K observed in Figure 4.3 (b). The large signal of mass 42 above 500 K following UV irradiation is consistent with the photo-generation of acetate in conjunction with the ejected methyl radical, in agreement with previous studies.

A typical depletion curve for mass 15 (data points) for an 18 μsec delay was obtained at 100 K for co-adsorbed O_2 and acetone on TiO_2 and a bi-exponential fit to the data (dashed line) is given in Figure 4.4. The UV radiation was introduced at time zero, and at 380 seconds the UV light was blocked from entering the vacuum chamber. The signal intensities for delay measurements were corrected for reactant depletion from the surface. This correction was done by using bi-exponential fits to depletion measurements obtained at the most probable laser delay.

Velocity distributions of methyl radicals produced in the photodecomposition of acetone were determined from measurements of $CH_3\cdot$ yield as a function of pump-probe laser delay. Figure 4.5 displays the $CH_3\cdot$ flux from a surface as a function of laser delay time under identical conditions as the experiment presented in Figure 4.4. A single narrow peak at 18 μsec is observed with a tail to long delay times. The corresponding

velocity and translational energy distributions are given in Figure 4.6 (a) and (b) respectively. The velocity distribution (data points) has a peak at around 1550 m s^{-1} with a shoulder on the low velocity side. The CH_3· velocity distribution was fit to the sum of two Gaussian functions (solid trace), with one Gaussian function attributed to a low velocity component with a peak at 620 m s^{-1} and the second Gaussian function due to a high velocity component with a peak at 1540 m s^{-1}. The individual Gaussian functions are shown in the figure as dashed lines. A variable transformation of data, the overall fit, and the two individual components of the fit, was made from velocity to translational energy and is presented in Figure 4.6 (b). The mean translational energies obtained from the individual components of the fit are 0.018 eV and 0.19 eV. Possible interpretations of the velocity and translational energy distributions are discussed in the next section.

A question central to studies of the photodecomposition of organics on TiO_2 is; what is the role of oxygen? In order to investigate this problem, a study of the photodecomposition of acetone as a function of different TiO_2 surface preparations was conducted and presented in here. Methyl radical signal from measurements made at a fixed delay of 18 μsec is shown as a function of time in Figure 4.7 for the different surface preparations. For this series of experiments the TiO_2 crystal was exposed to 80 L of O_2 at a temperature of 100 K, flashed to the temperatures indicated in the figure, allowed to return to 100 K, and subsequently dosed with 1 ML of acetone. Time zero corresponds to the introduction of UV radiation, which was later blocked from entering the chamber at about 320 seconds. Measurements were also made for a TiO_2 surface that had not been exposed to molecular oxygen and is displayed in the lower trace of Figure 4.7. The curves are displaced vertically for clarity. Essentially no signal due to methyl

radical was detected without exposing TiO_2 to molecular oxygen as evident in the figure. Experiments in which TiO_2 was pre-exposed to O_2 all show a spike in methyl yield upon introduction of the UV light followed by a significantly slower decay in CH_3· radical signal. The intensity of the spike and its duration increases with increasing anneal temperature of the O_2 adlayer. Rates of the kinetically fast and slow regions were approximated from fitting the data to bi-exponential decay functions and showed a trend of increasing decomposition rate with temperature. Note that no O_2 desorption from TiO_2(110) surfaces was detected above 400 K as seen in thermal desorption measurements of molecular oxygen in the previous chapter. Thus any oxygen present on the surface after flashing to 410 K (the experiment represented by the upper trace in Figure 4.7) is likely O atoms or O_2 that is destined for dissociation at a higher substrate temperature. The integrated yield of CH_3· radicals was obtained by extrapolating the bi-exponential fits to zero signal. The normalized yields for the experiments in which the adlayer was flashed to 100 K, 225 K and 410 K are 1.0, 0.78, and 0.46, respectively. However, it is possible that the methyl yield is underestimated for the upper two traces (flash to 225 Kor 410 K) if the rate of CH_3· ejected from the surface occurred to fast for all ions to be counted.

4.3.2 Butanone on reduced TiO_2

Thermal desorption spectra of butanone adsorbed on a reduced TiO_2(110) surface are shown in Figure 4.8 for various coverages. The temperature profile and coverage dependence observed here for butanone are similar to the TPD measurements of acetone on TiO_2 (Figure 4.1). The sharp peak at about 130 K does not appear to saturate and is

assigned to multilayer butanone consistent with acetone TPD spectra and assignments made by others.[50] The TPD spectrum of butanone shown in Figure 4.8 that marks the onset of the multilayer peak as is considered to correspond to 1 ML of butanone on TiO_2. As in the case of acetone on TiO_2, the high temperature peaks appearing at about 400 Kand 460 K are attributed to surface roughening based on the similarity between TPD spectra of the two molecules. Interestingly, butanone TPD spectra in Figure 4.8 differ slightly from those presented in a study by Henderson.[50] This is surprising given that TPD measurements of acetone on reduced TiO_2 reported here and by Henderson are so similar.

A TOF mass spectrum of gas phase butanone (1.4×10^{-8} Torr) collected with an ionization energy of 13.1 eV is given in Figure 4.9 (a). Peaks arising from background gases (H, H_2, and H_2O) are labeled in the figure. The parent ion (mass 72) is seen with relatively low intensity. Also present in the mass spectrum are fragments of mass 29 and 43 (corresponding to cleavage of a CH_3CH_2–$C(O)CH_3$ bond) and mass 57 corresponding to cleavage of a a $CH_3CH_2C(O)$–CH_3 bond.

All measurements of butanone photodecomposition reported in this study were made at a substrate temperature of 200 K, and in an environment of 5×10^{-8} Torr O_2 gas in an effort to improve the signal-to-noise of decomposition products. It has been previously demonstrated that photodecomposition of simple ketones on TiO_2 is enhanced at sample temperatures up to about 260 K.[16] Figure 4.9 (b) shows the TOF mass spectrum obtained at a laser delay of 60 μsec for a pump-probe experiment of O_2 and butanone co-adsorbed on a reduced TiO_2 surface. The ionization energy employed was 13.1 eV. The voltage on the MCP detector was momentarily switched off for the arrival

time corresponding to mass 32 to avoid saturating the detector due to intense signal from background O_2. Two sharp features marked with asterisks in Figure 4.9 (b) are the edges of the O_2 (g) peak that was not completely removed due to not pulsing the detector voltage off for a wide enough delay range. Peaks arising from background gases seen in Figure 4.9 (b) are also labeled in the figure. The small peak due to mass 15 and features in the region of C_2 species, specifically masses 26, 27, 28 and 29 are attributed to surface photochemical processes. No other masses were observed for species ejected from the surface during UV exposure.

A mass spectrum was collected under identical conditions as the experiment represented in Figure 4.9 (b) using a different VUV ionization energy to aid in product identification. This mass spectrum is shown in Figure 4.10. Curve (a) gives the fragmentation pattern of the ejected decomposition products in the C_2 region when photons of 10.8 eV energy are used for ionization. The only features in the C_2 region for curve (a) are a peak at mass 29 and a relatively small peak at mass 27. Curve (b) was collected with a ionization energy of 13.1 eV and is the same data shown in Figure 4.9 (b). Again, masses 26 through 29 are clearly present, and the peak marked with an asterisk is due to signal from gas-phase O_2. No other masses attributed to photochemical processes occurring at the adsorbate-oxide interface were detected at any laser delay when either ionization energy was used.

Velocity distributions were determined for masses 27, 28 and 29 in order to gain insight into the dynamics of the photo-induced chemistry as well as aid in species identification. Unfortunately, the signal to noise for masses 15 and 26 was too poor to gain information on the velocity distributions for their corresponding species.

Determining velocity distributions from laser delay scans was not as straight forward for butanone as it was in the case for acetone due to experimental artifacts and the congestion of peaks in the C_2 region of the mass spectrum. In short, additional corrections were needed for background contributions to the ion signal that if not made would systematically alter the data. The additional correction procedures are presented in Appendix B. After background, depletion, and flux corrections were made, a series of variable transformations were made from time to velocity and then from velocity to translational energy using the appropriate Jacobian. The velocity distribution for the species corresponding to mass 29 is displayed in Figure 4.11 (a). Filled circles represent the data which was fit to the sum of two Boltzmann distributions (solid curve). The individual components to the overall fit are also shown (dashed curves) displaying fast and slow channels. The translational energy distribution is given in Figure 4.11 (b). Again the data are represented by filled circles, and the solid curve is the fit to the velocity data after variable transformation to energy.

Translational energy distributions for species corresponding to masses 27 and 28 are presented in Figure 4.12 (a) and (b) respectively. Here, the filled circles represent the data and the solid traces in both (a) and (b) are the same fit to the translational energy distribution of mass 29 with the only modification to the fit being a multiplication factor to adjust the vertical scale so that the fit overlapped the data points. All three masses fit the same translational energy distribution very well and thus are all likely due to a single species. A likely candidate is the ethyl radical (mass 29) that may fragment into masses 28, 27, and 26. Differences in the TOF mass spectra obtained with different ionization energies may be attributed to the dependence of the ethyl radical cross section for

dissociative ionization on photon energy. The vertical adjustments to the fits correct for the different dissociative ionization cross sections to produce each mass. Species identification is discussed further in the next section.

4.4 Discussion

4.4.1 Acetone photodecomposition products

The experiments reported here are for the most part in agreement with previous studies on the photodecomposition of acetone on single crystal TiO_2(110) surfaces.[16,50,56] Acetone photodecomposition on TiO_2(110) surfaces does not precede without co-adsorption of oxygen. The requirement of oxygen for photoreaction is demonstrated in the bottom trace in Figure 4.7, which shows methyl yield as a function of UV irradiation time of the acetone-oxide interface in the absence of molecular oxygen either in the gas phase or adsorbed on the TiO_2 surface. Almost no signal is detected for methyl in the bottom trace, however when O_2 and acetone are co-adsorbed on TiO_2 the methyl yield is greatly enhanced as seen in the upper three traces of Figure 4.7. Oxygen and acetone form a surface bound intermediate on TiO_2(110) surfaces which has a low barrier for formation.[16] The structure of this intermediate was suggested to be acetone diolate based on a O–C–O bond order of 1.5 as determined by vibrational spectra obtained by HREELS.[56] It was further suggested that the diolate is active for photolysis whereas adsorbed acetone in an η^1 configuration is not. The oxygen species involved in the formation of the intermediate is not currently known. Henderson proposed a reaction mechanism for the photodecomposition of ketones on TiO_2 that involves a photo-induced

cleavage of a C–C bond of the diolate resulting in an alkyl radical being ejected into the vacuum leaving an acetate molecule bound to the substrate.

The data generated in the current study are consistent with the mechanism presented above in that acetate and methyl radical are produced as seen in Figures 4.2 and 4.3. Evidence for methyl radical production is shown in Figure 4.2 (b), a typical mass spectrum obtained at a laser delay of 18 μsec (delay in which the peak intensity for mass 15 occurs) upon UV irradiating the oxide with co-adsorbed O_2 and acetone at 100 K. TOF mass spectra at other delays differ only in the signal intensity for masses 15 and 32, and no other masses due to species originating from the interface were detected. The occurrence of mass 32 in the mass spectra indicates that O_2 PSD from the interface occurs concurrently with methyl radical production. This finding is in agreement with previous studies that have observed O_2 desorption during ketone photodecomposition on single crystal TiO_2 surfaces.[55] Significant contribution to mass 15 signal from dissociative ionization of acetone desorbing from the surface can be ruled out based on the fact that mass 15 is not observed in TOF spectra of gas phase acetone obtained with the same photon ionization energy as shown in Figure 4.2 (a). Also, the fact that masses 43 and 58 are absent in Figure 4.2 (b) argue against acetone or acetyl radical desorption from the surface during UV irradiation of the adsorbate-oxide interface. Thus mass 15 is assigned to methyl radical ejected into the vacuum due to a photochemical process at the adsorbate-oxide interface in agreement with earlier studies. Additionally, post-irradiation TPD measurements aid identification of a surface bound product. Figure 4.3 (b) gives an example of a post-irradiation TPD for surface co-adsorbed with acetone and oxygen. Mass 42 features observed above 500 K are attributed to acetate formation concurrent

with methyl radical. It has been previously shown that acetate decomposes to ketene on TiO_2 upon heating and desorbs above 500 K in TPD measurements.[56] Additionally, increase in both ketene and CH_3· production with along with a decrease acetone during UV irradiation of the acetone-TiO_2 interface in the presence of gas phase oxygen has been observed in previous studies.[16] Although some of the intermediate thermally decomposes to yield acetate, comparison of mass 42 traces in Figure 4.3 show that a substantially greater amount of acetate is produced via photolysis than thermally.

Earlier investigations of acetone photodecomposition on TiO_2 have demonstrated that annealing the acetone–oxygen adlayer to about 250 K prior to photolysis resulted in a significantly enhanced yield of methyl radical and suggested a relatively small activation barrier for formation of the acetone intermediate was overcome by annealing. Experiments performed in the present study observe an increase in methyl yield after thermal activation of the adlayer as well. Moreover, the work presented here demonstrates that the reaction channels and the products formed are not significantly altered by small amounts of heating. Delay scans of methyl radical ejected via irradiation of the acetone-oxygen adlayer at 100 K were identical to within experimental error regardless of whether or not the adlayer was first flashed to 200 K before irradiation at 100 K. This is consistent with enhancement of the photoreaction by annealing being attributed to a greater yield of an intermediate.

4.4.2 Acetone photodecomposition mechanism and velocity distributions

Velocity distributions for methyl radicals ejected from a TiO_2(110) surface during photodissociation of the adsorbed acetone or intermediate have been determined and are

presented in Figure 4.6 (a) (data points). Two channels for methyl ejection from the surface have been identified based on an empirical fit to the data (solid line) by the sum of two Gaussian functions. The two individual components of the fit (dashed traces) represent to the two channels and are referred to as either fast (prompt) or slow throughout this report. Below, possible excitation mechanisms responsible for acetone photodecomposition are discussed as well as the possible origins of the two channels for methyl ejection. Typically, four excitation mechanisms are considered for UV induced desorption: direct optical excitation of the adsorbate, direct optical excitation of the adsorbate-substrate complex, substrate-mediated electronic excitation, and photo-induced thermal desorption. Based on the large amount of energy required to cleave a C–C bond of acetone (about 350 kJ mol^{-1} based on known heats of formation) and the low photon flux used to initiate chemistry at the interface, the photo-induced thermal desorption mechanism is not considered further.

Here, the possibility of direct excitation of acetone is considered as a mechanism for dissociation. In the present study about 1 ML of acetone was adsorbed on the surface which is expected to be in excess of O_2 (a). It has been shown that O_2 adsorption on a TiO_2(110) surface saturates at one to three time the vacancy concentration.[21,26] This gives an upper limit for O_2 (or O atom) coverage of about 0.06 to 0.18 ML (or 0.12 to 0.36 ML) in the our investigation. Hence a large fraction of the adsorbed acetone is expected to be in the η^1-acetone configuration with a smaller faction interacting with oxygen to form the intermediate. The η^1-acetone has essentially the same structure as the free molecule.[56] Therefore, it is likely that much of the acetone on the surface during the photochemistry experiment is very similar to the free molecule. The photolysis of

gas-phase acetone has been extensively studied and some of the relevant conclusions are given below.[59] Acetone dissociation occurring via molecular excitation to the first excited singlet state (S_1) yields an acetyl and methyl radical with an onset for dissociation of 4.05 eV.[58] It has been suggested that dissociation takes place on the triplet surface (T_1) after intersystem crossing from the excited S_1 state. The partitioning of energy is mediated by an exit barrier on the T_1 surface with the CH_3· photofragment mean translational energy relatively insensitive to excitation energy and is about 0.61 eV.[60,61] The energy release into translation in the photolysis of gas-phase acetone is substantially higher than the $<E_t>$ of CH_3· radical desorbed via the fast channel, 0.19 eV, from the photodecomposition of acetone on TiO_2. This indicates a mechanism other than direct photolysis of the adsorbate may occur. Also, the excitation energy employed in the present study (3.7 eV) is significantly lower then the onset for photolysis of acetone in the gas-phase (4.05 eV) arguing against direct adsorbate mediated dissociation. However, it is possible the electronic structure of acetone is perturbed by chemisorption such that the absorption spectrum is red shifted relative to the free molecule. The alteration of a molecule's electronic structure via chemisorption would be substrate dependent and it is not known if adsorption on TiO_2 would shift the absorption spectrum of acetone enough for photolysis to occur via direct adsorbate excitation at 3.7 eV photon energy. An additional argument against this excitation mechanism is the lack of reaction in the absence of O_2. The above arguments favor an alternative to direct adsorbate excitation as a mechanism for acetone dissociation, nonetheless it cannot be ruled out. Additional studies such of the methyl yield dependence on excitation energy would help shed light on the excitation pathway since the cross section of photolysis of acetone in the

gas-phase increases with excitation energy above the threshold for dissociation.[62] An alternative approach would be to investigate the photochemistry of multilayer acetone, since the effects of the surface would only be felt by the first couple of layers.

Direct excitation of the adsorbate-substrate complex is another possible pathway for acetone dissociation. Thermal desorption and HREELS measurements have demonstrated that a portion of the acetone adsorbed on TiO_2 in the presence of oxygen forms an intermediate diolate species,[56] thus direct excitation of the diolate, diolate-TiO_2 complex, or acetone-TiO_2 complex must be considered. However, little is known about the structure or electronic properties of the aforementioned species and therefore justifying such a mechanism would prove difficult. Evidence in support of a substrate mediated reaction is that O_2 (a) is necessary for photodecomposition of ketones on the surface. Additionally, photochemical studies by Henderson using a Hg arc lamp have shown acetone photodecomposition on TiO_2(110) surfaces ceases to occur below the band gap energy of TiO_2 (3.05 eV) supportive of a substrate mediated excitation mechanism.[16] However, in the aforementioned study, the bandwidth of the lamp was quite large and cutoff filters were used to omit photon energies greater than the band gap, which also resulted in reducing the photon flux. Further investigations of the photochemistry dependence on excitation energy using a more defined UV light source (narrower bandwidth) are warranted.

Two channels for methyl radical ejection from the surface are identified in this report. The origins of the two channels however, can not be resolved with certainty without further experiments. Possible explanations for the two channels include multiple excitation mechanism occurring concomitantly, a dynamical energy loss, or multiple

states of the diolate intermediate. Here, a dynamical energy loss during the dissociation process, as was discussed in the previous chapter for the case of O_2 photodesorption, is considered. The energy difference between the two channels (0.15 eV) happens to coincide well with the first overtone of the ν_2 umbrella mode of the methyl radical (fundamental ν_2 frequency of 0.076 eV).[63] Attempts to force fit the data by inserting a third Gaussian function at a fixed energy equal to the fundamental frequency described the data well. The "forced" fit resulted in less then ten percent of the methyl yield contributing to what may be assigned to the fundamental vibration loss while about 40 percent corresponding to what may be loss due to first overtone.

Photolysis of gas-phase d_6-acetone results in methyl radicals with excited umbrella vibrational modes, however, an inverted distribution of vibrational energy levels has not been observed.[64] Hence, while the energy difference between the two channels matches the umbrella mode frequency, an inverted population of vibrational states would be unexpected for acetone decomposition. In order to confirm this analysis, the velocity distribution of d_6-acetone co-adsorbed with O_2 on titania should be determined. Additionally, vibrational state-resolved product distributions may aid in determining whether collision induced energy transfer is a viable explanation for the origin of two channels. A second possible dynamical loss attributed to excitation of a surface-optical phonon modes of TiO_2(110) can be ruled out since the three fundamental surface phonon vibrations (54 meV, 95 meV, and 46 meV)[46] do not correspond to the energy difference between the two channels. Thirdly, collisionally induced energy transfer between the surface and photofragment may occur resulting in a methyl translational energy loss. This would be possible if the diolate adsorbs on the surface in an orientation so that one

carbonyl carbon – methyl bond is directed towards the vacuum and the other toward the surface. In the former case the recoil velocity of the methyl radical is directed toward the vacuum and would correspond to the fast channel, while in the later case the recoil velocity is toward the surface and would correspond to the slow channel. A collision induced loss in methyl radical translational energy has been suggested to occur in photolysis of methyl iodide on TiO_2(110).[65] Collisions between CH_3· and the surface require consideration of multiple factors such as concurrent excitation and relaxation of methyl vibrational modes and/or surface phonons, and thus are not easily discernable with the techniques employed here. However, measurements of the angular distributions of methyl radicals ejected into the vacuum via the individual channels may provide insight into the mechanism. Molecules detected after a scattering event may have a broader angle distribution as was seen in CH_3I photolysis. Thus it would be of value for future experiments measuring the angle distributions of ejected methyl radicals to be performed.

4.4.3 Effect of oxygen

Co-adsorption of molecular oxygen is a prerequisite for acetone photodecomposition on TiO_2. The role of oxygen as well as the active oxygen species involved in the photochemistry is still unknown. In an attempt to identify the active oxygen species involved (O atom or O_2 species) a series of measurements of methyl production as a function of UV exposure time were made for different surface treatments and shown in Figure 4.7. In these experiments 80 L of O_2 was dose onto TiO_2 at 100 K and the substrate was flashed to the temperatures indicated in the figure. Acetone

(~ 1 ML) was subsequently dosed at 100 K and the methyl yield was monitored at an 18 μsec delay while the surface was irradiated with UV light. At this delay there should be little contribution to the signal from the slow velocity channel. Oxygen on titania at 100 K exists mostly in the molecular form, while after flashing to above 400 K only O atoms are thought to remain. It is apparent upon inspection of the figure that the rate of acetone photodecomposition depends on the state of oxygen on the surface. Several possible interpretations of the data are possible. One explanation may be that an intermediate complex with a low cross section for methyl ejection forms with O_2 species at 100 K, while a different complex with a higher cross section for this photochemistry forms with the O atoms. In this case, the increased rate of $CH_3\cdot$ formation at high temperature would be attributed to a greater number of O atoms available for formation of an acetone-oxygen complex. A second rationalization of the data may be that a single intermediate is produced and the rate limiting step is formation of this intermediate as others have suggested.[16] In this case O_2 would be thermally converted to an active state that reacts more readily with acetone to form a photoactive complex. Since the methyl radical is observed after the oxygen adlayer has been flashed to 410 K this species is likely an O atom. At 100 K a small amount of the active intermediate is initially present forming the initial spike, and the rate limiting step as the reaction proceeds is the formation of the intermediate (O_2 photodissociation). Evidence for photodissociation of O_2 on TiO_2 has been suggested by others.[2] Given the two explanations the latter seems more likely since if different species were responsible for the different rates, one might expect that the species would have different kinetic energy distributions while all of the measurements displayed in Figure 4.7 detected methyl radicals at a single velocity.

Velocity distributions for the different surface treatments need to be measured to more definitely differentiate between the two explanations.

Oxygen thermal desorption spectra shown in the previous chapter show no O_2 desorbs above 400 K. Thus any oxygen present on the surface after flashing to 410 K is likely O atoms present after dissociation at an O_{br} vacancy at low temperature or dissociation at Ti^{IV}(5f) sites at elevated temperature. Unfortunately the active oxygen species can not be unambiguously assigned as O atoms since an O_2 species that is a precursor for dissociation at a higher substrate temperature (and thus not detected) may exist on the surface at 400 K.

4.4.4 Butanone photochemistry and product identification

The photodecomposition of butanone was found to be very similar to acetone in that it involved cleavage of a carbon-carbonyl carbon bond (α-cleavage) to yield a radical ejected into the gas-phase and a surface bond carboxylate. Furthermore, the photochemistry is enhanced at elevated substrate temperatures and in the presence of oxygen, consistent with formation of a butanone-oxygen complex active for photofragmentation. In acetone, however, both of the carbon-carbonyl bonds are identical yielding methyl radical upon cleavage of this bond. Butanone differs in this respect in that α-cleavage may produce either a methyl or ethyl radical. Studies by Henderson of butanone photodecomposition on TiO_2(110) surfaces suggest a preferential α-cleavage to yield primarily ethyl radical and surface bound acetate.[50] It was postulated that ethyl radical undergoes secondary chemistry at the interface and ethane, ethylene,

and ethyl radical desorb into vacuum. This conclusion was based on analysis of mass spectra that included masses 27 to 30 and were obtained with electron impact ionization.

In agreement with studies by Henderson, TOF mass spectra obtained in this study show that the major product ejected into the gas-phase is a C_2 species, with a small signal for methyl radical (Figure 4.9 (b)). Gas-phase butanone undergoes dissociative ionization with a 13.1 eV ionization energy and produces fragments of masses 72, 57, 43, and 29 as seen in Figure 4.9 (a). Figure 4.9 (b) shows that PSD of the parent molecule is not observed in pump-probe experiments at this or other laser delays. Thus it is unlikely that contribution from dissociative ionization contributes significantly to masses in the C_2 region in surface photochemistry measurements, and these masses likely arise from photochemistry at the adsorbate-oxide interface. It is unclear whether signal due to methyl radical is from dissociative ionization of ethyl radical or from a second α-cleavage reaction pathway occurring at the interface. Unfortunately, the small signal obtained for mass 15 prohibits identification of its origin by correlating velocity measurements.

The results presented here however, differ from those reported by Henderson, in that our results are not consistent with ethyl radical secondary chemistry occurring at the interface. Figures 4.11 and 4.12 show that masses 27, 28 and 29 all follow the same translational energy distribution indicating they arise from a single species. Therefore the measurements obtained in this study do not show any evidence for secondary chemistry under UHV conditions. However under the higher pressure conditions in which TiO_2 will be used for removal of organic pollutants, the alkyl radicals detected in this study may be involved in radical chain reactions that further oxidize organic material. The

reason for the disagreement between our observations and those of Henderson is not clear at this time.

An advantage of using laser ionization techniques as opposed to electron impact is being able to select well defined photon energies to aid in product identification. Evidence for attributing masses in the C_2 region to ethyl radical stems from the ionization energy dependence of the mass fragmentation patterns. Figure 4.10 displays TOF mass spectra of ejected species produced in the photodecomposition of butanone collected with two different ionization energies, 10.8 eV (upper trace) and 13.1 eV (lower trace). The photochemistry occurred on a TiO_2 surface that was pre-exposed to O_2 and butanone at 100 K and investigated at a substrate temperature of 200 K in a background of O_2 gas (5×10^{-8} Torr). A study of the photoionization of ethyl radicals determined the onset of mass 28 in dissociative ionization to be above 12.1 eV, consistent with our mass spectra shown in Figure 4.10.[66] Also, the dependence of the relative intensities of all the masses observed in Figure 4.10 on ionization energy compare well with mass spectra collected with photons of 12.1 eVor 13.8 eV reported in the aforementioned study. We conclude that photo-induced dissociation of a butanone-oxygen intermediate at the interface produces primarily a single species ejected into the gas phase which is consistent with ethyl radical. However a minor reaction pathway for α-cleavage to yield methyl radical might also operate under the present conditions.

4.4.5 Butanone velocity distributions

Butanone and acetone were found to have similar thermal and photo-induced interactions with TiO_2 both with and without co-adsorbed oxygen. Both molecules

adsorb in a η^1 configuration and form a diolate species when co-adsorbed with oxygen molecules.[50] UV light above the TiO_2 band gap energy induces an α-cleavage, ejecting an alkyl radical into the vacuum and leaving an acetate molecule on the surface. Given the similar absorption spectrum at the pump energy employed,[67] and the similarities in structure and chemical behavior, it is likely both acetone and butanone follow the same photodecomposition mechanism on TiO_2. Therefore possible mechanistic pathways for butanone photodecomposition will not be discussed here since acetone decomposition mechanisms were discussed in section 4.4.2. In summary, the specific excitation mechanism leading to photodecomposition can not be resolved by the present set of experiments, however the data obtained in the current investigation as well as those reported by others is consistent with a substrate mediated excitation mechanism.

An empirical fit to the ethyl radical velocity distribution indicate two channels for ethyl ejection operate under the experimental conditions employed. Here, we turn are attention to the origin of the two channels for ethyl ejection. The individual components of the ethyl velocity distribution have mean translational energies of 24 meV and 97 meV. Interestingly, the slow channel for ethyl ejection is lower than thermal energy (2kT ~ 35 meV) at 200 K indicating that a single initial state of the diolate intermediate exists and the slow channel arises via a dynamical energy loss. Alternatively, ethyl radical may be trapped momentarily on the surface prior to desorption as was observed for O_2 photodesorption in the previous chapter, however one might expect such a reactive species to have a short lifetime at the adsorbate-oxide interface. Given that there is no evidence for secondary chemistry, we favor the former explanation. The energy difference between the two channels is about 74 meV which does not correlate well with

a loss to a surface optical phonon of TiO_2 (~ 30% error). The observed kinetic energy difference between the two channels happens to coincides well (< 10% error) with the frequency of the CH_2 pyramidal bending mode of the methylene group of the ethyl radical (ν_9).[68] An excitation of the ν_9 mode of the ethyl radical (C_s symmetry) upon fragmentation of the relevant C–C bond of the butanone diolate intuitively makes sense given the geometric distortion that occurs for the methylene group as it is transformed from tetrahedral to a nearly planer configuration. While we feel that excitation of the ν_9 mode is a more likely source of the second channel then trapping of such a reactive species on the surface, these experiments can not distinguish between the two processes.

A final consideration is to compare the relative translational energy distributions of the methyl and ethyl radicals produced via photodecomposition of their similar parent molecules (diolate intermediates). The mean translational energies for the fast and slow channels in butanone are about 50% the value of the mean kinetic energy distributions in the fast and slow channels in acetone, respectively (the overall mean kinetic distributions differ by about 33%). This result is consistent with the butanone intermediate (or ethyl) having a greater number of degrees of freedom then the acetone intermediate (or methyl). One would expect that the excess energy available after α-cleavage is very similar in the two systems given the same pump energy used and similar bond dissociation energies for the relevant C–C bonds in the free acetone and butanone molecules. Thus if the excess energy is distributed over the different degrees of freedom of each diolate intermediate (photofragment) in a similar manner, then the lower number of vibrational modes of the acetone diolate (methyl) would allow for more energy to be partitioned into translational motion. However, one must be careful in making such correlations between the DOF and

kinetic energy distributions since the energy partitioned into the photofragments will depend on many factors including the lifetime of the transition states as bond cleavage may occur prior to complete statistical energy distribution within parent molecule. Attempts at using a model to predict the partitioning of excess energy into translational or internal degrees of freedom would require additional information about the geometric and electronic structure of the intermediate complex.

4.5. Summary

The photodecomposition of two simple aliphatic ketones, acetone and butanone, at the TiO_2(110) surface were used as model systems in order gain insight into the initial steps of the processes that occur in the photo-oxidation of organic pollutants on TiO_2. Reaction products were determined by postirradiation TPD spectroscopy and pump-probe TOF mass spectroscopic techniques. Translational energy distributions were measured to gain insight into the reaction dynamics. Decomposition of the ketones occurred via a two step process, one thermal and the other photo-induced. Both acetone and butanone were first activated for photo-induced fragmentation by forming a ketone-oxygen complex with co-adsorbed O_2 that has a small barrier for formation.[16,50] Photons of energy exceeding TiO_2 band-gap resulted in a cleavage of a carbon-carbonyl carbon bond of the intermediate releasing either methyl or ethyl radical (for acetone or butanone, respectively) into the vacuum with acetate remaining bound to the substrate. No evidence for secondary chemistry involving the radicals was observed, however it will likely play a role under the higher pressure conditions relevant for removal of organic pollutants in wastewater or air.

The excitation mechanism was not unambiguously determined; however both the results reported here and in the literature are consistent with a substrate mediated excitation mechanism. Translational energy distributions of the alkyl radicals were observed to be bimodal indicating two channels for photodecomposition. The average kinetic energies of the fast channels for both ketones are indicative of a photo-induced process. The mean energy of the slow channel for ethyl ejection was found to be sub-thermal and thus is likely due to a dynamical loss, perhaps the CH_2 pyramidal deformation mode. Alternatively, the ethyl radical may be momentarily trapped on the substrate prior to desorption. The origin of the slow channel of methyl radical was less clear, but based on similarities in structure between acetone, butanone, and their respective ketone-oxygen complexes; it is likely that a single intermediate is involved in photodecomposition.

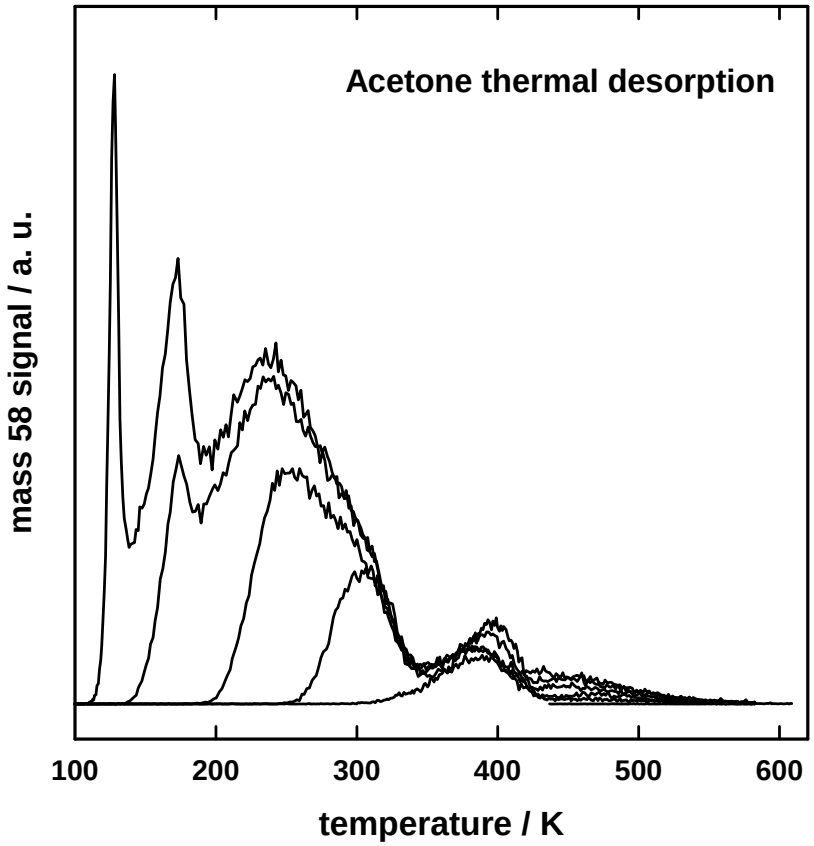

Figure 4.1: Acetone TPD spectra (m/e = 58) from a reduced TiO_2(110) surface for various acetone exposures through a directional doser.

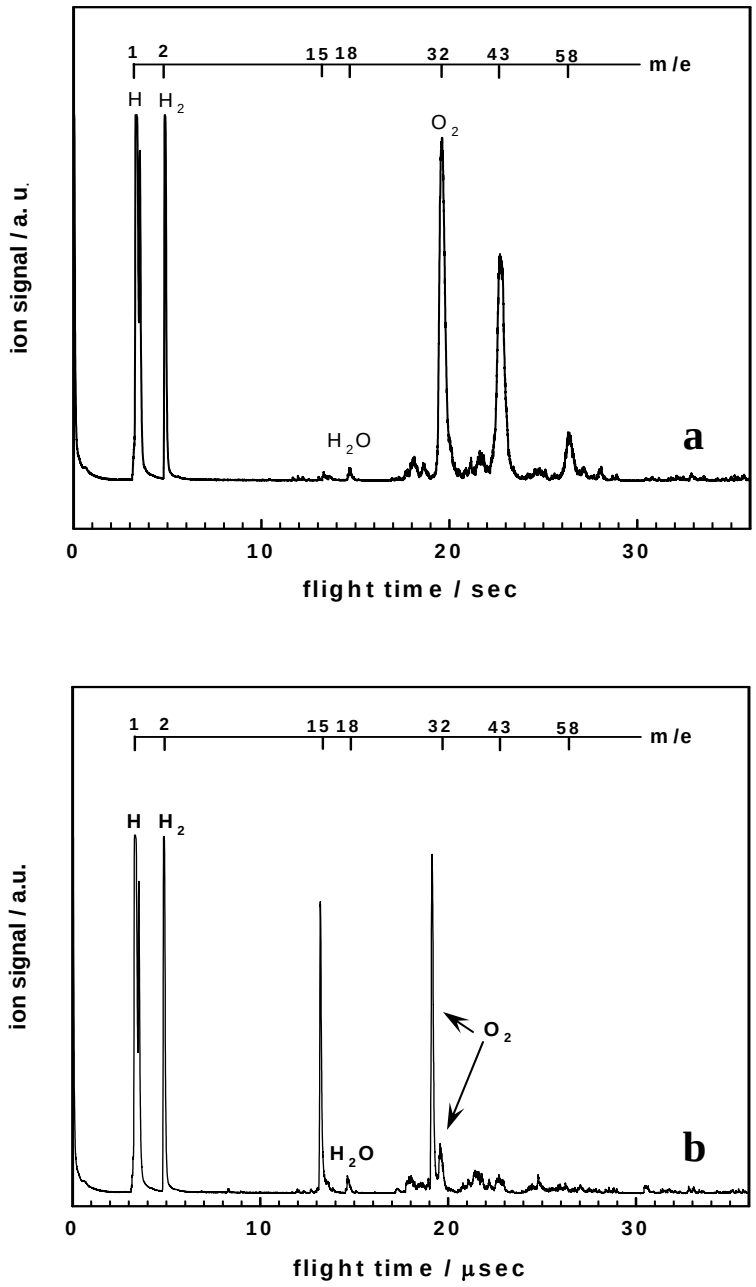

Figure 4.2: TOF spectra obtained with a photoionization wavelength of 94.74 nm (13.1 eV) for (a) gas-phase acetone at 5×10^{-8} Torr and (b) species desorbing from a reduced TiO_2(110) surface at 100 K with an adlayer of acetone and molecular oxygen. The excitation energy for the data in curve b was 335 nm (3.7 eV) and the data was collected at a laser delay of 18 μsec.

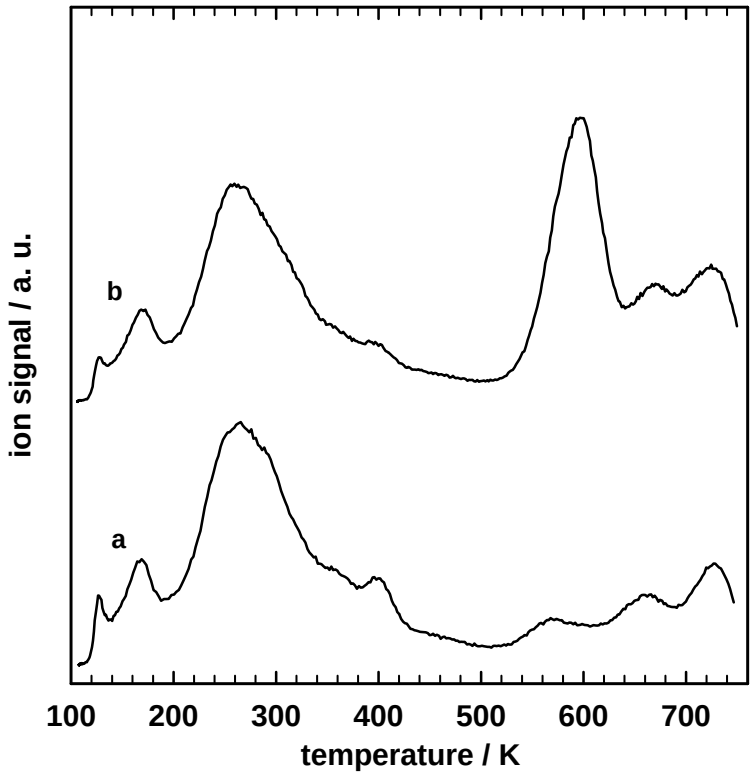

Figure 4.3: TPD spectra for mass and 42 of an acetone-oxygen adlayer on a reduced TiO_2(110) surface obtained (a) in the dark and (b) after irradiating with 335 nm UV light.

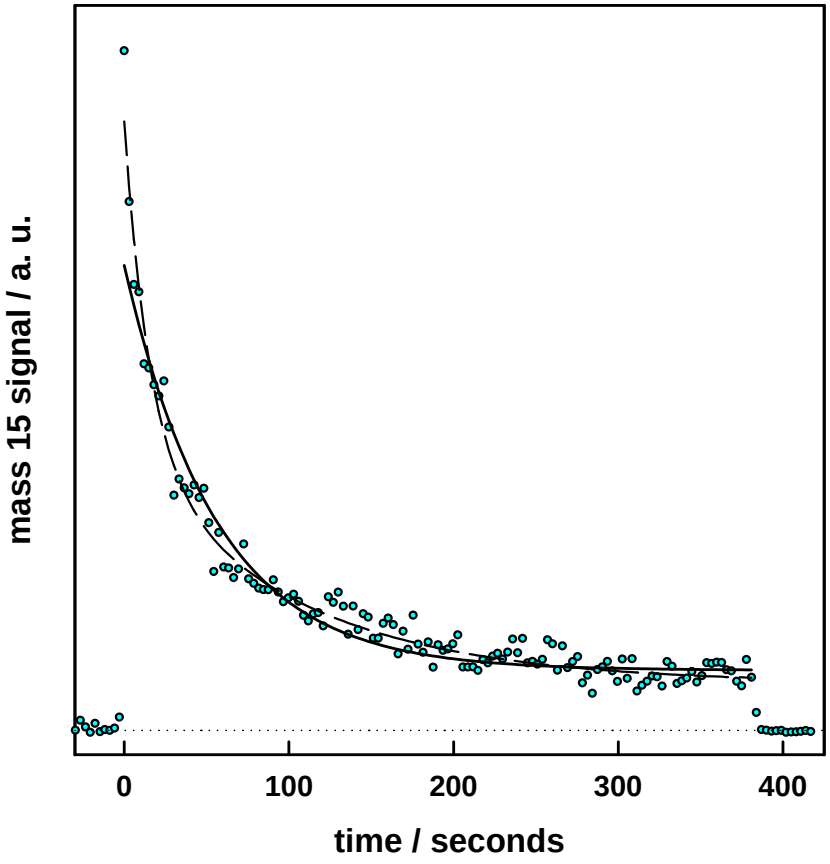

Figure 4.4: Photodesorption signal for mass 15 as a function of time exposed to 335 nm UV radiation at a laser delay of 17 μsec and a substrate temperature of 100 K. Time zero corresponds to the introduction of the UV light. Filled circles are data points, solid line and dashed line are an exponential fit and a bi-exponential fit to the data respectively.

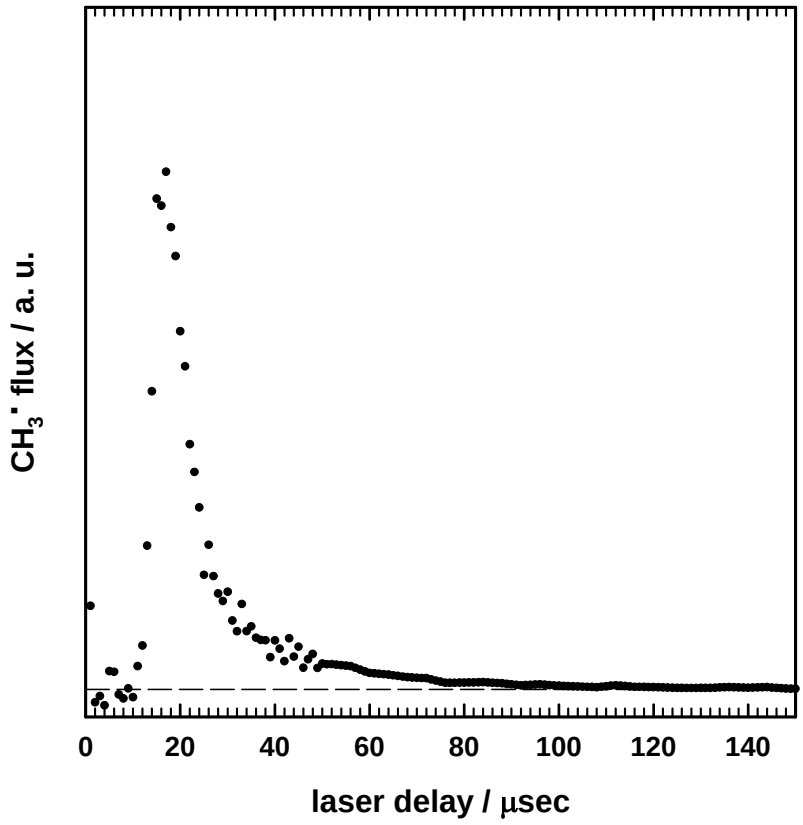

Figure 4.5: Photodesorption of CH_3· from a reduced TiO_2(110) surface pre-exposed to 80 L O_2 and 1 ML acetone at 100 K as a function of laser delay at an excitation energy of 3.7 eV. The data shown here has been flux corrected as well as corrected for depletion of reactant coverage.

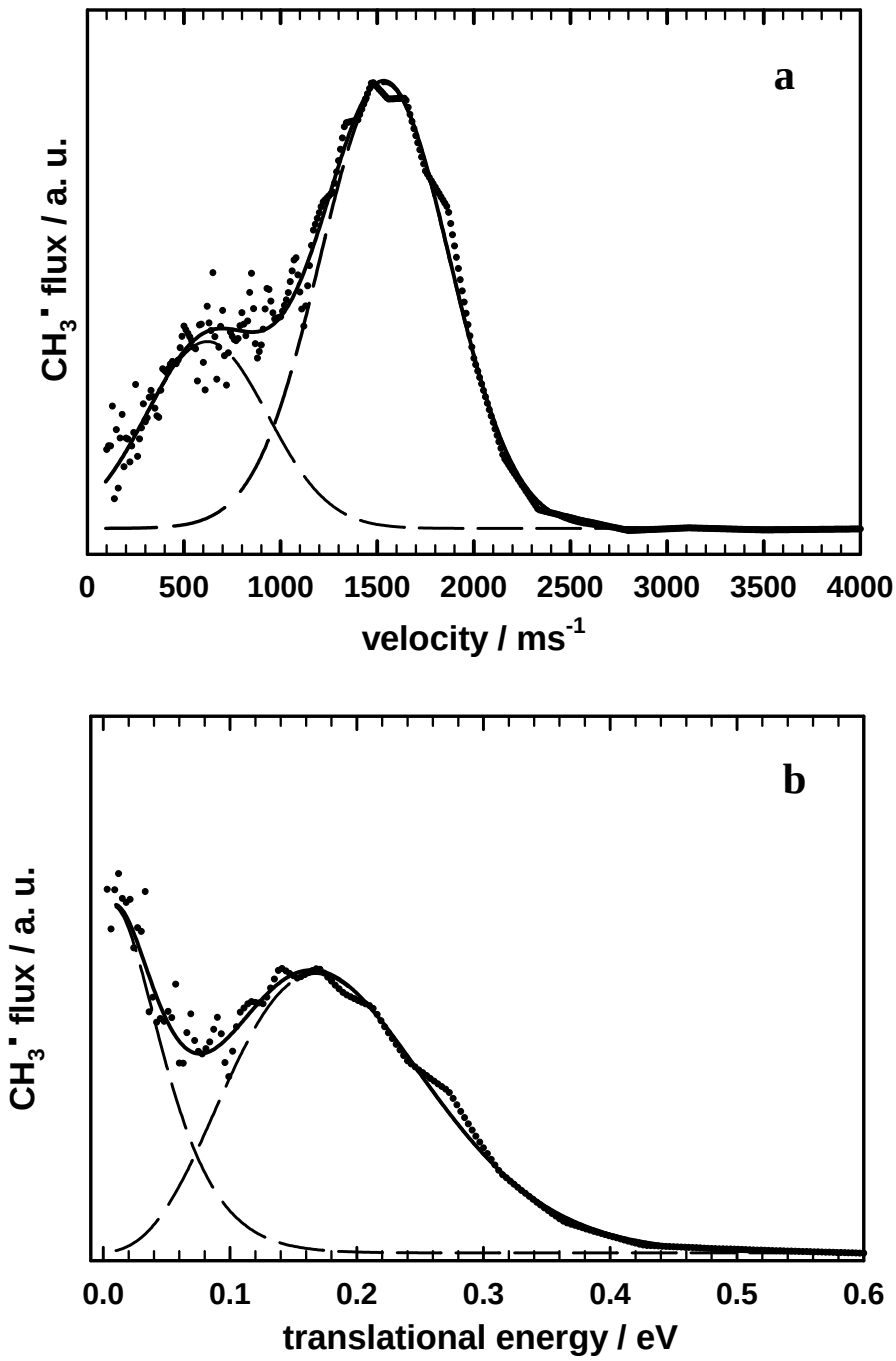

Figure 4.6: (a) velocity distribution and (b) translational energy distribution for CH_3· ejected from a adlayer of acetone and oxygen on a reduced TiO_2(110) surface at 100 K upon irradiating with 3.7 eV photons. Filled circles correspond to the data, dashed lines are Gaussian fits to the data in the velocity domain, and solid lines are the sum of the two individual Gaussian functions. Both the data and the fits were transformed from the velocity domain to the energy domain as described in the text. The above distributions are the same data presented in Figure 4.5.

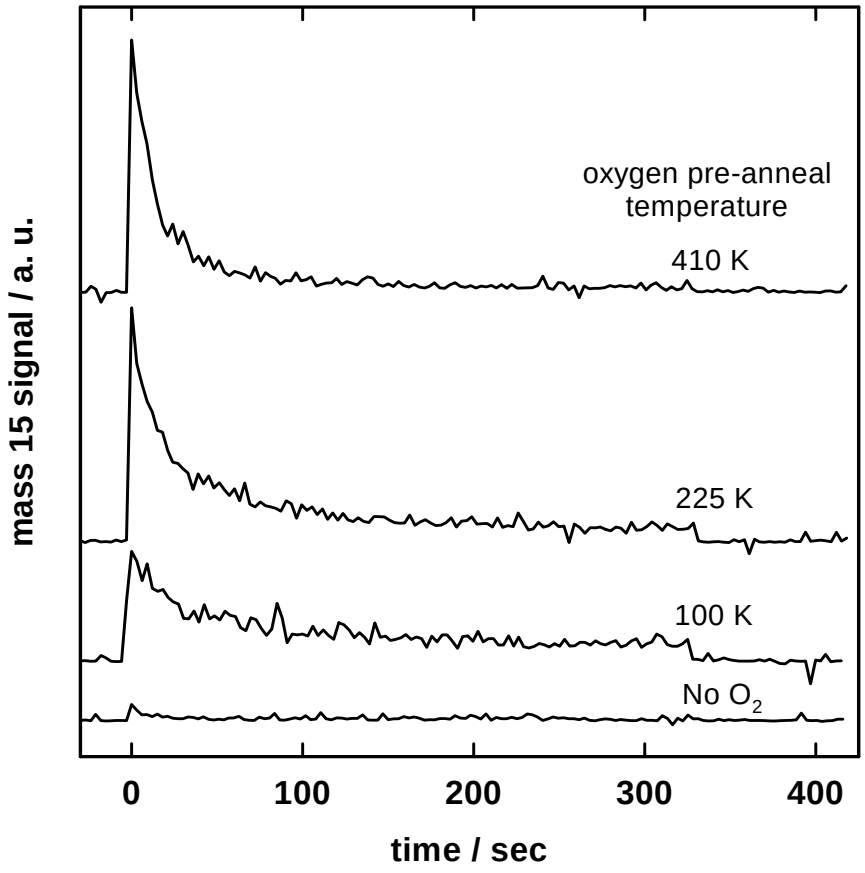

Figure 4.7: *Upper three traces:* Photo-induced ejection of methyl radical from an acetone-oxygen adlayer on a reduced TiO_2(110) surface prepared in the following way. The sample was dosed with 80 L of O_2 at 100 K, flashed to the temperature indicated in the figure, dosed with acetone at 100 K, and irradiated with 3.7 eV photons at 100 K. *Lower trace:* Photo-induced ejection of methyl radical from a reduced TiO_2 surface pre-exposed to 1 ML acetone at 100 K, and irradiated with 3.7 eV photons at 100 K

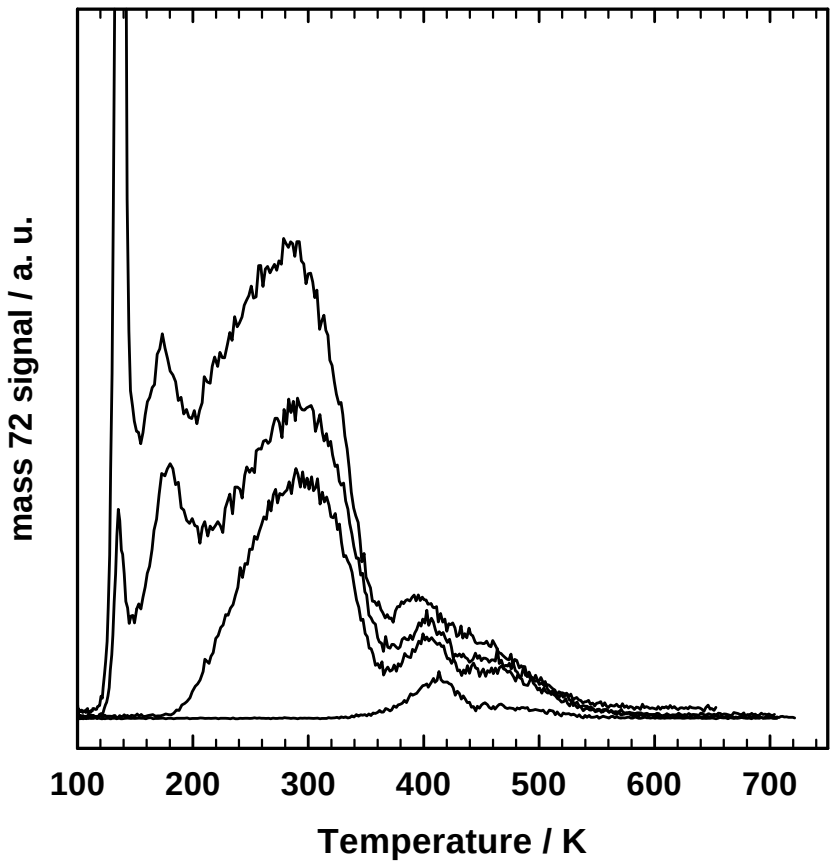

Figure 4.8: 2-Butanone TPD spectra (m/e = 72) from a reduced TiO_2(110) surface for various butanone exposures through a directional doser.

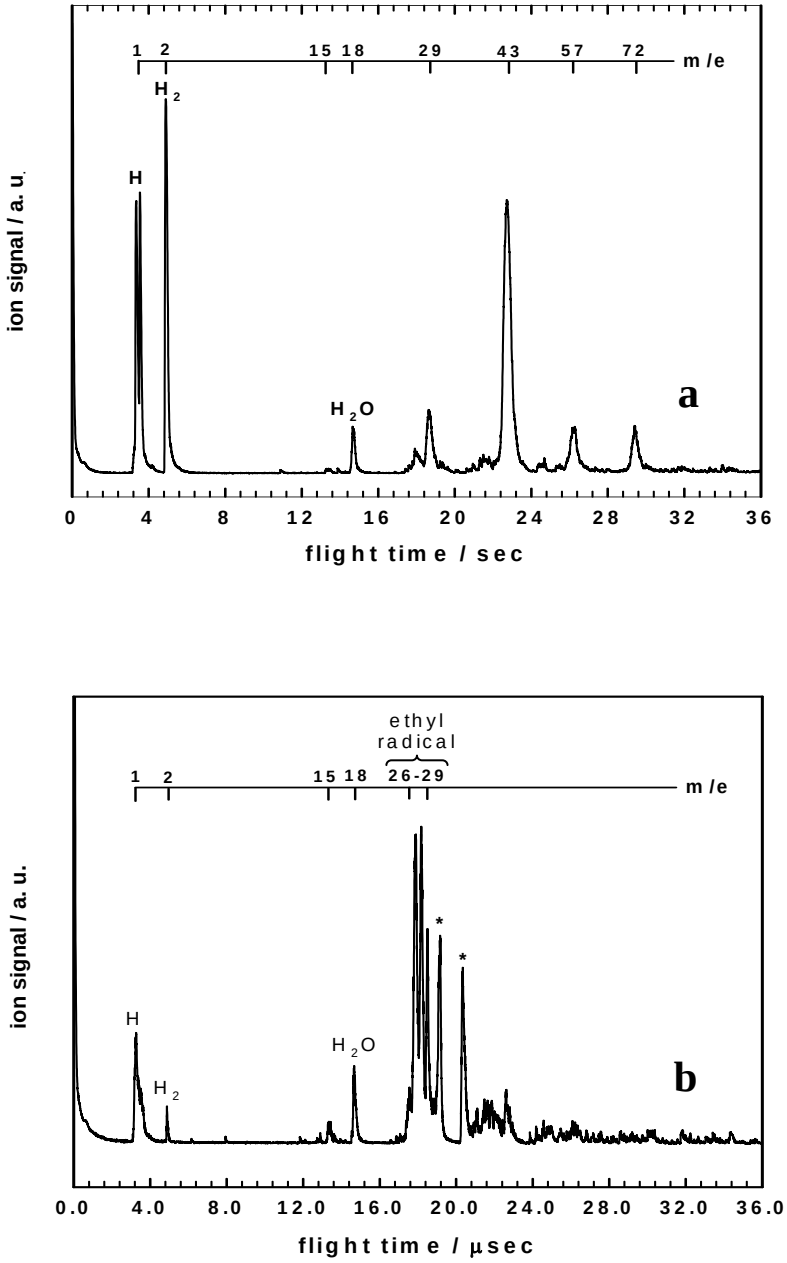

Figure 4.9: TOF spectra obtained with a photoionization wavelength of 94.74 nm (13.1 eV) for (a) gas-phase 2-butanone at 5×10^{-8} Torr and (b) species desorbing from a reduced TiO_2(110) surface at 200 K with an adlayer of butanone and molecular oxygen. The data in (b) was collected with an excitation energy of 335 nm (3.7 eV), at a laser delay of 60 μsec, and in the presence of 5×10^{-10} Torr O_2.

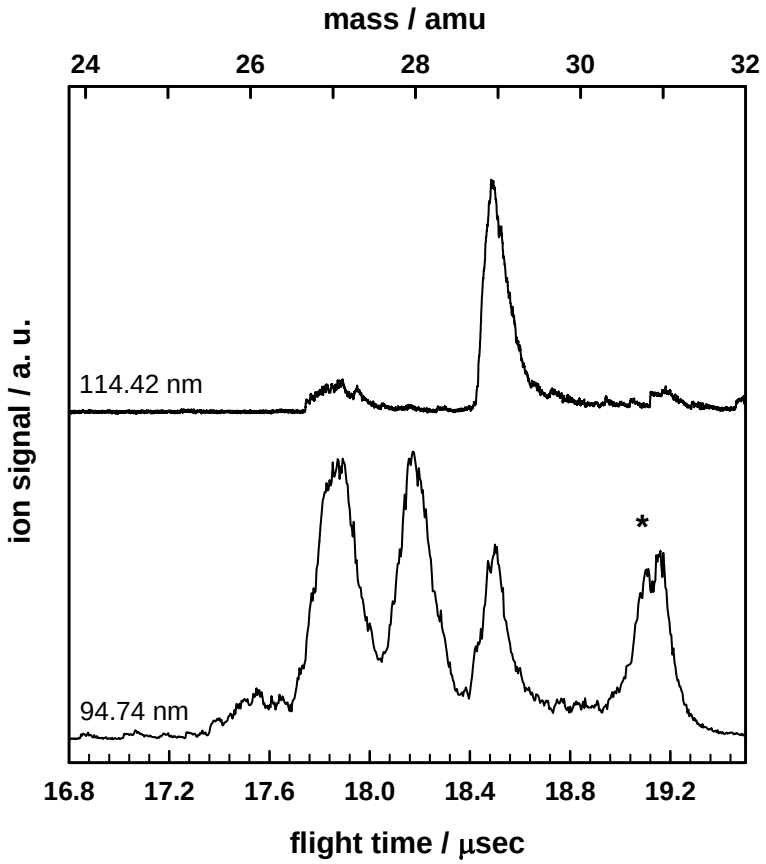

Figure 4.10: TOF spectra obtained for species desorbing from a reduced TiO_2(110) surface at 200 K with an adlayer of butanone and molecular oxygen. The data was collected with an excitation energy of 335 nm (3.7 eV), at a laser delay of 60 μsec, and in the presence of 5×10^{-10} Torr O_2. The mass spectra were obtained with the photoionization energy indicated in the figure.

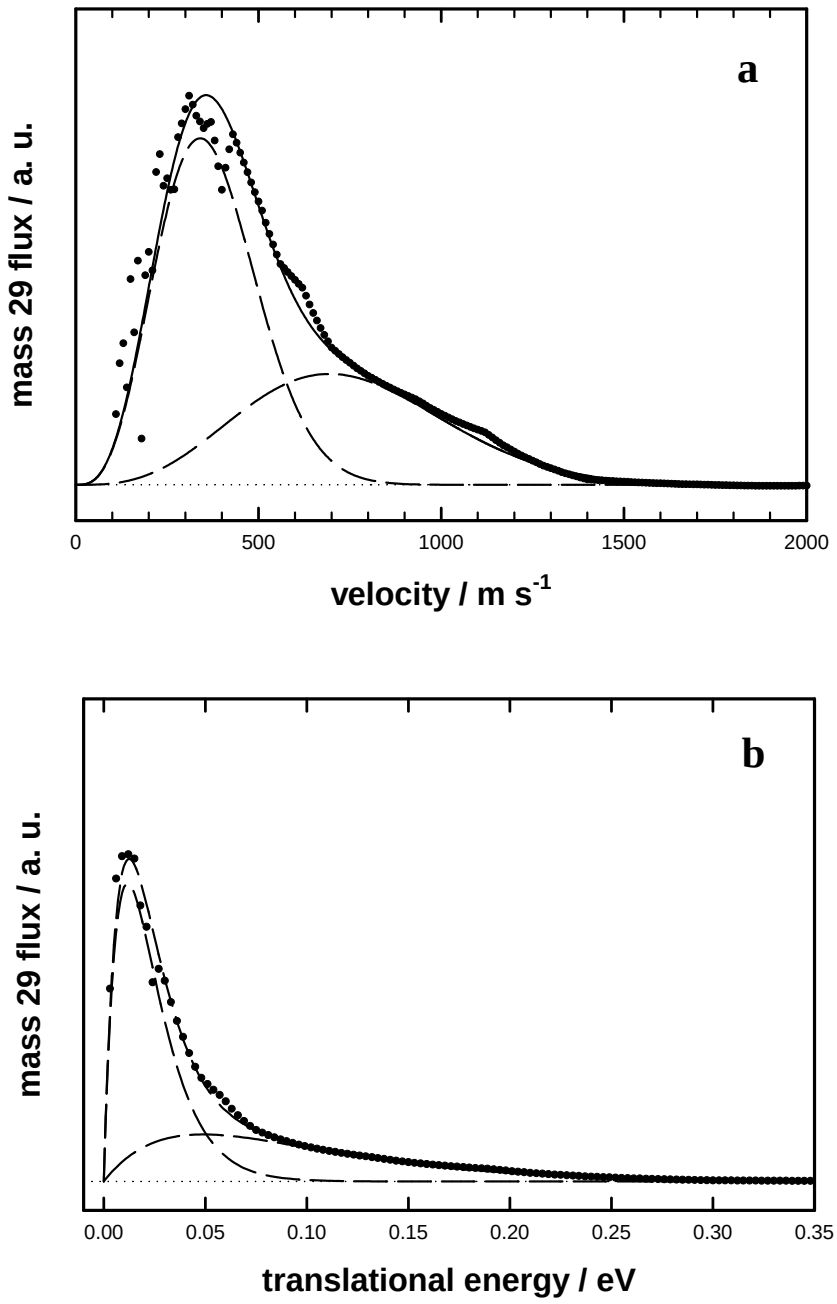

Figure 4.11: (a) velocity distribution and (b) translational energy distribution for CH_3CH_2· (mass 29) ejected upon irradiating an adlayer of 2-butaone and oxygen on a reduced TiO_2(110) surface at 200 K and in the presence of 5×10^{-10} Torr O_2 with 3.7 eV photons. Filled circles correspond to the data, dashed lines are Boltzmann fits to the data in the velocity domain, and solid lines are the sum of the two individual Boltzmann functions. Both the data and the fits were transformed from the velocity domain to the energy domain as described in the text.

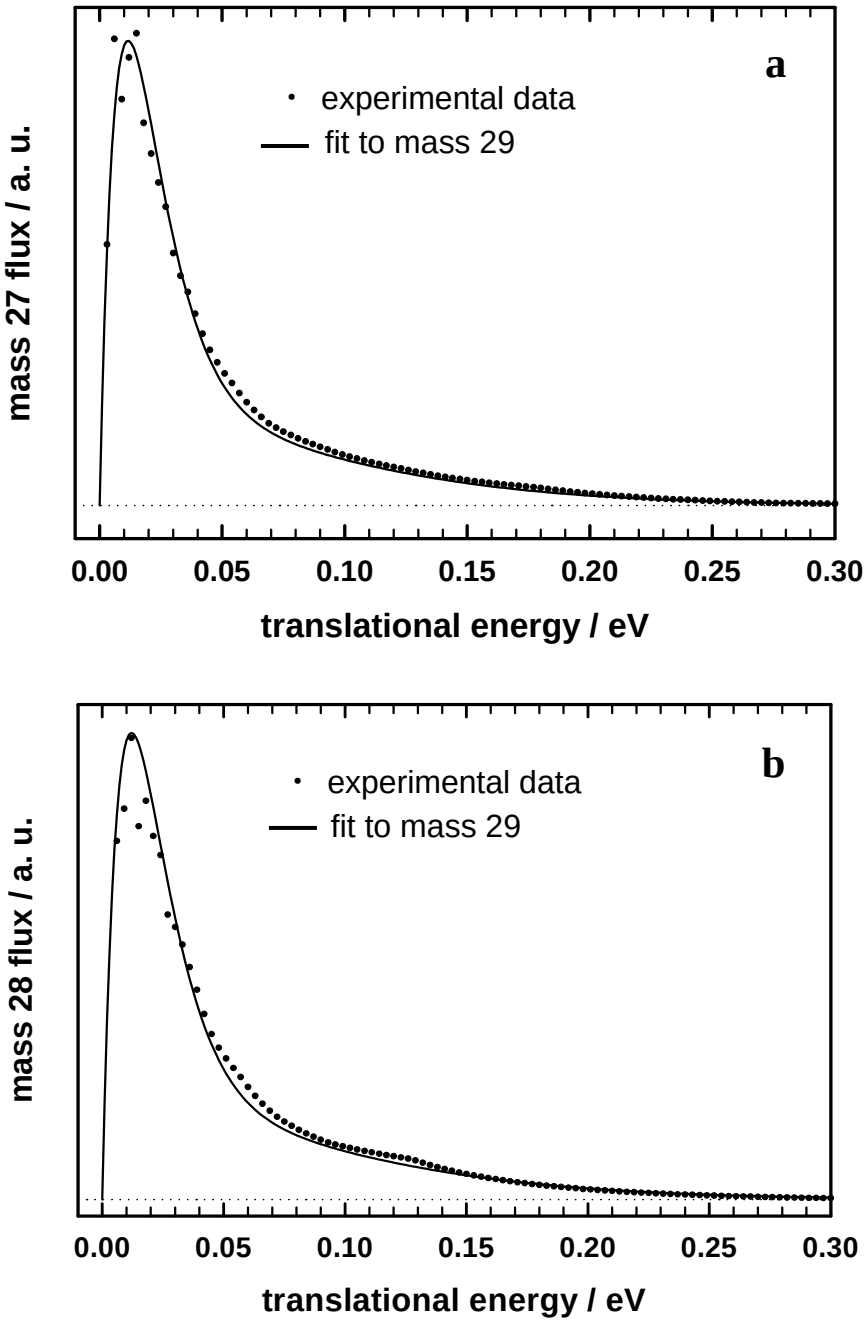

Figure 4.12: Translational energy distributions for CH_3CH_2· ejected upon irradiating an adlayer of 2-butaone and oxygen on a reduced TiO_2(110) surface at 200 K and in the presence of 5×10^{-10} Torr O_2 with 3.7 eV photons. Data was collected by monitoring (a) mass 27 and (b) mass 28. Filled circles correspond to the data, and solid lines are the fit to mass 29 given in Figure 4.11 and normalized to overlap the data points.

Bibliography:

Anpo, M., Che, M., Fubini, B., Garrone, E., Giamello, E., and Paganini, M. C., "*Generation of Superoxide Ions at Oxide Surfaces*." *Top. Catal.*, *8*, 189 (1999).

Atkins, P., *Physical Chemistry*, W.H. Freeman and Company, New York, 1998.

Attwood, A. L., Edwards, J. L., Rowlands, C. C., and Murphy, D. M., "*Identification of a Surface Alkylperoxy Radical in the Photocatalytic Oxidation of Acetone/O_2 over TiO_2*." *J. Phys. Chem. A*, *107*, 1779 (2003).

Bard, A. J., "*Photoelectrochemistry*." *Science (Washington, D. C.)*, *207*, 139 (1980).

Berger, T., Sterrer, M., Diwald, O., Knozinger, E., Panayotov, D., Thompson, T. L., and Yates, J. T. J., "*Light-Induced Charge Separation in Anatase TiO_2 Particles*." *J. Phys. Chem. B*, *109*, 6061 (2005).

Brinkley, D., and Engel, T., "*Active Site Density and Reactivity for the Photocatalytic Dehydrogenation of 2-Propanol on TiO_2(110)*." *Surf. Sci.*, *415*, L1001 (1998).

Comsa, G., and David, R., "*Dynamical Parameters of Desorbing Molecules.*" *Surf. Sci. Rep.*, *5*, 145 (1985).

Coronado, J. M., Kataoka, S., Tejedor-Tejedor, I., and Anderson, M. A., "*Dynamic Phenomena During the Photocatalytic Oxidation of Ethanol and Acetone Over Nanocrystalline TiO_2: Simultaneous FTIR Analysis of Gas and Surface Species*." *J. Catal.*, *219*, 219 (2003).

de Lara-Castells, M. P., and Krause, J. L., "*Periodic Hartree-Fock Study of the Adsorption of Molecular Oxygen on a Reduced TiO_2 (110) Surface.*" *J. Chem. Phys.*, *115*, 4798 (2001).

de Lara-Castells, M. P., and Krause, J. L., "*Theoretical Study of the Interaction of Molecular Oxygen with a Reduced TiO_2 Surface.*" *Chem. Phys. Lett.*, *354*, 483 (2002).

de Lara-Castells, M. P., and Krause, J. L., "*Theoretical Study of the UV-Induced Desorption of Molecular Oxygen from the Reduced TiO_2(110) Surface.*" *J. Chem. Phys.*, *118*, 5098 (2003).

de Lara-Castells, M. P., Mitrushenkov, A. O., Roncero, O., and Krause, J. L., "*Adsorption and Nonadiabatic Processes in the Photodesorption of Molecular Oxygen from the Reduced TiO_2(110) Surface.*" *Isr. J. Chem.*, *45*, 59 (2005).

Diebold, U., "*The Surface Science of Titanium Dioxide*." *Surf. Sci. Rep.*, *48*, 53 (2003).

Diebold, U., Lehman, J., Mahmoud, T., Kuhn, M., Leonardelli, G., Hebenstreit, W., Schmid, M., and Varga, P., "*Intrinsic Defects on a TiO_2(110)(1x1) Surface and their Reaction with Oxygen: A Scanning Tunneling Microscopy study.*" *Surf. Sci.*, *411*, 137 (1998).

Dohnalek, Z., Kim, J., Bondarchuk, O., White, J. M., and Kay, B. D., "*Physisorption of N_2, O_2, and CO on Fully Oxidized TiO_2(110)*." *J. Phys. Chem. B*, *110*, 6229 (2006).

Eppink, A. T. J. B., and Parker, D. H., "*Velocity Map Imaging of Ions and Electrons Using Electrostatic Lenses: Application in Photoelectron and Photofragment Ion Imaging of Molecule Oxygen*." *Rev. Sci. Instrum.*, *68*, 3477 (1997).

FitzPatrick, B. L., Maienschein-Cline, M., Butler, L. J., Lee, S.-H., and Lin, J. J., "*Determing the Partial Photoionization Cross-Sections of Ethyl Radicals*." *J. Phys. Chem. A*, *111*, 12417 (2007).

Fleck, L. E., Niu, B., Beuhler, R. J., and White, M. G., "*State-Resolved Dynamics of Infrared Photodesorption of CO from Ag(111)*." Laser Techniques for Surface Science II. San Diego, California: SPIE-The International Society for Optical Engineering, 298, 1995.

Fox, M. A., and Dulay, M. T., "*Heterogeneous Photocatalysis*." *Chem. Rev.*, *93*, 341 (1993).

Frank, S. N., and Bard, A. J., "*Heterogeneous Photocatalytic Oxidation of Cyanide Ion in Aqueous Solutions at TiO_2 Powder*." *J. Am. Chem. Soc.*, *99*, 303 (1977).

Fujishima, A., and Honda, K., "*Electrochemical Photolysis of Water at a Semiconductor Electrode*." *Nature (London)*, *238*, 37 (1972).

Gaya, U. I., and Abdullah, A. H., "*Heterogeneous Photocatalytic Degradation of Organic Contaminants Over Titanium Dioxide: A Review of Fundamentals, Progress, and Problems*." *J. Photochem. Photobiol., C*, *9*, 1 (2008).

Gierczak, T., Burkholder, J. B., Bauerle, S., and Ravishankara, A. R., "*Photochemistry of Acetone Under Tropospheric Conditions*." *Chem. Phys.*, *231*, 229 (1998).

Gravelle, P. C., Juillet, F., Meriaudeau, P., and Teichner, S., "*Surface Reactivity of Reduced TiO_2*." *Faraday Discuss. Chem. Soc.*, *52*, 140 (1971).

Haas, Y., "*Photochemical α-Cleavage of Ketones: Revisiting Acetone*." *Photochem. Photobiol. Sci.*, *3*, 6 (2004).

Hall, G. E., Bout, V., and Sears, T. J., "*Photodissociation of Acetone at 193 nm: Rotational- and Vibrational-State Distributions of Methyl Fragments by Diode Laser Absorption/Gain Spectroscopy*." *J. Chem. Phys.*, *94*, 4182 (1991).

Hashimoto, K., Irie, H., and Fujishima, A., "*TiO_2 Photocatalysis: A Historical Overview and Future Prospects*." *Jpn. J. Appl. Phys.*, *44*, 8269 (2005).

Heller, A., "*Chemistry and Applications of Photocatalytic Oxidations of Thin Organic Films*." *Acc. Chem. Res.*, *28*, 503 (1995).

Henderson, M. A., "*Acetone Chemistry on Oxidized and Reduced TiO_2(110)*." *J. Phys. Chem. B*, *108*, 18932 (2004).

Henderson, M. A., "*Ethyl Radical Ejection during Photodecomposition of Butanone on TiO_2(110)*." *Surf. Sci.*, *in Press*, (2008).

Henderson, M. A., "*The Interaction of Water With Solid Surfaces: Fundamental Aspects Revisited*." *Surf. Sci. Rep.*, *46*, 1 (2002).

Henderson, M. A., "*Photooxidation of Acetone on TiO_2(110): Conversion to Acetate via Methyl Radical Ejection*." *J. Phys. Chem. B*, *109*, 12062 (2005).

Henderson, M. A., "*Relationship of O_2 Photodesorption in Photooxidation of Acetone on TiO_2*." *J. Phys. Chem. C*, *112*, 11433 (2008).

Henderson, M. A., "*Structural Sensitivity in the Dissociation of Water on TiO_2 Single-Crystal Surfaces*." *Langmuir*, *12*, 5093 (1996).

Henderson, M. A., Epling, W. S., Perkins, C. L., Peden, C. H. F., and Diebold, U., "*Interaction of Molecular Oxygen with the Vacuum-Annealed TiO_2(110) Surface: Molecular and Dissociative Channels*." *J. Phys. Chem. B*, *103*, 5328 (1999).

Henrich, V. E., Dresselhaus, G., and Zeiger, H. J., "*Observation of Two-Dimensional Phases Associated with Defect States on the Surface of TiO_2*." *Phys. Rev. Lett.*, *36*, 1335 (1976).

Herzberg, G., *Molecular Spectra and Molecular Structure Volume I - Spectra of Diatomic Molecules.*, Krieger Publishing Company, Malabar, Florida, 1950.

Holbert, V. P., Garrett, S., J., Stair, P. C., and Weitz, E., "*The Photochemistry of CD_3I Adsorbed on the TiO_2(110) surface*." *Surf. Sci.*, *346*, 189 (1996).

Hugenschmidt, M. B., Gamble, L., and Campbell, C. T., "*The Interaction of H_2O with a TiO_2(110) Surface*." *Surf. Sci.*, *302*, 329 (1994).

Kimmel, G. A., and Petrik, N. G., "*Tetraoxygen on Reduced TiO_2(110): Oxygen Adsorption and Reactions with Bridging Oxygen Vacancies*." *Phys. Rev. Lett.*, *100*, 196102 (2008).

Linsebigler, A., Lu, G., and Yates, J. T. J., "*CO Photooxidation on TiO_2(110)*." *J. Chem. Phys.*, *100*, 6631 (1996).

Linsebigler, A., Lu, G., and Yates, J. T. J., "*Photocatalysis on TiO_2 Surfaces: Principles, Mechanisms, and Selected Results.*" *Chem. Rev.*, *95*, 735 (1995).

Lu, G., Linsebigler, A., and Yates, J. T. J., "*The Adsorption and Photodesorption of Oxygen on the TiO_2(110) Surface.*" *J. Chem. Phys.*, *102*, 4657 (1995).

Lu, G., Linsebigler, A., and Yates, J. T. J., "*The Photochemical Identification of Two Chemisorption States for Molecular Oxygen on TiO_2(110).*" *J. Chem. Phys.*, *102*, 3005 (1995).

Naccache, C., Meriaudeau, P., Che, M., and Tench, A. J., "*Identification of Oxygen Species Adsorbed on Reduced Titanium Dioxide.*" *Trans. Faraday Soc.*, *67*, 506 (1971).

North, S. W., Blank, D. A., Gezelter, J. D., and Longfellow, C. A., "*Evidence for Stepwise Dissociation Dynamics in Acetone at 248 and 193 nm.*" *J. Chem. Phys.*, *102*, 4447 (1995).

Onda, K., Li, B., and Petek, H., "*Two-Photon Photoemission Spectroscopy of TiO_2(110) Surfaces Modified by Defects and O_2 or H_2O Adsorbates.*" *Phys. Rev. B: Condens. Matter*, *70*, 045415 (2004).

Pacansky, J., and Dupuis, M., "*Assignment of the Infrared Spectrum for the Ethyl Radical.*" *J. Am. Chem. Soc.*, *104*, 415 (1982).

Paxton, A. T., and Thien-Nga, L., "*Electronic Structure of Reduced Titanium Dioxide.*" *Phys. Rev. B: Condens. Matter*, *57*, 1579 (1998).

Perkins, C. L., and Henderson, M. A., "*Photodesorption and Trapping of Molecular Oxygen at the TiO_2(110)-Water Ice Interface.*" *J. Phys. Chem. B*, *105*, 3856 (2001).

Raillard, C., Hequet, V., Le Cloirec, P., and Legrand, J., "*TiO_2 Coating Types Influencing the Role of Water Vapor on the Photocatalytic Oxidation of Methyl Ethyl Ketone in the Gas Phase.*" *Appl. Catal., B*, *59*, 213 (2005).

Rao, R. M., Beuhler, R. J., and White, M. G., "*Nonthermal Photodesorption of N_2 from Ag(111).*" *J. Chem. Phys.*, *109*, 8016 (1998).

Rasmussen, M. D., Molina, L. M., and Hammer, B., "*Adsorption, Diffusion, and Dissociation of Molecular Oxygen at Defected TiO_2(110): A Density Functional Theory Study.*" *J. Chem. Phys.*, *120*, 988 (2004).

Richter, L. J., Buntin, S. A., King, D. S., and Cavanagh, R. R., "*State-Resolved Studies of the Laser-Induced Desorption of NO from Si(111) 7x7: Low Coverage Results.*" *J. Chem. Phys.*, *96*, 2324 (1992).

Rocker, G., Schaefer, J. A., and Gopel, W., "*Localized and Delocalized Vibrations on TiO_2(110) Studied by High-Resolution Electron-Energy-Loss Spectroscopy*." *Phys. Rev. B: Condens. Matter*, *30*, 3704 (1984).

Rusu, C. N., and Yates, J. T. J., "*Defect Sites on TiO_2(110). Detection by O_2 Photodesorption*." *Langmuir*, *13*, 4311 (1997).

Shapira, Y., McQuistan, R. B., and Lichtman, D., "*Relationship Between Photodesorption and Surface Conductivity in ZnO.*" *Phys. Rev. B: Condens. Matter*, *15*, 2163 (1977).

Snelson, A., "*Infrared Matrix Iodide and Dimethyl Mercury*." *J. Phys. Chem.*, *74*, 537 (1969).

Tang, H., Levy, H., Berger, H., and Schmid, P. E., "*Urbach tail of Anatase TiO_2*." *Phys. Rev. B: Condens. Matter*, *52*, 7771 (1995).

Thompson, T. L., and Yates, J. T. J., "*Control of a Surface Photochemical Process by Fractal Electron Transport Across the Surface: O_2 Photodesorption from TiO_2(110)*." *J. Phys. Chem. B*, *110*, 7431 (2006).

Thompson, T. L., and Yates, J. T. J., "*Monitoring Hole Trapping in Photoexcited TiO_2(110) Using a Surface Photoreaction.*" *J. Phys. Chem. B*, *109*, 18230 (2005).

Thompson, T. L., and Yates, J. T. J., "*Surface Science Studies of the Photoactivation of TiO_2-New Photochemical Processes*." *Chem. Rev.*, *106*, 4428 (2006).

Thompson, T. L., and Yates, J. T. J., "*TiO_2-Based Photocatalysis: Surface Defects, Oxygen and Charge Transfer*." *Top. Catal.*, *35*, 197 (2005).

Waits, L. D., Horwitz, R. J., and Guest, J. A., "*Translational energy study of CH# photofragments following 1(n,p*) excitation of acetone*." *Chem. Phys.*, *155*, 149 (1991).

Wendt, S., Sprunger, P., T., Lira, E., Madsen, G. K. H., Li, Z., Hansen, J. O., Matthiesen, J., Blekinge-Rasmussen, A., Laegsgaard, E., Hammer, B., and Besenbacher, F., "*The Role of Interstitial Sites in the Ti3d Defect State in the Band Gap of Titania.*" *Science (Washington, D. C.)*, *320*, 1755 (2008).

Xu, W., and Raftery, D., "*In Situ Solid-State Nuclear Magnetic Resonance Studies of Acetone Photocatalytic Oxidation on Titanium Oxide Surfaces*." *J. Catal.*, *204*, 110 (2001).

Yujing, M., and Mellouki, A., "*The Near-UV Cross Sections for Several Ketones*." *J. Photochem. Photobiol., A*, *134*, 31 (2000).

Zuckermann, H., Schmitz, B., and Haas, Y., "*Dissociation Energy of an Isolated Triplet Acetone Molecule*." *J. Phys. Chem.*, *92*, 4835 (1988).

List of References:

(1) Diebold, U. *Surf. Sci. Rep.* **2003**, *48*, 53.

(2) Hashimoto, K.; Irie, H.; Fujishima, A. *Jpn. J. Appl. Phys.* **2005**, *44*, 8269.

(3) Gaya, U. I.; Abdullah, A. H. *J. Photochem. Photobiol., C* **2008**, *9*, 1.

(4) Heller, A. *Acc. Chem. Res.* **1995**, *28*, 503.

(5) Fox, M. A.; Dulay, M. T. *Chem. Rev.* **1993**, *93*, 341.

(6) Linsebigler, A.; Lu, G.; Yates, J. T. J. *Chem. Rev.* **1995**, *95*, 735.

(7) Thompson, T. L.; Yates, J. T. J. *Chem. Rev.* **2006**, *106*, 4428.

(8) Fujishima, A.; Honda, K. *Nature (London)* **1972**, *238*, 37.

(9) Frank, S. N.; Bard, A. J. *J. Am. Chem. Soc.* **1977**, *99*, 303.

(10) Bard, A. J. *Science (Washington, D. C.)* **1980**, *207*, 139.

(11) Atkins, P. *Physical Chemistry*; 6 ed.; W.H. Freeman and Company: New York, 1998.

(12) Berger, T.; Sterrer, M.; Diwald, O.; Knozinger, E.; Panayotov, D.; Thompson, T. L.; Yates, J. T. J. *J. Phys. Chem. B* **2005**, *109*, 6061.

(13) Wendt, S.; Sprunger, P., T.; Lira, E.; Madsen, G. K. H.; Li, Z.; Hansen, J. O.; Matthiesen, J.; Blekinge-Rasmussen, A.; Laegsgaard, E.; Hammer, B.; Besenbacher, F. *Science (Washington, D. C.)* **2008**, *320*, 1755.

(14) Rao, R. M.; Beuhler, R. J.; White, M. G. *J. Chem. Phys.* **1998**, *109*, 8016.

(15) Fleck, L. E.; Niu, B.; Beuhler, R. J.; White, M. G. Laser Techniques for Surface Science II, San Diego, California, 1995; p 298.

(16) Henderson, M. A. *J. Phys. Chem. B* **2005**, *109*, 12062.

(17) Perkins, C. L.; Henderson, M. A. *J. Phys. Chem. B* **2001**, *105*, 3856.

(18) Henderson, M. A. *Surf. Sci. Rep.* **2002**, *46*, 1.

(19) Eppink, A. T. J. B.; Parker, D. H. *Rev. Sci. Instrum.* **1997**, *68*, 3477.

(20) Dohnalek, Z.; Kim, J.; Bondarchuk, O.; White, J. M.; Kay, B. D. *J. Phys. Chem. B* **2006**, *110*, 6229.

(21) Henderson, M. A.; Epling, W. S.; Perkins, C. L.; Peden, C. H. F.; Diebold, U. *J. Phys. Chem. B* **1999**, *103*, 5328.

(22) Onda, K.; Li, B.; Petek, H. *Phys. Rev. B: Condens. Matter* **2004**, *70*, 045415.

(23) Anpo, M.; Che, M.; Fubini, B.; Garrone, E.; Giamello, E.; Paganini, M. C. *Top. Catal.* **1999**, *8*, 189.

(24) Naccache, C.; Meriaudeau, P.; Che, M.; Tench, A. J. *Trans. Faraday Soc.* **1971**, *67*, 506.

(25) de Lara-Castells, M. P.; Mitrushenkov, A. O.; Roncero, O.; Krause, J. L. *Isr. J. Chem.* **2005**, *45*, 59

(26) Lu, G.; Linsebigler, A.; Yates, J. T. J. *J. Chem. Phys.* **1995**, *102*, 4657.

(27) Kimmel, G. A.; Petrik, N. G. *Phys. Rev. Lett.* **2008**, *100*, 196102.

(28) Paxton, A. T.; Thien-Nga, L. *Phys. Rev. B: Condens. Matter* **1998**, *57*, 1579.

(29) Rasmussen, M. D.; Molina, L. M.; Hammer, B. *J. Chem. Phys.* **2004**, *120*, 988.

(30) de Lara-Castells, M. P.; Krause, J. L. *J. Chem. Phys.* **2001**, *115*, 4798.

(31) de Lara-Castells, M. P.; Krause, J. L. *Chem. Phys. Lett.* **2002**, *354*, 483.

(32) Lu, G.; Linsebigler, A.; Yates, J. T. J. *J. Chem. Phys.* **1995**, *102*, 3005.

(33) Rusu, C. N.; Yates, J. T. J. *Langmuir* **1997**, *13*, 4311.

(34) Thompson, T. L.; Yates, J. T. J. *J. Phys. Chem. B* **2005**, *109*, 18230.

(35) Thompson, T. L.; Yates, J. T. J. *J. Phys. Chem. B* **2006**, *110*, 7431.

(36) de Lara-Castells, M. P.; Krause, J. L. *J. Chem. Phys.* **2003**, *118*, 5098

(37) Hugenschmidt, M. B.; Gamble, L.; Campbell, C. T. *Surf. Sci.* **1994**, *302*, 329.

(38) Henderson, M. A. *Langmuir* **1996**, *12*, 5093.

(39) Brinkley, D.; Engel, T. *Surf. Sci.* **1998**, *415*, L1001.

(40) Thompson, T. L.; Yates, J. T. J. *Top. Catal.* **2005**, *35*, 197.

(41) Linsebigler, A.; Lu, G.; Yates, J. T. J. *J. Chem. Phys.* **1996**, *100*, 6631.

(42) Richter, L. J.; Buntin, S. A.; King, D. S.; Cavanagh, R. R. *J. Chem. Phys.* **1992**, *96*, 2324.

(43) Shapira, Y.; McQuistan, R. B.; Lichtman, D. *Phys. Rev. B: Condens. Matter* **1977**, *15*, 2163.

(44) Comsa, G.; David, R. *Surf. Sci. Rep.* **1985**, *5*, 145.

(45) Herzberg, G. *Molecular Spectra and Molecular Structure Volume I - Spectra of Diatomic Molecules.*; 2nd ed.; Krieger Publishing Company: Malabar, Florida, 1950.

(46) Rocker, G.; Schaefer, J. A.; Gopel, W. *Phys. Rev. B: Condens. Matter* **1984**, *30*, 3704.

(47) Diebold, U.; Lehman, J.; Mahmoud, T.; Kuhn, M.; Leonardelli, G.; Hebenstreit, W.; Schmid, M.; Varga, P. *Surf. Sci.* **1998**, *411*, 137.

(48) Gravelle, P. C.; Juillet, F.; Meriaudeau, P.; Teichner, S. *Faraday Discuss. Chem. Soc.* **1971**, *52*, 140.

(49) Henrich, V. E.; Dresselhaus, G.; Zeiger, H. J. *Phys. Rev. Lett.* **1976**, *36*, 1335.

(50) Henderson, M. A. *Surf. Sci.* **2008**, *in Press*.

(51) Attwood, A. L.; Edwards, J. L.; Rowlands, C. C.; Murphy, D. M. *J. Phys. Chem. A* **2003**, *107*, 1779.

(52) Coronado, J. M.; Kataoka, S.; Tejedor-Tejedor, I.; Anderson, M. A. *J. Catal.* **2003**, *219*, 219.

(53) Xu, W.; Raftery, D. *J. Catal.* **2001**, *204*, 110.

(54) Raillard, C.; Hequet, V.; Le Cloirec, P.; Legrand, J. *Appl. Catal., B* **2005**, *59*, 213.

(55) Henderson, M. A. *J. Phys. Chem. C* **2008**, *112*, 11433.

(56) Henderson, M. A. *J. Phys. Chem. B* **2004**, *108*, 18932.

(57) Tang, H.; Levy, H.; Berger, H.; Schmid, P. E. *Phys. Rev. B: Condens. Matter* **1995**, *52*, 7771.

(58) Zuckermann, H.; Schmitz, B.; Haas, Y. *J. Phys. Chem.* **1988**, *92*, 4835.

(59) Haas, Y. *Photochem. Photobiol. Sci.* **2004**, *3*, 6.

(60) Waits, L. D.; Horwitz, R. J.; Guest, J. A. *Chem. Phys.* **1991**, *155*, 149.

(61) North, S. W.; Blank, D. A.; Gezelter, J. D.; Longfellow, C. A. *J. Chem. Phys.* **1995**, *102*, 4447.

(62) Gierczak, T.; Burkholder, J. B.; Bauerle, S.; Ravishankara, A. R. *Chem. Phys.* **1998**, *231*, 229.

(63) Snelson, A. *J. Phys. Chem.* **1969**, *74*, 537.

(64) Hall, G. E.; Bout, V.; Sears, T. J. *J. Chem. Phys.* **1991**, *94*, 4182.

(65) Holbert, V. P.; Garrett, S., J.; Stair, P. C.; Weitz, E. *Surf. Sci.* **1996**, *346*, 189.

(66) FitzPatrick, B. L.; Maienschein-Cline, M.; Butler, L. J.; Lee, S.-H.; Lin, J. J. *J. Phys. Chem. A* **2007**, *111*, 12417.

(67) Yujing, M.; Mellouki, A. *J. Photochem. Photobiol., A* **2000**, *134*, 31.

(68) Pacansky, J.; Dupuis, M. *J. Am. Chem. Soc.* **1982**, *104*, 415.

Appendix A.

The procedure used to empirically fit the velocity distributions and abstract the mean translational energies are described here. A typical fit is shown in Figure A1, and the fit parameters are given in Tables 1 through 3. Measurements for determining the velocity distributions are collected as a function of pump-probe laser delay. The delay curves were corrected for depletion of O_2 from the surface by dividing the delay curve by the rate of O_2 photodesorption that was measured for each experiment. In addition, all delay curves were converted to flux distributions by weighting by t^{-1} since laser ionization is a density sensitive detection method. The flight time and distance was used in conjunction with the proper Jacobian to transform the flux and depletion corrected distributions from time-of-flight to the velocity distribution.

The velocity distributions were fit as follows. The two prompt channels were each fit to a Gaussian function of the form

$$f = ae^{-\frac{1}{2}\left(\frac{v-v_0}{w}\right)^2} \tag{A1}$$

where *a* is a normalization factor, v is the velocity, v_o is the peak velocity, and w is the width. The slow channel was fit to two Boltzmann distributions given by the equation[44]

$$f = Av^3 e^{-\left(\frac{mv^2}{2kT}\right)} \tag{A2}$$

where *A* is a normalization factor, v is the velocity, m is the mass of molecular oxygen k is the Boltzmann constant, and T is the substrate temperature. An example fit is shown in Figure A1 where the dashed lines represent the two individual components for the slow channel (a and b), as well as fits to the two prompt channels (c and d). The solid line is the sum of the individual components. Parameters of the fits to velocity distributions measured at substrate temperature of 100 K, 200 K, and 260 K are given in Tables 1, 2, and 3 respectively.

In order to obtain a mean translational energy for each channel, further conversion of the data from velocity to translational energy was done using the simple expression relating velocity to kinetic energy ($E = \frac{1}{2}mv^2$) and the relevant Jacobian transformation. The mean translational energies for each fit component are also given in Tables 1-3 along with the integrated peak areas. The mean translational energies of the slow channels for each distribution are given in the text of dissertation as a weighted average of the mean energies of the two individual Boltzmann components.

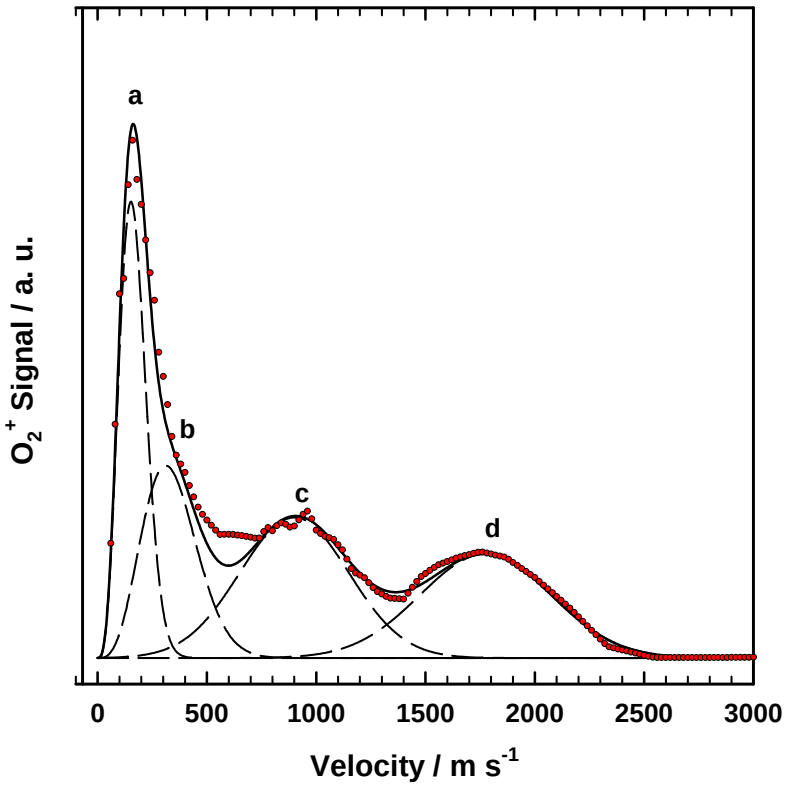

Figure A1: *Filled circles:* Velocity distribution of O_2 upon PSD from a reduced TiO_2(110) surface pre-exposed to 80 L O_2 at 100 K. The data shown here was collected with an excitation energy of 4.16 eV, and at a substrate temperature of 100 K. *Dashed lines (a) and (b):* Fits to individual peaks using the Boltzmann functions. *Dashed lines (c) and (d):* Fits to individual peaks using the Gaussian functions. *Solid line:* Sum of the individual fits.

Table 1: Velocity Distribution Fit Parameters for a Substrate Temperature of 100 K, and an Excitation Energy of 4.16 eV.

	Gaussian Function**			Boltzmann Function‡		$<E_t>$	Peak
Peak*	a (a.u.)	v_o	w	A (a.u.)	T (K)	(eV)	Area
a				2.2×10^{-8}	30	0.010	24%
b				1.09×10^{-9}	125	0.023	20%
c	5.4×10^{-3}	900	250			0.14	30%
d	4×10^{-3}	1775	300			0.54	26%

Table 2: Velocity Distribution Fit Parameters for a Substrate Temperature of 200 K, and an Excitation Energy of 4.16 eV.

	Gaussian Function**			Boltzmann Function‡		$<E_t>$	Peak
Peak*	a (a.u.)	v_o	w	A (a.u.)	T (K)	(eV)	Area
a				1.72×10^{-10}	41	0.011	12.6%
b				2.3×10^{-11}	208	0.037	43.6%
c	1.05×10^{-4}	980	252.5			0.17	21.6%
d	1.01×10^{-4}	1725	270			0.51	22.2%

Table 3: Velocity Distribution Fit Parameters for a Substrate Temperature of 260 K, and an Excitation Energy of 4.16 eV.

	Gaussian Function**			Boltzmann Function‡		$<E_t>$	Peak
Peak*	a (a.u.)	v_o	w	A (a.u.)	T (K)	(eV)	Area
a				8.1×10^{-10}	110	0.021	19.2%
b				1.95×10^{-10}	300	0.053	34.4%
c	2.1×10^{-3}	1020	220			0.18	16.8%
d	2.7×10^{-3}	1725	300			0.51	29.5%

*Peaks a-d are label in Figure A1.
**Parameters are for equation A1, with v_o and w in ms^{-1}
‡Parameters are for equation A2

Appendix B.

Obtaining laser delay scans was not as straight forward for butanone as it was in the case for acetone due to the congestion of peaks in the C_2 region of the mass spectrum. Since the masses in the C_2 region are separated by one amu, a narrow gate (peak integration limit) had to be set in each measurement to minimize signal contribution from adjacent peaks. The time-of-flight of species desorbing from the interface depends on the velocity imparted along the mass spectrometer axis by photochemistry occurring at the surface (neutral flight time) as well as by the acceleration field once the species is ionized. Conversely, arrival times of gas-phase species only depend on velocity imparted by the TOF lens array. During data collection, as the laser delay was scanned from short to long time (high to low velocity) the arrival time of a species from the surface would move toward long delay time (low velocity) and the gate was set to move with the peak of interest. A problem arose during data collection in that the background signal changed systematically with laser delay as the gate moved into and out of signal contributions from background gases, particularly hydrocarbons from small amounts of mechanical pump oil. In order to correct for this, several measurements were made under identical conditions except that the excitation laser was blocked (background scan). The background measurements were made at different times throughout the day and averaged together. A typical background scan is displayed in Figure B1. The solid line in the figure is a fit to the data by an exponential rise to a limiting value. The delay measurements were corrected by subtraction of the fit to the background scans from the data. The data was then corrected for depletion of reactants by dividing the data by a depletion scan made at an appropriate laser delay. Finally the delay scans were flux corrected by multiplying spectra by t^{-1}. After the raw data was corrected for background contributions, depletion of reactants, and flux it was converted to velocity distributions.

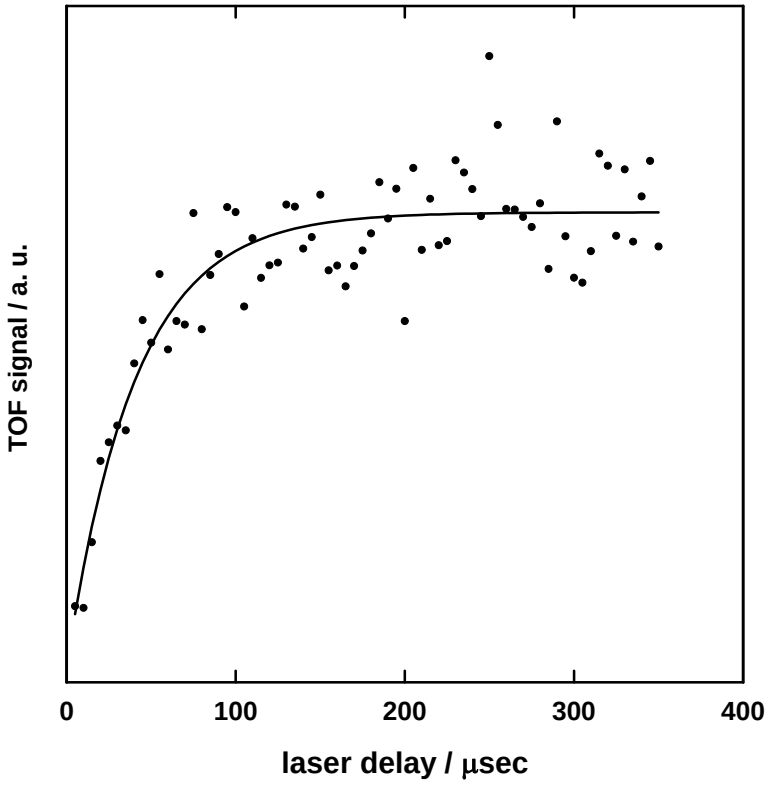

Figure B1: Typical background scan to be used for background correction of laser delay measurements. TOF signal obtained with a gate set for mass 29. Ionization energy of 13.1 eV was used, and the pump laser was blocked from the chamber. The background correction was applied to delay curves of ethyl radical ejection during the photodecomposition of 2-butanone on a $TiO_2(110)$ sample at 200 K in the presence of 5×10^{-10} torr O_2. Filled circles are data points, and the solid line is a fit to the data by an exponential rise to a maximum.